Functional Supramolecular Materials Based on Multiple Hydrogen-Bonding Motifs and the Associated Molecular Interaction Mechanism

by

Jingsi Chen

A thesis submitted in partial fulfillment of the requirements for the degree of

Doctor of Philosophy

in

Materials Engineering

Department of Chemical and Materials Engineering
University of Alberta

Abstract

Engineered multifunctional polymers with stimuli-responsive and self-healing properties have drawn increasing attention in recent years for the development of "smart" materials with a broad range of applications. Hydrogen bonding, as one of the most developed approaches in supramolecular chemistry, has been extensively exploited for generating self-assembled structures and functional materials. However, the integration of on-demand multifunctionalities (e.g., excellent mechanical properties, sensitive response to external stimuli and rapid healing ability) in one platform still remains a challenge. Besides, the single-molecular level understanding of the interaction mechanism between hydrogen-bonding motifs, which plays a crucial role in developing desired hydrogen-bonded structures, is limited. In this thesis, a review of hydrogen-bonded supramolecular materials and their properties is presented first, followed by three original studies regarding the development of multifunctional supramolecular materials (i.e., micelles, conductive composites, conductive hydrogels) based on a hydrogen-bonding motif 2-ureido-4[1H]-pyrimidinone (UPy), and an original research elucidating the UPy dimerization mechanism is described as well.

Polymeric micelles with core-shell structures have been recognized as attractive platforms for drug delivery. In the first project, a thermo-responsive core cross-linked polymeric micelle was developed based on a double hydrophilic block copolymer of poly(ethylene glycol)-b-poly(N-isopropylacrylamide) (PEG-b-PNIPAm), with UPy functionality incorporated throughout PNIPAm block to direct the core cross-linking via self-complementary multiple hydrogen bonds. The PNIPAm core of the micelles

exhibited reversible thermo-sensitive swelling/shrinking behavior, where the stability and responsive properties of the obtained micelles with varying UPy side-group content were investigated by dynamic light scattering, atomic force microscopy and fluorescence spectroscopy. The temperature-controlled loading and release of pyrene molecules were demonstrated, indicating the potential of the synthesized micelles as drug carriers.

Flexible conductive materials, which mimic human skin's functions, has gained special interest in the development of next-generation electronics. In the second project, an electrically conductive composite combining stretchability, self-healing, adhesiveness and sensing capability was prepared via a facial solution casting method, by triggering the in situ polymerization of pyrrole in a supramolecular polymer matrix cross-linked by UPy groups. The elastomer composite with the incorporation of 7.5 wt% conductive polypyrrole displayed a mechanical strength of 0.72 MPa with an elongation over 300%, and a complete self-healing of both mechanical and electrical properties was achieved within 5 min. Besides, the elastic material exhibited strong adhesiveness to a broad range of inorganic and organic substrates, which was further fabricated as a strain sensor for the successful detection of large and subtle human motions including finger bending and pulse beating.

In the third project, a novel type of multifunctional conductive polymer hydrogel was fabricated by incorporating UPy groups as cross-linking points into a conventional brittle polyaniline/poly(4-styrenesulfonate) (PANI/PSS) hydrogel, leading to a platform with the integration of high conductivity, excellent stretchability, injectability, and rapid self-healing capability. The formation of interpenetrating PANI/PSS network offered the hydrogel a superior conductivity of 13 S/m and a linear response (gauge factor=3.4) to

external strain (≈300%), exhibiting accurate and reliable detection of various human activities, including large motions of human body (e.g., finger and wrist bending) and subtle movements of muscles (e.g., swallowing, speaking, pulse beating). Taking advantage of the reversibility of the non-covalent cross-links, the hydrogels could be facilely molded into different shapes and injected from a needle, along with a complete self-healing within 30 s upon damage.

To further reveal the interaction mechanism of the hydrogen-bonding groups from a molecular perspective, in the fourth project, single-molecule force spectroscopy (SMFS) was employed to characterize the binding strength and dynamics of UPy-UPy dimers in aqueous environment, and the hydrophobic effect was investigated by tethering alkylene spacers of different lengths to the hydrogen-bonding moieties. The rupture force and unbinding energy of self-complementary UPy-UPy dimers were found to be remarkably enhanced with increasing spacer length, demonstrating cooperative effect between hydrogen bonding and hydrophobic interactions at the single-molecular level. In good agreement, molecular dynamics (MD) simulations on the interactions of UPy-UPy dimers also indicated higher structural stability with longer hydrophobic spacers.

This thesis work has developed three novel multifunctional supramolecular materials based on a multiple hydrogen-bonding motif UPy, and has elucidated the related hydrogen-bonding interactions at the single-molecule level. This work expands the applicability of hydrogen-bonding motifs to different multifunctional materials ranging from drug carriers to flexible electronics, providing new insights and approaches to the development of advanced functional materials based on multiple hydrogen bonds for diverse biomedical and engineering applications.

Preface

This thesis is an original work conducted by Jingsi Chen under the supervision from Dr. Hongbo Zeng and Dr. Thomas Thundat, containing published contents from the peer-reviewed journals and a book as described below.

Part of Chapter 1 of this thesis has been published as Li, L.; Chen, J.; Yan, B.; Zeng, H., Intrinsic Self-Healing Polymeric Materials for Engineering and Environmental Applications. In *Smart Materials for Advanced Environmental Applications*, The Royal Society of Chemistry, 2016; 139-164. I was responsible for the manuscript composition of Section 5.2 "Self-Healing Polymeric Materials via Reversible Bond Formation".

Chapter 2 of this thesis has been published as Chen, J.; Yan, B.; Wang, X.; Huang, Q.; Thundat, T.; Zeng, H., Core Cross-Linked Double Hydrophilic Block Copolymer Micelles Based on Multiple Hydrogen-Bonding Interactions. *Polym. Chem.* **2017,** *8*, 3066-3073. I was responsible for materials synthesis, data collection and analysis, as well as the manuscript composition. Dr. Bin Yan instructed the polymer synthesis and data analysis. Dr. Xiaogang Wang, Dr. Qingxue Huang and Dr. Thomas Thundat contributed to the manuscript revision. Dr. Hongbo Zeng was the corresponding author and was involved in the experimental design and manuscript composition.

Chapter 3 of this thesis has been published as Chen, J.; Liu, J.; Thundat, T.; Zeng, H., Polypyrrole-Doped Conductive Supramolecular Elastomer with Stretchable, Rapid Self-Healing, and Adhesive Properties for Flexible Electronic Sensors. *ACS Appl. Mater. Interfaces* **2019,** *11*, 18720-18729. I was responsible for materials synthesis, data collection and analysis, as well as the manuscript composition. Dr. Jifang Liu and Dr. Thomas Thundat contributed to the manuscript revision. Dr. Hongbo Zeng was the

corresponding author and was involved in the experimental design and manuscript composition.

Chapter 4 of this thesis has been published as Chen, J.; Peng, Q.; Thundat, T.; Zeng, H., Stretchable, Injectable and Self-Healing Conductive Hydrogel Enabled by Multiple Hydrogen Bonding toward Wearable Electronics. *Chem. Mater.* **2019**, *31,* 4553-4563. I was responsible for materials synthesis, data collection and analysis, as well as the manuscript composition. Qiongyao Peng and Dr. Thomas Thundat contributed to the manuscript revision. Dr. Hongbo Zeng was the corresponding author and was involved in the experimental design and manuscript composition.

Chapter 5 of this thesis has been published as Chen, J.; Wu, M.; Gong, L.; Zhang, J.; Yan, B.; Liu, J.; Zhang, H.; Thundat, T.; Zeng, H., Mechanistic Understanding and Nanomechanics of Multiple Hydrogen-Bonding Interaction in Aqueous Environment. *The J. Phys. Chem. C* **2019,** *123*, 4540–4548. I was responsible for materials synthesis, force measurements data collection and analysis, as well as the manuscript composition. Dr. Min Wu conducted the molecular dynamics simulations. Lu Gong assisted with the force measurements. Dr. Jiawen Zhang, Dr. Bin Yan, Dr. Jifang Liu, Dr. Hao Zhang and Dr. Thomas Thundat contributed to the manuscript revision. Dr. Hongbo Zeng was the corresponding author and was involved in the experimental design and manuscript composition.

Dedicated to

My parents, my husband Hui, and our family member Gulu

Acknowledgements

My Ph. D. study and this thesis would not be possible without the help of many individuals.

My foremost gratitude goes to Dr. Hongbo Zeng, who provides me the great opportunity to study in University of Alberta and guided me into the fantastic world of functional polymers. I really appreciate his elaborate guidance through my graduate study, and his immense knowledge, thoughtful insights and passion for science encourage me to pursue my future career in this field.

My sincere gratitude goes to Dr. Thomas Thundat for his constant encouragements and valuable suggestions. His enthusiasm for scientific research and broad perspective inspire me to think about the world more scientifically.

I would like to thank all my group members, both past and present, for their support, advice and friendship. Especially thanks to Dr. Bin Yan who helped me with the polymer synthesis and various analytical techniques.

Financial support from Alberta Innovates is also appreciated.

Last but not least, I would like to thank my parents, for their continuous support and love during my study overseas. My special thanks go to my husband Hui who gave me support and encouragements during my dark days, and we spent lots of happy hours together over the past nine years. Looking forward to more years of laugh with holding each other's hands.

Table of Contents

List of Tables

List of Figures

Abbreviations and Symbols

CD   cyclodextrin

CB[n]   cucurbit[n]uril

3D   three-dimensional

PTHF   poly(tetrahydrofuran)

BTA   benzene-1,3,5-tricarboxamide

UPy   2-ureido-4[1H]-pyrimidinone

PBA   poly(n-butyl acrylate)

PS   polystyrene

PA6ACA   acryloyl-6-aminocaproic acid

DMAEMA   2-(dimethylamino)-ethyl methacrylate

PEG   poly(ethylene glycol)

SFA   surface forces apparatus

SMFS   single-molecule force spectroscopy

AFM   atomic force microscopy

FJC   freely jointed chain

M-FJC   modified freely jointed chain

WLC   worm-like chain

DHBC   double hydrophilic block copolymers

PPy   polypyrrole

RAFT   reversible addition-fragmentation chain transfer

NIPAm   N-isopropylacrylamide

PANI   polyaniline

PSS	poly(4-styrenesulfonate)
$P(E_{1-x}-U_x)C$	poly(ethyl-co-urea carbonate)
PNIPAm	poly(N-isopropylacrylamide)
HEMA	2-hydroxyethyl methacrylate
LCST	lower critical solution temperature
AIBN	2,2′-Azobis(2-methylpropionitrile)
DMSO	dimethyl sulfoxide
DMF	N,N-dimethylformamide
$CHCl_3$	chloroform
$CDCl_3$	deuterated chloroform
CaH_2	calcium hydride
NMR	nuclear magnetic resonance
DLS	dynamic light scattering
CTA	chain transfer agent
DP	degree of polymerization
RMS	root-mean-square
PDI	polydispersity index
PEGMA	poly(ethylene glycol) methyl ether methacrylate
AA	acrylic acid
PDMS	polydimethylsiloxane
CuPcTs	copper phthalocyanine-3,4′,4″,4‴-tetrasulfonic acid tetrasodium salt
APS	ammonium persulfate
FTIR	Fourier transform infrared spectroscopy

GPC	gel permeation chromatography
TGA	thermogravimetric analysis
SEM	scanning electron microscopy
PC	polycarbonate
GF	gauge factor
NaSS	4-styrenesulfonic acid sodium salt
NaOH	sodium hydroxide
TEMED	N,N,N′,N′-tetramethylethylenediamine
HCl	hydrochloric acid
ANI	aniline
$FeCl_3$	iron(III) chloride hexahydrate
MD	molecular dynamics
CDI	1,1′-carbonyldiimidazole
TA	thioctic acid
DCC	N,N'-dicyclohexylcarbodiimide
DMAP	4-dimethylaminopyridine
DCM	methylene chloride
PME	particle mesh Ewald
PMF	potential of mean force
WHAM	weighted histogram analysis method
K_a	association constant
T_g	glass transition temperature
N	number of Kuhn segments

l_k	Kuhn length
x	extension of polymer chain
F	applied force
L_c	contour length
k_B	Boltzmann constant
T	temperature
K_s	segment elasticity
ΔG	energy barrier
k_{on}	kinetic on-rate constant
k_{off}	kinetic off-rate constant
x_B	dissociation distance
R_f	loading rate
F_R	most probable rupture force
Mn	number average molecular weight
Mw	weight average molecular weight
I_n	fluorescence intensity
δ	chemical shift
D_H	hydrodynamic diameter
G'	storage modulus
G''	loss modulus
I	current
R	resistance
U	voltage

ω	angular frequency
R_s	sheet resistance
σ	conductivity
η^*	viscosity
γ	strain
E	extension
L_{planar}	monomer length in planar conformation
$L_{helical}$	monomer length in helical conformation

CHAPTER 1   Introduction

1.1 Functional Supramolecular Polymers

Beyond conventional polymers generated by permanent covalent bonds, supramolecular polymers, which combine polymer science with supramolecular chemistry, are assembled from building blocks via reversible noncovalent interactions such as hydrogen bonding, metal-ligand coordination, ionic interactions, host-guest interactions, and π-π stacking,[1-3] where the building units can be either low-molecular-weight monomers or polymer chains.[4,5] Compared to strong covalent interactions, the primary supramolecular binding motifs possess a broad range of binding strengths, as illustrated in **Figure 1.1**.[6] The modulated strength and the directionality of the noncovalent connections allow the supramolecular polymers to exhibit characteristics of traditional polymers,[7,8] and more importantly, their dynamic and reversible nature impart the resultant polymers capability to tune the structures and properties upon appropriate external stimuli.[9,10] Taking advantage of these unique features, supramolecular polymers have emerged as a popular research area over the past three decades, with efforts spend on in-depth understanding of molecular interactions as well as development of advanced functional materials for practical applications in diverse fields.[11]
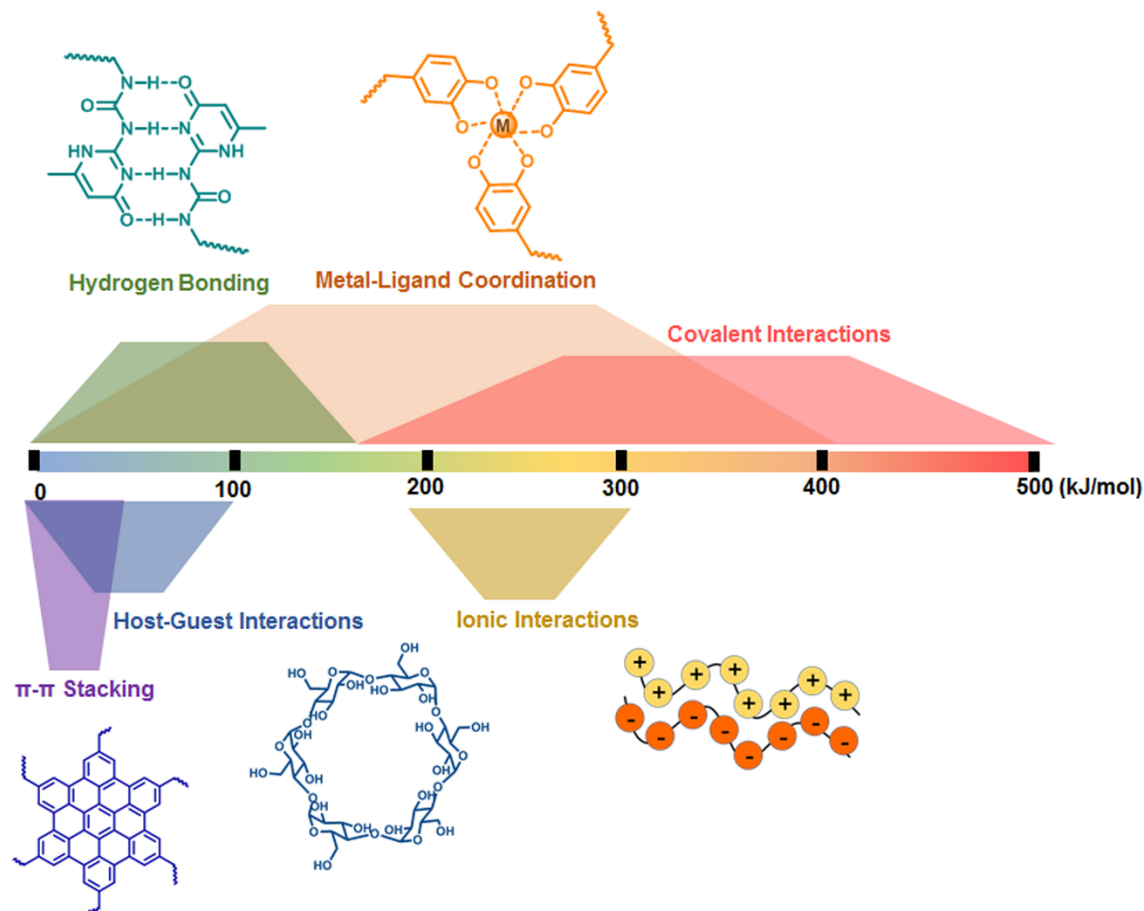
Figure 1.1. Schematic representations of some primary supramolecular binding motifs and their typical range of binding strength.

1.1.1 Driving Forces

1.1.1.1 Hydrogen Bonding

Hydrogen bonds ubiquitously exist in biological systems and hydrogen-bonding interactions play an essential role in various biological processes such as DNA pairing and protein folding.[12] Owing to its affinity and reversibility, hydrogen bonding has evolved as one of the most developed approaches to generate synthetic supramolecular polymers.[13] As single hydrogen bond is generally weak with binding energy in the range

of 10~25 kJ/mol,[14] multiple hydrogen bonding groups, which can form triple, quadruple or sextuple hydrogen bonds within two complementary moieties, are favorable to direct the self-assembly of stable structures, due to their relatively high strength, excellent reversibility, and complementary recognition.[15] The association strength between multiple hydrogen bonding units depends on the nature of donor (D)/acceptor (A), solvent, number of hydrogen bonds, and the arrangements of D/A sites. **Figure 1.2** shows examples of several multiple hydrogen bonding groups and their association constants (K_a) in chloroform.[16-19] The viscosity of hydrogen-bonded supramolecular polymers is generally reduced at elevated temperatures, rendering the materials thermo-responsiveness and easy processability.

(a) K_a= 800 M^{-1} **(b)** K_a= 2.4×10^4 M^{-1} **(c)** K_a= 6×10^7 M^{-1} **(d)** K_a= 3×10^8 M^{-1}
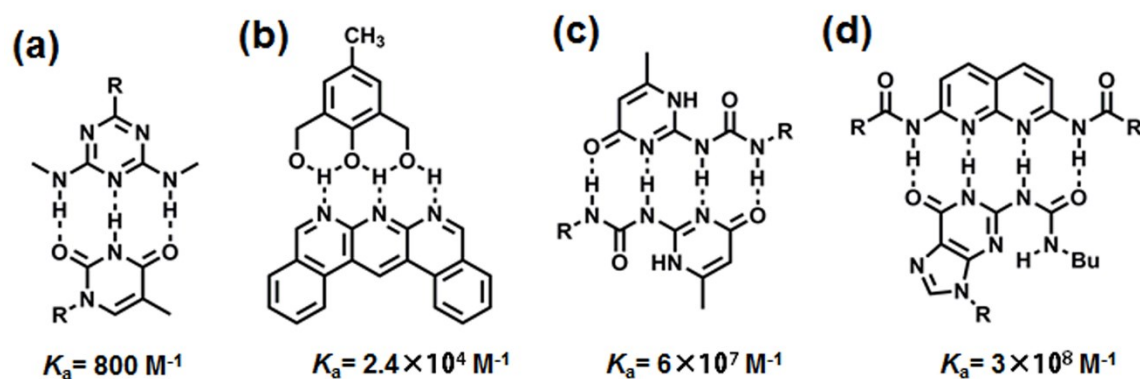
Figure 1.2. Examples of supramolecular hydrogen-bonding motifs and their association constants in chloroform designed by (a) Binder et al.[16] (b) Leigh et al.[17] (c) Meijer et al.[18] (d) Zimmerman et al.[19]

1.1.1.2 Metal-Ligand Coordination

Metal-ligand coordination offers variable binding energies as well as redox and photophyical properties, which has been widely used for the construction of metal-organic frameworks and self-assemblies.[20] Responsive, supramolecular materials

3

utilizing metal-ligand interactions are particularly attractive because the reversibility and physical properties of the coordination complexes can be facilely tuned by incorporating different metal ions and ligands.[21] Rowan et al. reported a class of organic/inorganic hybrid materials self-assembled from telechelic rubbery polymers end-capped with 2,6-bis(benzimidazolyl)-4-oxypyridine derivatives. The polymer chain was extended by forming complexes with a range of metal ions (e.g., Fe^{2+}, Co^{2+}, Zn^{2+}, Cd^{2+}).[22,23] This concept of metallo-supramolecular polymers was also demonstrated by Schubert and coworkers, using terpyridine-functionalized building blocks and divalent metal ions to prepare switchable polymers via dynamic metal-ligand interactions.[24] The coordination between Fe^{3+} and catechol ligands inspired by mussel adhesive proteins has attracted enormous attention, with the mono complex dominating at pH < 5.6, the bis complex at 5.6 < pH < 9.1 and the tris complex at pH > 9.1, leading to "smart" materials with properties readily controlled by the pH of the surrounding environment.[25]

1.1.1.3 Ionic Interactions

Ionomers are a class of polymers containing up to 15 mol% ionic groups along the polymer backbone.[26] The ion pairs aggregate into discrete regions, which act as crosslinks exerting influence on the mechanical and physical properties of ionomers.[27] They are commonly used for commercial applications such as molded coatings, packaging films, and membranes in fuel cells.[28] The reversible nature of ionic interactions leads to rearrangement of the clustered regions and contributes to the self-healing behavior, which

was demonstrated by projectile testing of poly(ethylene-co-methacrylic acid)-based ionomers.[29] Besides, the mixing of oppositely charged polyelectrolytes can result in self-

assembled hydrogels and coacervates with various applications in biomedical engineering.[30]

1.1.1.4 Host-Gest Interactions

Macrocyclic host-gest complexation is formed via complementary shape and size recognition between the cavity of the macrocyclic host and the guest molecule, where the internal characteristics of the host provide noncovalent interactions (e.g., hydrophobic interactions, hydrogen bonds, van der Waals interactions) to bind the guest.[10] Among various developed host-guest systems, two primary host molecules employed in supramolecular chemistry are cyclodextrins (CDs) and cucurbit[n]urils (CB[n]s).[31,32] CDs consist of six to eight D-glucose units via α-1,4-glycosidic linkages, which possess a hydrophilic external surface to facility the solubility and a hydrophobic cavity to lock a variety of inorganic, organic or biological molecules.[33] CDs have been incorporated into different polymeric systems to induce the formation of hydrogels, displaying temperature, pH, and redox sensitivity.[34] CB[n]s are built from glycoluril repeating units and exhibit higher binding strengths compared to CDs due to additional ion-dipole interactions.[35] Since the cavity of CB[8] is larger than the other derivatives, it can bind two guest molecules simultaneously, and the ternary complex provides a facile approach toward multicomponent systems.[36]

1.1.1.5 π-π Stacking

π-π stacking interactions are the association between electronically complementary aromatic π systems, and play an important role in supramolecular chemistry.[37] Computational studies on model compounds indicated that a "chain-folding" motif comprising two π-electron-deficient diimide units separated by a triethylenedioxy

linking unit provides an ideal stereoelectronic center for binding complementary π-electron-rich aromatic groups.[38] Since the strength and directionality of π-π stacking usually decrease in nonpolar solvents, an effective strategy to generate stable supramolecular assemblies is to combine π-π stacking and other noncovalent interactions in one system. For example, by blending a chain-folding polyimide with a low-molecular-weight polyurethane with pyrenyl end-groups, a tough and elastomeric material was produced. The polymer network contained both hydrogen bonding moieties (ureas and urethanes) and complementary π-π stacking residues, showing significant enhancement of tensile modulus and its mechanical properties could be repeatedly regained at elevated temperature.[39]

1.1.2 Supramolecular Architectures

1.1.2.1 Linear Polymers

When monomers or polymers are end-functionalized with supramolecular binding motifs, which are referred to as "ditopic monomeric species", supramolecular linear polymers are formed through the recognition of the self-complementary (AA type) or hetero-complementary (AB type) units, and their structures are determined by both the recognition type and the monomer features.[40] Homopolymers are generally produced from a single monomer modified with AA type groups, while different kinds of monomers functionalized with AB type units can lead to head-to-tail connections for the construction of alternating copolymers and block copolymers.[41] The degree of polymerization is mainly dependent on the binding strength of the end groups and affected by the surrounding environment.[42] Besides, the stacking and aggregation of the functional motifs can induce rod-like or wormlike structures. For instance, the discotic

liquid crystals were assembled by the stacking of planar aromatic cores with flexible alkyl side chains dissolved in the solvents.[43]

1.1.2.2 Dendrimers and Hyperbranched Polymers

Supramolecular dendritic polymers, which are formed via the identical recognition of the dendritic building blocks, possess numerous terminals and weak intermolecular entanglement, exhibiting unique physiochemical properties such as low viscosity and high solubility.[44] Compared to conventional dendrimers, the self-assembly process in the supramolecular dendritic polymers allows facile synthesis and switchable structures in response to external stimuli. However, the uniform topology of the dendritic structure is difficult to achieve due to the dynamic nature of the noncovalent interactions.[3] Hyperbranched polymers are commonly utilized in biomedical applications, especially drug delivery systems, attributed to their highly branched globular morphology and abundant inner cavities. Host-guest interactions have been extensively applied for the preparation of hyperbranched polymers, where the supramolecular polycations constructed by the recognition between adamantane and CDs were able to show high DNA condensation ability and gene transfection activity.[45]

1.1.2.3 Three-Dimensional (3D) Networks

When polymer building blocks are connected via the noncovalent interactions between the side groups or main chains, supramolecular 3D networks are established with a combination of the properties gained from the polymer units and the reversible cross-linking.[46] Phase separation can be detected in the supramolecular networks due to the stacking, clustering and crystallization of the cross-linking points.[47] Based on the dynamics of the utilized supramolecular interactions, the macroscopic properties of the

prepared materials can be readily modulated by various stimuli such as temperature, pH, light and electric/magnetic field, suggesting their potential application in diverse fields. For example, pH-sensitive hydrogen-bonded hydrogels were developed as carriers for anti-cancer drugs which could be delivered at the acidic tumor sites, [48] and shape-memory materials were facilely fabricated by incorporating supramolecular cross-linking into a permanently bonded network.[49]

1.1.3 Properties and Functions

1.1.3.1 Stimuli-Responsive Materials

Most supramolecular interactions tend to be weakened at elevated temperatures, resulting in a reduced viscosity of the resultant supramolecular polymers, which endows thermoplasticity and thermo-responsiveness to the materials.[46] When CB[8]/viologen/naphthoxy complex served as the cross-linking in a hydrogel system, the hydrogel could undergo reversible sol-gel transition during heating/cooling cycles with tunable microstructures.[50] A photo-switchable hydrogel was fabricated by inclusion complexation between γ-CD and two accommodated coumarin units. Due to the reversible photo-dimerization/cleavage of the coumarin, the mechanical property of the hydrogel was controlled by UV radiation as well as temperature.[51] Catechol-metal and catechol-boronate complexations have been applied for the design of pH-responsive materials, and the hydrogels based on phenylborate esters were demonstrated to display responsiveness to monosaccharides such as glucose, galactose, and fructose.[52,53] Owning to the redox-responsive properties of metal ions, the supramolecular polymers linked by the coordination between ditopic ligands and copper ions exhibited a modulated degree of

polymerization and viscosity, which were dependent on the oxidation state of the copper ions.[54]

1.1.3.2 Self-Healing Materials

One of the most fascinating properties of biological systems is that they can repair damages inflicted by external stimuli autonomously,[55] which is rarely achieved in synthetic polymeric systems. Inspired by nature, the development of self-healing polymers, which possess the ability to repair themselves after environmental attack, is currently an active field of study around the world.[56-58] The self-healing polymers are expected to show significantly enhanced durability, making them promising candidates for applications susceptible to damage or in poorly accessible areas.[59] **Figure 1.3** shows the common healing principle of self-healing polymers. Physical damage to polymers will result in chain cleavage and/or slippage and subsequently form reactive chain ends. If these end groups are stable in the environment and can be brought into contact by rearrangements of polymer chains, the bonds will reform and repair the polymer network.[60] Therefore, the two essential elements for self-healing process are the reversibility of reactive groups and the mobility of polymer chains.[61] Taking advantage of the dynamic nature of the noncovalent bonds, the polymers assembled by supramolecular interactions hold great promise for the fabrication of self-healing materials.

| Undamaged network | Physical damage | Contact of reactive end groups | Bond reformation Network repair |
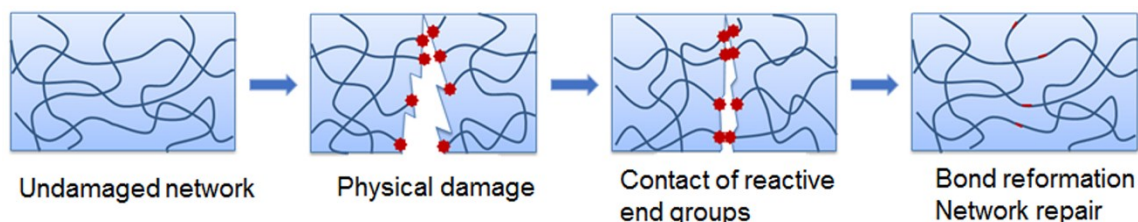
Figure 1.3. Schematic representation of the damage-repair process in self-healing polymers.

A serious of self-healing poly(acrylic acid) hydrogels were developed via facial free radical polymerization containing both covalently and ionically crosslinked networks.[62] The covalent crosslinking of polymers provided mechanical support to sustain the shape of the hydrogels, while the autonomous self-healing of the hydrogel was achieved through the dynamic ionic bonding between ferric ions and carboxylic groups. The remarkable self-healing property of the metallo-hydrogels could be nicely modulated by changing the chain length of the amphiphiles and the type of metal ions. The unique physical and chemical interactions offered by catechol groups have also been utilized for the design of self-healing materials, where the mixing of catechol-functionalized 4-arm PEG with a variety of trivalent metal ions (i.e., Fe^{3+}, V^{3+}, Al^{3+}) led to a series of hydrogels with self-healing capability enabled by metal-ligand interactions.[25,63] Moreover, in metal-free environments, self-healing ability could also be realized in catechol-functionalized polyacrylate and polymethacrylate materials, which was mainly attributed to bidentate hydrogen bonding between catechol groups and facilitated by other physical interactions.[64] An injectable hydrogel was prepared based on a thermo-responsive ABA tri-block copolymer consisting of catechol-functionalized poly(N-isopropylacrylamide) as A block and hydrophilic PEG as B block,[65] of which the rapid self-healing property was contributed not only by hydrogen bonding but also aromatic interactions (i.e., quadrupolar interactions and π−π stacking) between the catechol moieties.

The universal design of self-healing supramolecular systems is based on the scission and reformation of weak supramolecular interactions rather than stronger covalent bonds. This concept provides an upper limit to the strength of these materials as there is a dilemma between bonding strength and self-healing ability.[66] Up to now, most

healable supramolecular materials are soft elastomers with relatively low glass transition temperature (T_g). Supramolecular nanocomposites may offer a promising approach to enhancing the strength of the material by utilizing nanoscale particles[67] or high aspect-ratio fillers[68] as the strengthening phase. This class of supramolecular composites remains self-healing properties offered by the supramolecular polymer matrix and has the potential to generate materials with useful engineering applications, especially for high-modulus structural materials.

1.2 Hydrogen-Bonded Supramolecular Polymers

1.2.1 Hydrogen-Bonded Nanostructures

Phase segregation is an effective strategy to control the morphologies and properties of polymeric materials, where micelle-like phase segregation induced by clustering of hydrogen-bonding groups have been demonstrated to facilitate the intermolecular interaction and enhance the stability of the network.[69] When common nucleobases (i.e., adenine, cytosine, guanine, thymine) were utilized as end-functionalities of poly(tetrahydrofuran) (PTHF) macromonomers, the weak hydrogen-bonding interactions and π-π stacking between the nucleobase ends aided them to aggregate into "hard" domains which were connected by "soft" PTHF chains (**Figure 1.4a**). The phase separation differed in different solutions and were dependant on temperature.[70]

Lateral stacking hydrogen-bonding units can promote the formation of ordered structures such as nanofibers, nanotubes and nanorods.[2] Through the association of bifurcated hydrogen bonds, urea moieties have been widely incorporated into polymeric systems to adjust their mechanical properties including strength, hardness and adhesion.[71]

As presented in **Figure 1.4b**, a thermoplastic elastomer was developed based on a block copolymer, which was composed of soft poly(ε-caprolactone) segments and hard blocks containing two urea groups separated by a spacer. When small molecules also consisted of bisureas were added into the system, these molecules would self-assemble into supramolecular ribbons together with the hard blocks by the stacking of bisureas, and the formed nanofillers showed very high aspect ratio with monodispersed diameters of 5~6 nm, significantly enhancing the modulus and stiffness of the elastomer.[72,73]
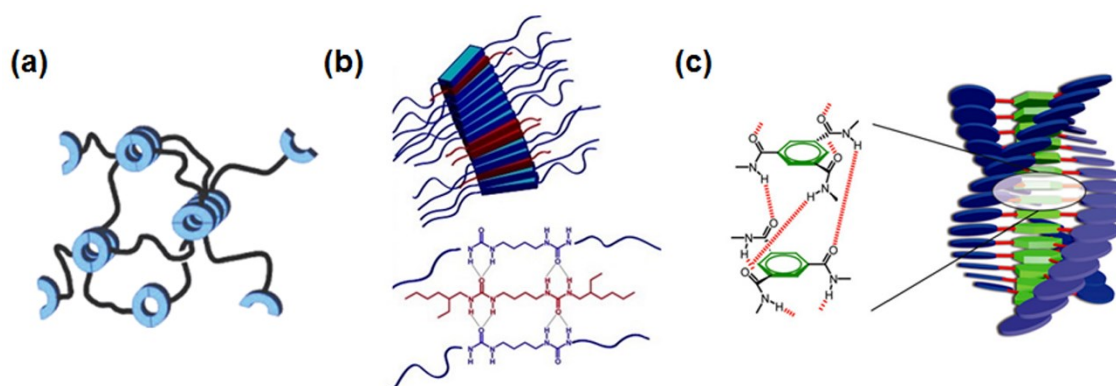
Figure 1.4. Schematic representation of (a) phase segregation in a hydrogen-bonded supramolecular network,[70] (b) supramolecular nanofiller formed via hydrogen bonding between bisureas,[72] (c) a helical architecture assembled by BTA with a combination of hydrogen bonding, π-π interactions, and solvophobic effects.[74] *Image was adapted and compiled from references 70, 72 and 74.*

DNA is one of the most well-known hydrogen bonded systems famous for the "double helix" structure. The 3D conformation of DNA originates from the complementary recognition between appropriate nucleotides via hydrogen bonding, which allows two strands to bind with each other and store information.[75] Helical architecture was also demonstrated by the self-assembly of C_3-symmetrical benzene-

1,3,5-tricarboxamide (BTA), which consisted of a single benzene core and three side chains connected by hydrogen-bonded amides (**Figure 1.4c**).[74] Chiral control of the discotic amphiphiles provided a facile method to regulate the shape and stack length of the columnar aggregates, suggesting great potential in the synthesis of enantiopure medicines.[76]

1.2.2 Hydrogen-Bonded Self-Healing Materials

A variety of self-healing polymers have been developed by incorporating hydrogen-bonding functionalities. In 2007, Leibler and coworkers designed thermo-reversible rubbers consisting of oligomers with multiple hydrogen bonding units.[77] These polymers were obtained using a two-step synthetic route, where fatty acids from renewable resources were condensed with an excess of diethylenetriamine, followed by reactions with urea. It resulted in the formation of a hydrogen-bonded network with a mixture of oligomers containing a large number of different hydrogen bonding residues, as depicted in **Figure 1.5**. When the hydrogen-bonded material was plasticized by dodecane and cut with a razor, it could be autonomously repaired by bringing the fractured surfaces together at room temperature, since the non-associated -C=O groups of amide and the amine-functionalized ends on the fractured surfaces tended to link with each other when brought into contact. Quadruple hydrogen-bonding unit 2-ureido-4[1H]-pyrimidinone (UPy) has become a preeminent motif in supramolecular chemistry since it was introduced by Meijer and coworkers,[78] because it is self-complementary with high dimerization constant and readily accessible in a one-step reaction from inexpensive starting materials. As the dimerization of UPy groups is reversible and highly thermally

responsive,[79] a number of UPy-based healable materials have been reported either by applying a heat trigger or contact pressure trigger.[80] The functional hydrogen-bonding groups can be employed as telechelic ends, chain-extended segments or pendant groups to form diverse supramolecular architectures.[81] The introduction of UPy groups to a series of polymers has led to corresponding thermally healable materials manufactured by Suprapolix, including polysiloxane, polyethers and polyesters.[82] At elevated temperatures, rearrangement of hydrogen-bonding interactions could be achieved due to reduced viscosity of polymers, while autonomous self-healing at room temperature occurred in low T_g materials which showed a higher level of dynamics of the polymer chains.[82] Taking advantage of high segmental mobility of polymer matrix, UPy groups were incorporated as side chains into soft poly(n-butyl acrylate), where dynamic dissociation/dimerization occurred at room temperature with a binding lifetime of about 1.2 seconds.[83]
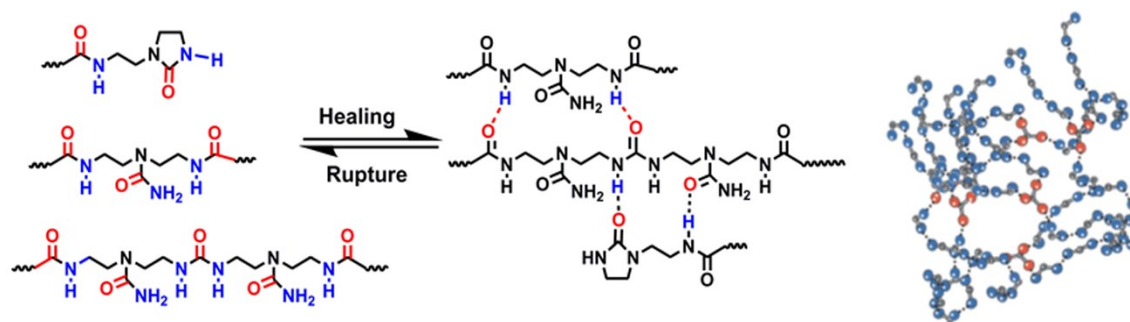
Figure 1.5. The hydrogen-bonded network of a self-healing rubber composed of a mixture of fatty diacids and triacids.[77] *Image was reproduced from reference 77.*

To construct materials with higher modulus, Guan and coworkers produced multiphase supramolecular thermoplastic elastomers with a hydrogen-bonding brush polymer consisting of a polystyrene backbone with polyacrylic amide side chains.[66]

These polymers could self-assemble into a two-phase nanostructure due to the immiscibility of polystyrene and polar side groups. The polystyrene backbones collapsed as discrete "hard" domains, which were connected by "soft" polyacrylic amid pendant chains with multiple hydrogen-bonding sites. The low T_g (~5 °C) of polymer matrix facilitated the regeneration of hydrogen bonds at room temperature with healing efficiency of 92% after 24 hours. Another heterogeneous strategy to achieve self-healing was designed by Hentschel et al. with poly(n-butyl acrylate)-b-polystyrene (PBA-PS) end-functionalized with UPy groups.[84] These multiphase supramolecular polymers retained the hard (PS) /soft (PBA) two-phase morphology with reversible hydrogen-bonding moieties in the soft matrix, which combined stiffness of thermoplastic elastomers with dynamic healing capabilities. This concept can be applicable to a wide range of multi-phase polymers and various types of supramolecular motifs for the design of stiff, strong, and tough self-healing polymers.

Plasticizing reduces the T_g of material and increases the mobility of polymer chains.[77] Hydrogel systems can be viewed as highly plasticized systems with water being the plasticizer and have the potential to show autonomous self-healing at room temperature. A permanently cross-linked hydrogel with self-healing property was developed by arming the hydrogel with acryloyl-6-aminocaproic acid (PA6ACA) side chains, which formed hydrogen bonds across two hydrogel interfaces through the amide and carboxylic functional groups (**Figure 1.6a**).[85] The healing process could be switched on and off by the change of pH due to protonation/deprotonation of carboxyl groups, correlating with association/dissociation of hydrogen bonds. Campo et al. reported a thermally regulated self-healing random copolymer comprising 2-(dimethylamino)-ethyl

methacrylate (DMAEMA) and UPy-based monomers as shown in **Figure 1.6b**, [86] where the reversibility of multivalent UPy groups imparted self-healing ability to the hydrogel. A tough stimuli-responsive supramolecular hydrogel was obtained by incorporating Upy groups into poly(ethylene glycol) (PEG) main chain.[87] As presented in **Figure 1.6c**, the bulk materials contain nanoscopic physical cross-links composed of UPy−UPy dimers. The hydrogen-bonding groups were embedded in segregated hydrophobic domains dispersed within the PEG matrix both in dry state and in water-swollen hydrogel. As UPy groups were shielded by isophorone spacers, they formed strong hydrogen-bonded arrays offering the gel elasticity and recovery of mechanical properties after deformation.
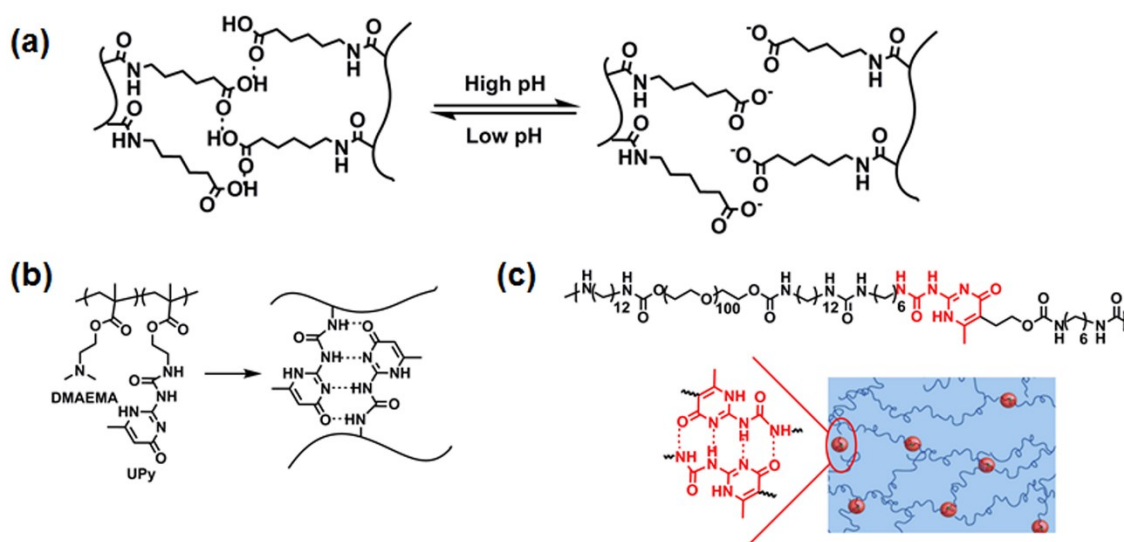
Figure 1.6. Hydrogen-bonded self-healing hydrogels. (a) pH-regulated self-healing mechanism of PA6ACA hydrogel.[85] (b) Chemical structure of poly(DMAEMA-co-UPy) and the dynamic dimerization of UPy moiety.[86] (c) Chemical structural of PEG-UPy chain-extended polymers and illustrative depiction of hydrogel morphology.[87] *Image was reproduced and compiled from references 85, 86 and 87.*

1.2.3 Hydrogen-Bonded Polymers in Aqueous Environment

The polarity of solvent plays a critical role in hydrogen-bonding interactions. When hydrogen-bonding motifs are surrounded by a certain solvent, the intermolecular interactions between solute-solute, solvent-solvent and solute-solvent are schematically depicted in **Figure 1.7**.[88] As a highly polar medium, water can greatly weaken the hydrogen-bonding strength between the bonded units, by providing competitive hydrogen bonds with the dissolved hydrogen-bond donors and acceptors.
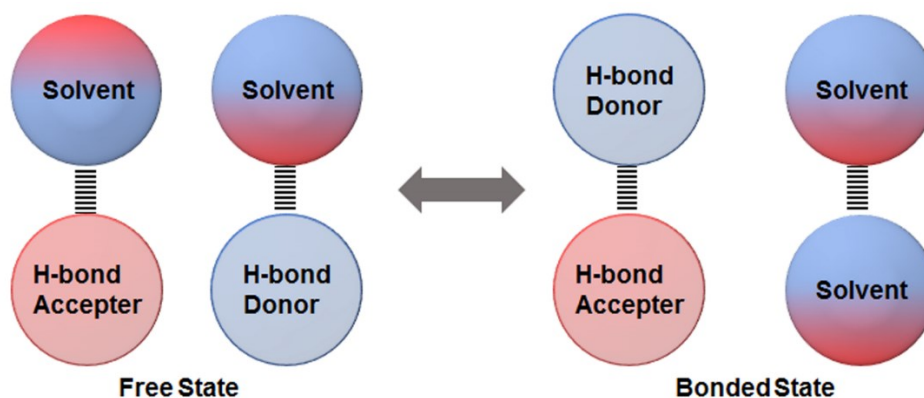
Figure 1.7. Schematic representation of intermolecular interactions of hydrogen-bonding motifs in solution.[88] *Image was reproduced from reference 88.*

A theoretical analysis proposed by Smith et al.[89] indicated that UPy-UPy binding energies could be reduced from 39 kcal/mol in vacuum to 17 kcal/mol in water, suggesting the interaction between N-H of the pyrimidinone ring and water molecules competed with dimerization. Therefore, hydrophobic shielding is generally evolved in the development of stable hydrogen-bonded structures in aqueous environment, either by employing long alkylene spacers,[90] adamantyl substituent[91] or forming micelles.[92] The self-healing kinetics of supramolecular polymers based on fatty acids was investigated

and it turned out that the self-healing reactions were dependent on external conditions.[93,94] Upon exposure to heat or moisture, the healing ability of freshly cut surfaces was diminished by new equilibrium resulting from redistribution of free hydrogen-bonding motifs. It is worth pointing out that water in the rubber not only acted as a plasticizer, which could increase the mobility of polymer network, but also interacted with hydrogen-bonding groups and changed the hydrogen bond structure. Adhesion mechanisms of UPy-modified poly(n-butyl acrylate) thin films was studied under humidity by surface forces apparatus (SFA).[95] With increasing relative humidity, water molecules interacted with free UPy functional groups on the surface as well as diffused into the bulk of the polymer, changing both the surface energy and viscosity of polymer films. The increased density of free UPy groups on the surface led to an enhanced adhesion between the polymer films.

1.3 Single-Molecule Force Spectroscopy(SMFS) of Supramolecular Interactions

1.3.1 Principle of Atomic Force Microscopy (AFM)-Based SMFS

Since the self-assembled structures and macroscopic properties of supramolecular polymers are highly dependant on the molecular interactions of binding motifs, the fundamental understanding of the binding strength and dynamics of the supramolecular interactions can pave the way for the design of desirable supramolecular architectures and bulk materials. With the development of precise experimental tools, single molecule techniques, which allow the direct detection of mechanical forces at molecular level, have drawn enormous attention to investigating diverse intramolecular and intermolecular interactions.[96] Among the most commonly used tools including cantilevers, microneedles, optical tweezers, and magnetic beads, AFM-based SMFS becomes predominant because

it provides a combination of high-resolution imaging with force spectroscopy, and is suitable to detect highly dynamic process (>10 μs).[97]

AFM was first introduced as an imaging tool in 1986, where the spatial resolution is determined by a piezoelectric transducer and the force signal is reflected by the cantilever defection monitored by a laser beam.[98] The principle of AFM-based SMFS is illustrated in **Figure 1.8**.[96,99,100] For the investigation of supramolecular interactions between two bonded units, generally speaking, both the AFM tip and the substrate are functionalized with one of the moieties, respectively, via either chemical or physical adsorption with a flexible polymer linker. During a typical force measurement cycle, the cantilever far away from the substrate (position 1) starts to approach towards the surface, and when the tip is in contact with the functionalized substrate, specific interactions can form between the binding groups (position 2). Usually a certain force is applied to facilitate the interaction between the tip and the surface, resulting in a repulsive signal. Upon separation, the polymer linker tends to be stretched, along with bending of the cantilever (position 3 and 4). At a certain position, the applied force reaches to the dissociation force of the weakest bond of the structure, leading to bond rupture and a sudden drop of the force-distance curve (position 5). The region showing increasing attractive force is related to the characteristics of the stretched polymer, while the maximum force is referred to as "rupture force" and employed for the investigation of molecular interactions.[101,102]
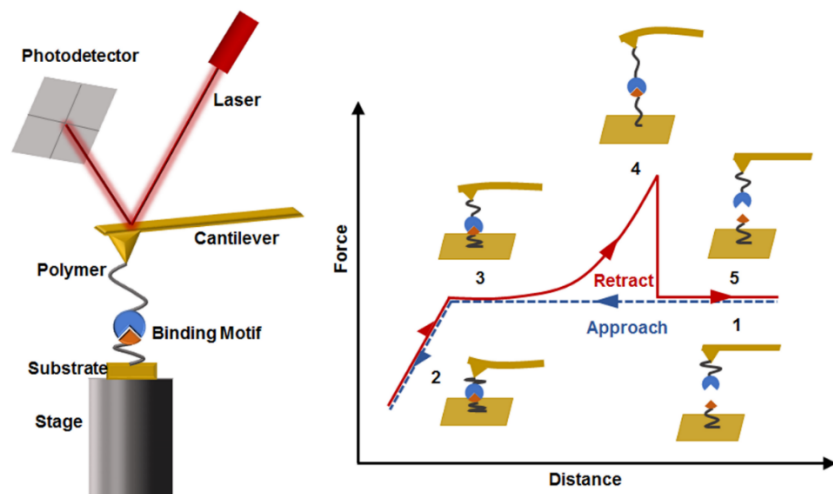
Figure 1.8. Schematic illustration of the experimental setup and representative force-distance curve of AFM-based SMFS.

1.3.2 Single Polymer Chain Stretching

Nanomechanical information of polymers and intramolecular interactions have been extensively studied by stretching a single polymer chain. When a flexible polymer chain with a random-coil conformation is stretched, the system will deviate from Brownian molecular motion due to the energy input by the applied force. At low force regime, the number of molecular conformation is reduced and the loss of entropy dominate the process, while high forces can generate deformation and stretching of bonds in molecular backbone, giving rise to enthalpic elasticity.[96,103] The interpretation of force-distance profiles obtained from SMFS measurements is based on the consideration of entropic contribution, and predominantly described by two statistical mechanical models, i.e., the freely jointed chain (FJC) model and the worm-like chain (WLC) model, [104-106] as displayed in **Figure 1.9**.
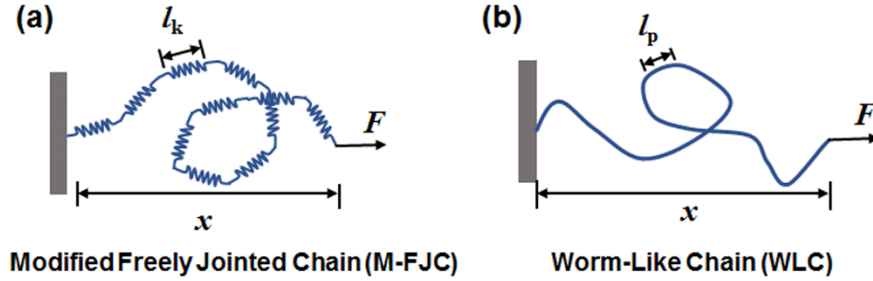
Figure 1.9. Schematic representation of modified freely jointed chain (M-FJC) model and worm-like chain (WLC) model.

In the FJC model, the polymer chain is treated as an aggregate consisting of N rigid Kuhn segments with an equal Kuhn length (l_k), which are connected via flexible joints. Upon extension, the segments tend to align along the direction of external force, and the extension of polymer chain x correlates with the applied force F by:

$$x = L_c \left[\coth\left(\frac{F \cdot l_k}{k_B T} - \frac{k_B T}{F \cdot l_k}\right) \right] \qquad (1.1)$$

where L_c, k_B and T represent contour length, segment elasticity, Boltzmann constant and temperature, respectively.[107] However, FJC model fails at high force regime, where enthalpic contribution is nonnegligible, and it can be modified by taking the elasticity of bonds into account. Therefore, the segment elasticity K_s has been introduced to each Kuhn segment by Bustamante and coworkers to optimize the FJC model, leading to a modified freely jointed chain (M-FJC) model with better fitting quality.[108]

$$x = L_c \left[\coth\left(\frac{F \cdot l_k}{k_B T} - \frac{k_B T}{F \cdot l_k}\right) \right] + N \cdot \frac{F}{K_s} \qquad (1.2)$$

In the WLC model, the polymer coil exhibits a continuous conformation and is regarded as a homogenous string with a persistence length l_p, a contour length L_c and a

constant elasticity. The relationship between force and chain extension can be expressed

as

$$F = \frac{k_B T}{l_p} [\frac{1}{4}(1-\frac{x}{L_c})^{-2} + \frac{x}{L_c} - \frac{1}{4}] \qquad (1.3)$$

This model combines both entropic and enthalpic contributions, and is commonly

employed to reproduce the force-extension profiles of various biological molecules.[109,110]

1.3.3 Molecular Interactions

Specific interactions originated from molecular recognition is characterized by the

rupture force probed during stretching. As shown in **Figure 1.10**, when an reversible

interaction between A and B groups is in equilibrium, the energy barrier of the

complexation ($\Delta G_{(0)}$) is defined as the energy difference between the free state and the

bound state, while the binding affinity is determined by the ratio of kinetic on-rate

constant k_{on} and off-rate constant k_{off}. When a force is applied on AB complex, the

system deviates from equilibrium, along with a reduced binding barrier $\Delta G_{(F)}$ and an

increased k_{off}.[111,112]

$$\Delta G_{(F)} = \Delta G_{(0)} - F \cdot x_B \qquad (1.4)$$

$$k_{off(F)} = k_{off(0)} \cdot e^{\frac{F \cdot x_B}{k_B T}} \qquad (1.5)$$

x_B represents the dissociation distance of the specific bond. During SMFS measurement,

the applied force is loading rate (R_f)-dependant, and according to Bell-Evans theory,[113,114]

the most probable rupture force (F_R) can be expressed by the following equation:

$$F_R = \frac{k_B T}{x_B} \ln(\frac{R_f \cdot x_B}{k_B T \cdot k_{off}}) \qquad (1.6)$$

Both x_B and k_{off} are obtained by conducting linear fitting on F_R versus $\ln R_f$, providing dynamic information of the interaction, and the binding energy is calculated by:

$$\Delta G = -k_B T \left(\frac{k_{off}}{k_{on}}\right) \qquad (1.7)$$
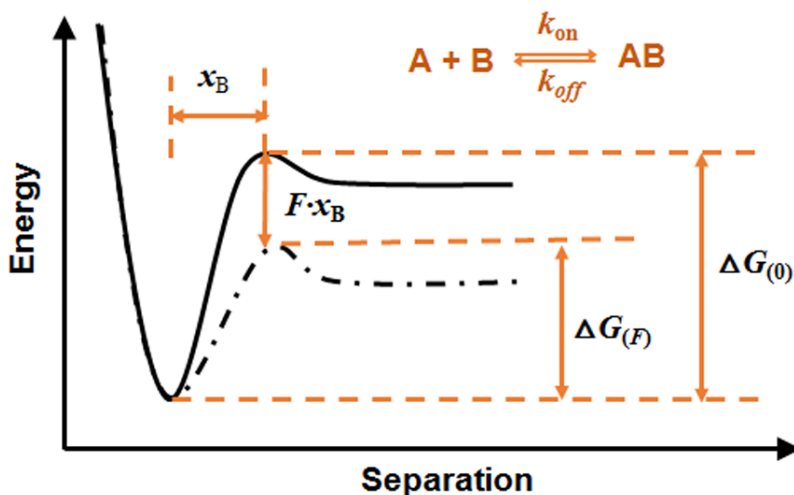
Figure 1.10. Schematic representation of the energy profile of AB complexation upon an applied force.

1.4 Objectives

The development of advanced multifunctional materials is becoming one of the most exciting and emerging areas of scientific interest. Combining stimuli-responsive properties with self-healing ability into engineered polymers will lead to a diverse range of applications, where supramolecular chemistry, especially hydrogen-bonding interaction, provides a promising approach. Up to now, extensive efforts have been devoted to the design of hydrogen-bonded functional materials; however, it still remains a challenge to achieve satisfying multifunctionalities, such as excellent mechanical

properties, sensitive response to external stimuli and rapid healing ability, in one platform. Besides, the understanding of the interaction mechanism between hydrogen-bonding motifs is limited from the molecular perspective, which is of great significance to direct self-assembled pathways and desired hydrogen-bonded structures.

The overall goal of this project is to develop multifunctional supramolecular polymers, including colloidal systems and bulk materials, based on multiple hydrogen-bonding UPy groups toward engineering and biomedical applications, and elucidate the interaction mechanism of the hydrogen-bonding motifs at the single-molecule level. The detailed objectives are listed as follows.

(1) Develop thermo-responsive micelles from double hydrophilic block copolymers (DHBCs), using UPy groups as core cross-linkers to form stable micelles with tunable thermo-responsiveness.

(2) Fabricate a multifunctional polypyrrole (PPy)-doped conductive polymer composite from hydrogen-bonded elastomer via solution casting method, which integrates highly stretchable, fast self-healing, adhesive and sensing abilities.

(3) Fabricate a novel type of multifunctional conductive polymer hydrogel that combines high conductivity with excellent mechanical properties (i.e., stretchability, injectability and self-healing ability), by incorporating UPy motifs into a conducting polymer network.

(4) Quantitatively characterize the pairwise interactions between hydrogen-bonded UPy dimers in water using AFM-based SMFS, and study the effects of hydrophobic interactions on the intermolecular hydrogen bonding.

1.5 Thesis Outline

Chapter 1 gives an overview of supramolecular materials and their properties, followed by a literature review on hydrogen-bonded supramolecular polymers and a brief introduction of AFM-based SMFS technique. The objectives of this work are presented.

Chapter 2 presents the synthesis and characterization of the thermo-responsive core cross-linked DHBC micelles. UPy-containing DHBCs were synthesized via reversible addition-fragmentation chain transfer (RAFT) polymerization with UPy-modified methacrylate monomers and N-isopropylacrylamide (NIPAm), using poly(ethylene glycol) (PEG) as a macro-initiator. In the developed copolymer PEG-b-P(NIPAm-co-UPy), the dimerization of incorporated UPy groups acts as core cross-linking sites and leads to a noncovalent network formed by hydrogen-bonding interactions. The temperature-induced swelling and shrinking of the self-assembled micelles were investigated, and the controlled drug delivery performance was demonstrated.

Chapter 3 introduces a facile solution casting method for the fabrication of a multifunctional conductive composite, by triggering the in situ polymerization of pyrrole within a UPy-functionalized elastomer matrix. Taking advantage of the hydrogen-bonded supramolecular polymer matrix, the prepared composite could be stretched over 400% with a complete and repeatable self-healing ability within 5 min after damage. Moreover, the composite has been demonstrated to display strong adhesiveness to various substrates including glass, metal and organic materials. The strain sensor fabricated from the composite possesses high sensitivity to successfully detect both large and subtle human motions including finger bending and pulse beating.

Chapter 4 reports the preparation of a stretchable, injectable and self-healing conductive hydrogel, which incorporates UPy cross-linking sites into a fragile conducting polyaniline/poly(4-styrenesulfonate) (PANI/PSS) network. Due to the dynamic and reversible dissociation/association process of the hydrogen bonds, the prepared composite can be readily stretched and injected from a needle, as well as display a rapid self-healing ability within 30 s upon damage. The electronic conduction assisted by ionic transport renders the hydrogel a superior conductivity of 13 S/m and a high sensitivity to external strain, which has been applied to monitor diverse human activities, including large motions of human body (e.g., finger and wrist bending) and subtle movements of muscles (e.g., swallowing, speaking, pulse beating).

Chapter 5 presents the characterization of the kinetic parameters and nanomechanical strength of a single UPy dimer in water with a combination of SMFS and molecular dynamics simulations, and the effect of hydrophobic interactions on the intermolecular hydrogen bonding was also investigated. It reveals that although the dimerization of UPy was disrupted by water to some extent, the binding strength could be remarkably enhanced by attaching longer hydrophobic spacers adjacent to the hydrogen-bonding moieties.

Chapter 6 outlines the major conclusions and contributions of this work, with suggestions for future research directions.

CHAPTER 2 Core Cross-Linked Double Hydrophilic Block Copolymer Micelles Based on Multiple Hydrogen-Bonding Interactions

2.1 Introduction

Polymeric micelles with typical core-shell morphology in aqueous media have found significant applications in diverse biomedical and engineering fields such as drug delivery,[115-117] diagnostic imaging,[118,119] sensing[120,121] and catalysis.[122] In recent years, double hydrophilic block copolymers (DHBCs) have attracted considerable attention,[123-125] in which water solubility of one or both blocks can be easily tuned by appropriate stimuli such as temperature, pH, and ionic strength.[126-129] The resultant stimuli-responsive micelles are explored as intelligent drug carriers[130-133] and catalysts.[134] However, the structural stabilization of DHBC micelles has become a main challenge for practical applications, since the dynamic nature of the micelles may lead to micelle-to-unimer transition after dilution or under certain solvent conditions. A variety of strategies have been developed to address this problem, and core cross-linking is one of the most effective approaches to maintain the structural integrity as well as stimuli-responsiveness of the micelles.[135-137] Compared to conventional covalent cross-linking which may reduce the biodegradability of micelles,[138] non-covalent cross-linking methods are able to not only reinforce the micelles but also render them with additional intelligence.[139,140] Diverse non-covalent interactions have been employed to build core cross-linked micelles, including strong hydrophobic interactions,[141] electrostatic interactions,[142,143] host-guest interactions,[144] metal-ligand coordination,[145,146] and hydrogen-bonding.[147-149]

Inspired by biological systems (e.g., double-helical DNA and protein β-sheets),[150] complementary multiple hydrogen bonds have become one of the most developed approaches to generate supramolecular polymers due to their versatility, directionality and biocompatibility.[2,151-154] Several hydrogen-bonding arrays have been successfully developed to direct the self-assembly of block copolymers and stabilize the cores of micelles.[155-157] For example, diblock copolymers poly(ethylene glycol)-b-poly(ethyl-co-urea carbonate) (PEG-P(E_{1-x}-U_x)C) were synthesized with the incorporation of urea-functional groups, and the hydrogen-bonding interactions between urea functionality enhanced the stability of the micelles as well as drug loading ability.[147] Kuang et al. prepared core cross-linked micelles from nucleobases-modified amphiphilic block copolymers, where the hydrogen bonds between adenine (A) and thymine (T) served as cross-linking sites to stabilize the micellar structures for controlled drug release.[149] Similarly, Fan et al. developed novel pH-responsive nanocarriers from polyacrylate block copolymers containing adenine (A) moieties, which formed multiple hydrogen bonds with the addition of uracil (U)-containing cross-linkers.[148] However, the reported weak hydrogen-bonding interactions only exist within a hydrophobic microenvironment and can be easily destroyed when exposed to water,[158] which is not desirable for fabrication of stable micelles. 2-ureido-4[1H]-pyrimidinone (UPy) units can undergo strong dimerization via quadruple hydrogen bonds (dimerization constant $>10^6$ M^{-1} in chloroform),[95,159,160] and possess high association constant in aqueous solutions.[89] UPy moieties have been successfully incorporated into water-soluble poly(ethylene glycol) (PEG) to form hydrogels via non-covalent hydrogen-bonding interactions.[48,87,161] Recently, the fabrication of hydrogen-bonded micelles and vesicles from compounds

with UPy and tris(tetraethylene glycol monomethyl ether) moieties was reported, and the stability of the assemblies were attributed to the dimerization of UPy groups.[162] In addition, Chen et al. prepared colloidal nanogels from UPy functionalized poly(N-isopropylacrylamide) (PNIPAm), and the interactions of the multiple hydrogen-bonding groups were demonstrated to be strong enough to preserve the integrity of hydrogel particles over a wide temperature range.[163]

Herein, we report a facile fabrication of core cross-linked micelles from thermo-responsive DHBCs by incorporating self-complementary multiple hydrogen-bonding groups. In this work, UPy-containing DHBCs were synthesized via reversible addition-fragmentation chain transfer (RAFT) polymerization with UPy-modified 2-hydroxyethyl methacrylate (HEMA) monomer and N-isopropylacrylamide (NIPAm), using poly(ethylene glycol) (PEG) as a macroinitiator. The schematic illustration for the formation of micelles is shown in **Figure 2.1**. It is well known that PNIPAm homopolymer is thermo-sensitive with lower critical solution temperature (LCST) of about 32 °C in water,[164] and PEG-b-PNIPAm diblock copolymers can undergo reversible unimers-micelle transition with the change of temperature.[165] In the developed copolymer PEG-b-P(NIPAm-co-UPy), the dimerization of incorporated UPy groups act as core cross-linking sites and lead to a non-covalent network formed by hydrogen-bonding interactions. The effects of hydrogen bonds on the stability of the self-assembled micelles were investigated as a function of temperature. To the best of our knowledge, this work represents the first report on the preparation and characterization of core cross-linked micelles via strong hydrogen-bonding interactions based on a well-defined thermo-responsive DHBC.
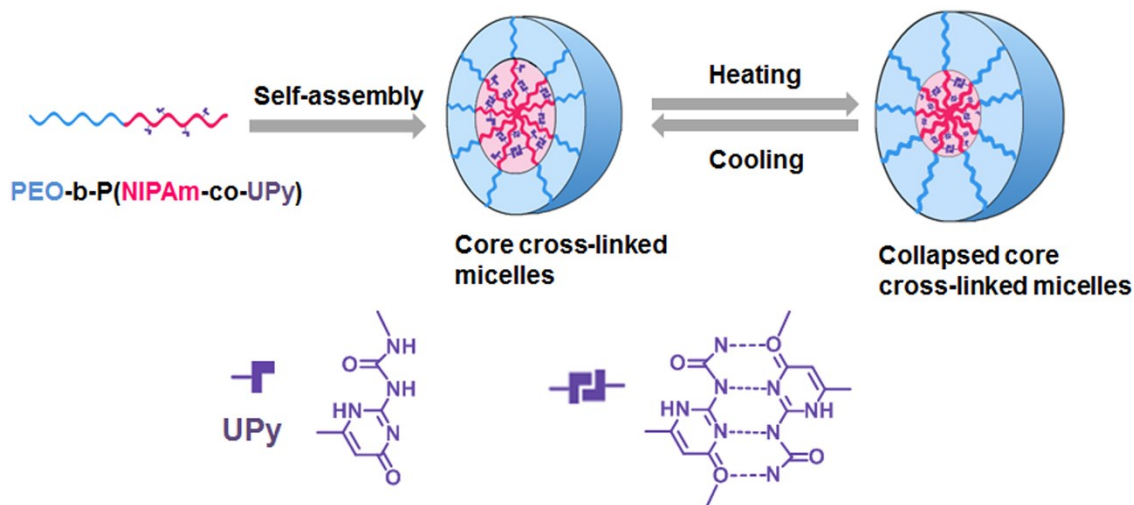
Figure 2.1. Schematic illustration of the fabrication of core cross-linked micelles with thermo-responsive cores from UPy-containing DHBCs PEG-b-P(NIPAm-co-UPy) through hydrogen-bonding interactions of UPy groups.

2.2 Experimental Methods

2.2.1 Materials

2-Amino-4-hydroxy-6-methylpyrimidine (98%, Aldrich), hexamethylene diisocyanate (98%, Fluka), dibutyltin dilaurate (95%, Aldrich), 2,2′-Azobis(2-methylpropionitrile) (AIBN, 98%, Aldrich), dimethyl sulfoxide (DMSO, anhydrous, 99.9%, Aldrich), N,N-dimethylformamide (DMF, 99%, Aldrich) were used as received. 2-Hydroxyethyl methacrylate (HEMA, 97%, Aldrich) was destabilized by passing it over a column of aluminum oxide. N-isopropylacrylamide (NIPAm, 97%, Aldrich) was purified by recrystallization from n-hexane. Chloroform ($CHCl_3$) was dried over calcium hydride (CaH_2) and distilled before use. All other reagents and solvents were used as obtained.

2.2.2 Synthesis

2-(6-isocyanatohexylaminocarbonylamino)-6-methyl-4[1H]-pyrimidinone (OCN-UPy). OCN-UPy was prepared according to the literature procedures.[166] A mixture of 2-amino-4-hydroxy-6-methylpyrimidine (5.00 g, 0.04 mol) in hexamethylene diisocyanate (40.32 g, 0.24 mol) was stirred at 100 °C under N_2 atmosphere for 24 h. 50 mL pentane was added in the flask after reaction and the resulting precipitate was filtered and washed with excess pentane for 3 times. The white powder was then dried under vacuum. ^{1}H NMR (CDCl$_3$, 400 MHz): δ_H (ppm)= 13.1 (s, 1H, CH$_3$CN$\underline{H}$), 11.9 (s, 1H, CH$_2$N$\underline{H}$(C=O)NH), 10.2 (s, 1H, CH$_2$N$\underline{H}$(C=O)NH), 5.8 (s, 1H, C$\underline{H}$=CCH$_3$), 3.3 (m, 4H, NH(C=O)NHC$\underline{H}_2$ + C$\underline{H}_2$NCO), 2.2 (s, 3H, C$\underline{H}_3$C=CH), 1.6 (m, 4H, NCH$_2$C$\underline{H}_2$), 1.4 (m, 4H, CH$_2$CH$_2$C$\underline{H}_2$CH$_2$CH$_2$).

UPy-containing methacrylate monomer (HEMA-UPy). Freshly distilled HEMA (1.30 g, 0.01 mol) was dissolved in chloroform (100 mL), and then OCN-UPy (5.86 g, 0.02 mol) was added to the solution. After the addition of 2 drops of dibutyltin dilaurate as catalyst, the mixture was stirred at 60 °C for 20 h. With completion of the reaction, another 100 mL of chloroform was added and the suspension was filtered to remove the solids. After concentrating the filtrate back to 100 mL by rotation evaporation, 5 g silica and 2 drops of dibutyltin dilaurate were added, and the mixture was heated at 60 °C for 1 h. The silica was removed by filtration and the chloroform in resulting solution was removed in vacuo. The obtained monomer was stored at 5 °C prior to use. ^{1}H NMR (CDCl$_3$, 400 MHz): δ_H (ppm)= 13.1 (s, 1H, CH$_3$CN$\underline{H}$), 12.0 (s, 1H, CH$_2$NH(C=O)N$\underline{H}$), 10.5 (s, 1H, CH$_2$N$\underline{H}$(C=O)NH), 6.1+5.6 (s, 2H, C=C$\underline{H}_2$), 5.8 (s, 1H, C$\underline{H}$=CCH$_3$), 4.9 (s, 1H, N$\underline{H}$(C=O)O), 4.3 (m, 4H, C$\underline{H}_2$O(C=O)), 3.3-3.2 (m, 4H, NH(C=O)NHC$\underline{H}_2$ +

CH$_2$NH(C=O)O), 2.2 (s, 3H, CH$_3$C=CH), 1.9 (s, 3H, (C=O)CCH$_3$), 1.7-1.2 (m, 8H, CH$_2$CH$_2$CH$_2$).

Block copolymer PEG-b-P(NIPAm-co-UPy). Poly (ethylene glycol)-based macro-RAFT agent PEG$_{113}$-CTA was synthesized by attaching the chain transfer agent 2-(dodecylthiocarbonothioylthio)-2-methylpropionic acid to the hydroxyl end group of poly(ethylene glycol) methyl ether (PEG$_{113}$-OH, Mn=5000).[167] Typical procedures employed for the RAFT synthesis of PEG-b-P(NIPAm-co-UPy) copolymer are as follows. A representative example of the copolymerization of 10 mol% UPy-HEMA with respect of NIPAm is given. The PEG$_{113}$-CTA macroinitiator (178 mg, 0.033 mmol), NIPAm (339 mg, 3 mmol), HEMA-UPy monomer (128 mg, 0.3 mmol) and AIBN (1.3 mg, 0.008 mmol) were dissolved in 10 mL DMSO. After being purged with continuous N$_2$ for 20 min, the mixture was stirred at 70 °C for 22 h. The solution was added dropwise into 300 mL diethyl ether and the precipitate was collected by filtration. Then the polymer was dried under vacuum overnight. For comparison, diblock copolymer PEG-b-P(NIPAm-co-HEMA) was also prepared by following the same route using 2-hydroxyethyl methacrylate instead of HEMA-UPy as comonomers.

2.2.3 Preparation of the Core Cross-Linked Micelles

To prepare the micellar aggregates, PEG-b-P(NIPAm-co-UPy) solutions were prepared by dissolving the DHBCs in DMF at a concentration of 5 mg/mL. Then, 5mL Milli-Q water was added into 5 mL of the stirred polymer solution via syringe pump at a rate of 12.5 μL/min, in order to induce the formation of micelles. Then 40 mL Milli-Q water was added quickly into the suspensions to quench the micellar structures. The

residual DMF was removed from the suspensions by dialyzing the resulting solutions against water for 3 days. The solutions were stored at 5 °C for further characterization.

2.2.4 Characterization of the Prepared Micelles

Nuclear magnetic resonance (NMR) Spectroscopy. All ^{1}H NMR spectra were recorded on an Agilent DD2 400 MHz spectrometer using deuterated chloroform (CDCl$_3$) as solvent. The testing temperature was 25 °C.

Dynamic light scattering (DLS). Zetasizer Nano ZSP (Malvern Instruments, UK) was used to measure the average particle sizes and size distributions of the micelles at different temperatures between 5~40 °C. The micelle solutions at a concentration of 0.3 mg/mL were passed through 0.45 μm pore size filters, and all samples were equilibrated at the desired temperature for 10 min prior to measurements.

Atomic force microscopy (AFM). Morphology and size distributions of the polymer micelles were determined by AFM imaging using a Bruker ICON AFM system (Bruker, Santa Barbara, CA) operated in ScanAsyst mode. The topological images were obtained under ambient conditions in air with Bruker ScanAsyst-Air probes (silicon nitride cantilever, spring constant=0.4 N/m). Samples for AFM imaging were prepared by depositing one drop of the micelle solutions (0.3 mg/mL) onto cleaned silica substrates, and the solvent was allowed to evaporate freely in air at 5 °C.

Fluorescence measurements. Low critical solution temperatures (LCSTs) of the diblock copolymers in water were determined by steady-state fluorescence measurements using pyrene as a probe. A typical fluorescence spectrum of pyrene in fluids exhibits five vibrational peaks, and the intensities of the first (I_1 at 373 nm) and third (I_3 at 384 nm) peaks are sensitive to the polarity of the probing microenvironment. The ratio of I_1/I_3 is

about 1.9 in water and drops to about 1.2 when pyrene molecules are solubilized in hydrophobic domains.[168] The conformation change of the polymers can be obtained from the measurement of the change in I_1/I_3 as a function of temperature. To obtain sample solutions, 0.2 mL solution of pyrene in methanol (6×10^{-3} mg/mL) was added to a serious of volumetric flasks and the methanol was evaporated. 10 mL micelle solutions (0.3 mg/mL) were added to each flask giving the pyrene concentration in the final solutions of 6×10^{-7} M. The samples were stirred and equilibrated for 24 h at room temperature prior to measurements. Fluorescence spectra were recorded on a Varian Cary Eclipse spectrometer (Varian Inc., USA). The sample temperature was controlled by a circulating water bath between 10~40 °C. The excitation and emission slit widths were set at 10 and 5 nm, respectively. The excitation wavelength was 335 nm and fluorescence emission spectra were recorded within 350~550 nm.

2.3 Results and Discussion

2.3.1 Preparation of PEG-b-P(NIPAm-co-UPy) Double Hydrophilic Block Copolymers

The diblock copolymer PEG-b-P(NIPAm-co-UPy) was synthesized by RAFT copolymerization using PEG-based chain transfer agent (PEG$_{113}$-CTA) with the presence of NIPAm and varying amounts of HEMA-UPy comonomers. The detailed synthesis route is illustrated in **Figure 2.2**. A series of polymerization reactions were carried out and the obtained block copolymers are named as BC-Ux, where x indicates the molar percentages of UPy-containing monomer with respect to NIPAm in the feed. To investigate the effect of UPy groups on the formation of micelles, a reference polymer with 10 mol% HEMA as comonomers instead of UPy moieties was prepared (BC-U0).
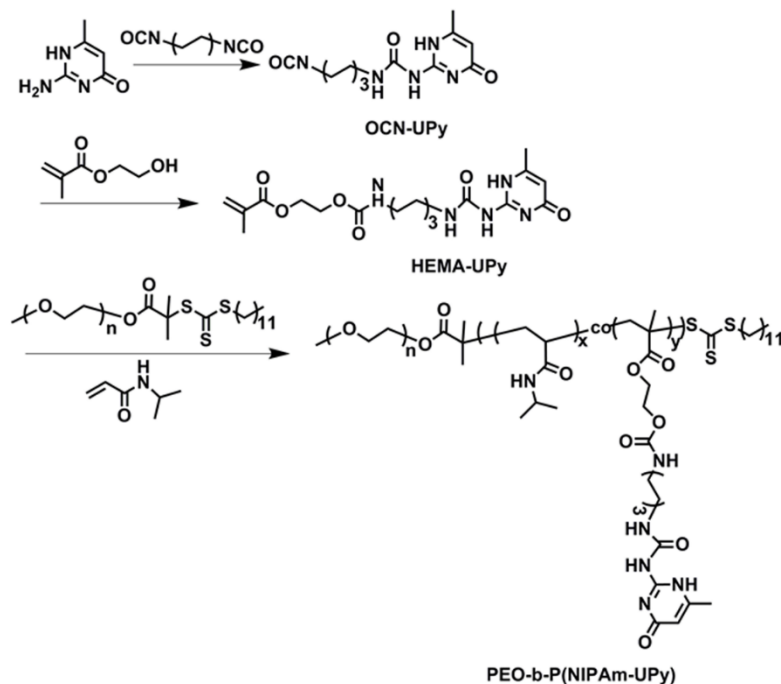
Figure 2.2. Synthesis route of diblock copolymer PEG-b-P(NIPAm-co-UPy).

^{1}H NMR was employed to characterize the structure of the diblock copolymers. **Figure 2.3a** shows the characteristic peaks of PEG-b-P(NIPAm-co-HEMA) in CDCl$_3$. Besides signal attributed to methylene protons of PEG block at 3.6 ppm (a), the spectrum also reveals the presence of characteristic signals of NIPAm residues at 5.9-7.0 ppm (b), 4.0 ppm (c), and 1.1 ppm (d),[135] and HEMA residues at 4.2 ppm (e), and 3.8 ppm (f),[169] suggesting the coexistence of these moieties. The ^{1}H NMR spectrum of the UPy functionalized polymer BC-U6 in CDCl$_3$ is shown in **Figure 2.3b**. Besides protons characteristic of PEG and NIPAm residues, we can clearly see the signals at 13.1 ppm (h), 12.0 ppm (i), and 10.5 ppm (j) by enlarging the spectrum signal in the range from 15.0 ppm to 9.0 ppm, which are ascribed to the urea NH protons of UPy groups and consistent with the previous researches by Meijer et al.[87,160,170] The characteristic chemical shifts of UPy group did not change during polymerization (**Figure S2.1** in

Appendix A). Comparing the integral values of PEG_{113} block to the ones for the characteristic peaks of NIPAm, HEMA and ureidopyrimidinone groups, the actual degrees of polymerization (DPs) of NIPAm, HEMA and HEMA-UPy in the prepared block polymers were calculated and summarized in **Table 2.1**.
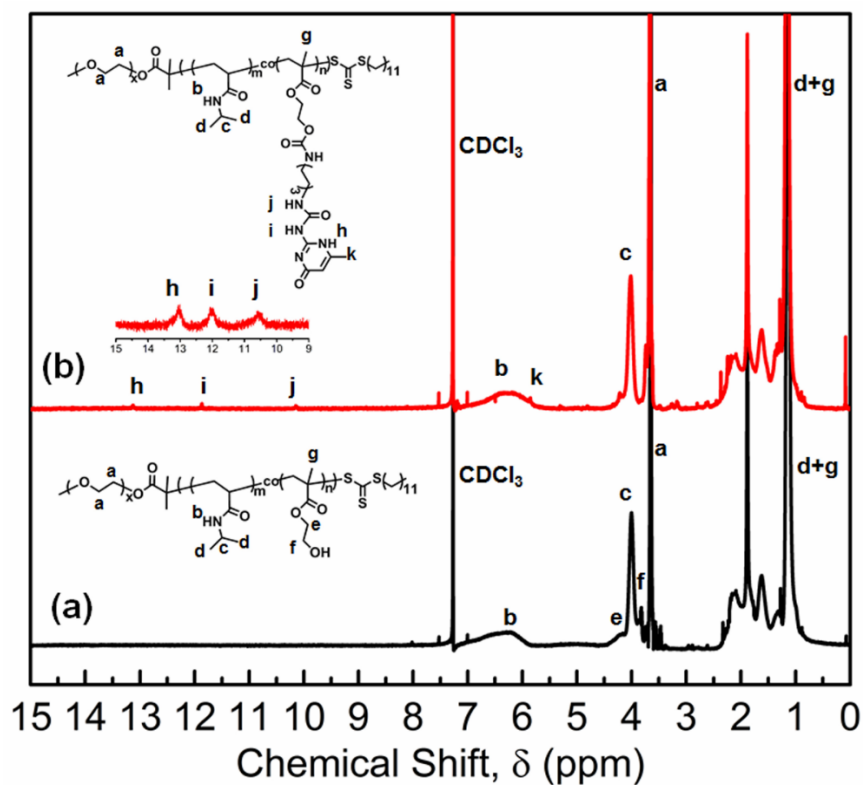
Figure 2.3. ^{1}H NMR spectra of (a) PEG-b-P(NIPAm-co-HEMA) (BC-U0) and (b) PEG-b-P(NIPAm-co-UPy) (BC-U6) diblock copolymers in CDCl₃.

Table 2.1. Characteristics of synthesized block copolymers determined by ^{1}H NMR.

Sample	Polymer	DP	UPy fraction (mol%)		Mn (g/mol)
			Feed	**Product**	
BC-U0	PEG113-b-P(NIPAm$_{84}$-co-HEMA$_7$)	91	0	0	15,767
BC-U3	PEG113-b-P(NIPAm$_{82}$-co-UPy$_2$)	84	3	2.4	15,477
BC-U6	PEG113-b-P(NIPAm$_{74}$-co-UPy$_4$)	78	6	5.4	15,419
BC-U10	PEG113-b-P(NIPAm$_{70}$-co-UPy$_6$)	76	10	8.6	15,813

2.3.2 Formation of Core Cross-Linked DHBC Micelles

As the obtained DHBCs were not soluble in water, the copolymers were initially dissolved as unimers in DMF and self-assembled into micelles via nanoprecipitation as presented in **Figure 2.1**.[171] To avoid large aggregates formed by direct dialysis,[172] mono-dispersed micelles were induced with the slow addition of water, where PNIPAm blocks could progressively associate into cores of micelles.[173] From the dynamic light scattering (DLS) data measured by Zetasizer, all of the polymers could form micelles exhibiting narrow size distributions at 40 °C due to the aggregation of hydrophobic PNIPAm chains. With increasing the amount of UPy groups, the micelles assembled from BC-U0, BC-U3, BC-U6 and BC-U10 showed average hydrodynamic diameters of 49.6, 44.3, 40.4, and 37.9 nm, respectively (**Figure S2.2** in **Appendix A**). Upon cooling to 5 °C, the PNIPAm blocks became soluble in water and the hydrogen-bonding groups were exposed to a hydrophilic environment. **Figure 2.4** illustrates the intensity-average hydrodynamic

diameter (D_H) distributions for aqueous solutions of polymers with different functional groups at 5 °C. Without the presence of UPy groups, the HEMA-containing polymer BC-U0 shows an average D_H about 10 nm, which indicates that the polymer chains directly dissolve in water as random coils because of the lack of strong core cross-links. The broad size distribution reveals that some loose aggregates are probably formed due to the association of HEMA moieties. With incorporation of a low content of UPy groups, BC-U3 assembled into aggregates with a very broad hydrodynamic diameter distribution from 10 to 400 nm, which indicates that quadruple hydrogen-bonding groups of different molecules interact with each other and the polymer chains are only partially dissolved in water. With increasing UPy functionality, the higher cross-link density leads to a stronger network formed among PNIPAm blocks, and stable core cross-linked micelles with relatively narrow size distributions could be obtained from BC-U6 and BC-U10. The average D_H of the micelles were determined to be 49.7 nm and 40.2 nm, respectively.
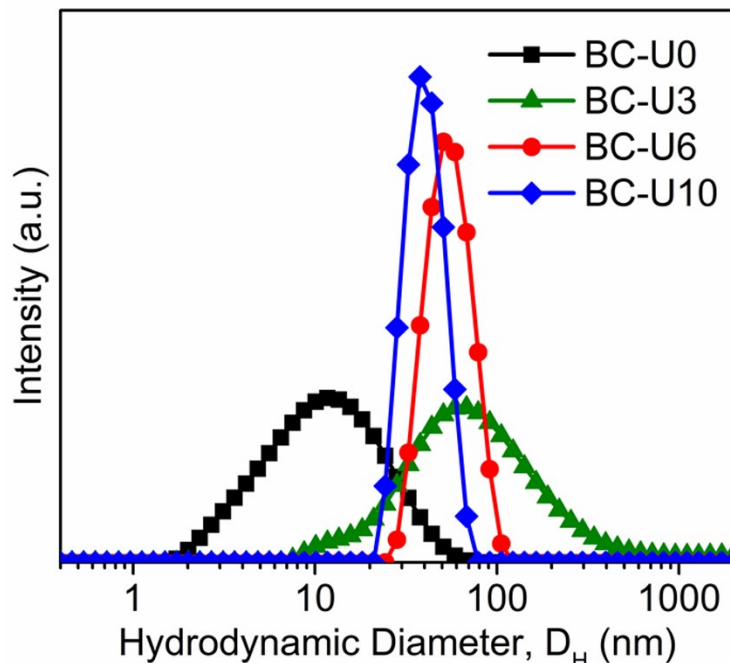
Figure 2.4. Hydrodynamic diameter distributions obtained from aqueous solutions of synthesized polymers BC-U0, BC-U3, BC-U6 and BC-U10 at 5 °C.

The morphology and the sizes of the polymer aggregates were also investigated by AFM in the dry state with samples prepared at 5 °C. As displayed in **Figure 2.5**, the surface of BC-U0 is relatively smooth with root-mean-square (RMS) roughness of ~1.6 nm, where no micellar structures could be detected. However, with the presence of quadruple hydrogen-bonding groups, BC-U3 is able to assemble into aggregates with sizes in a wide range, and the RMS roughness of the surface is 4.01 nm.
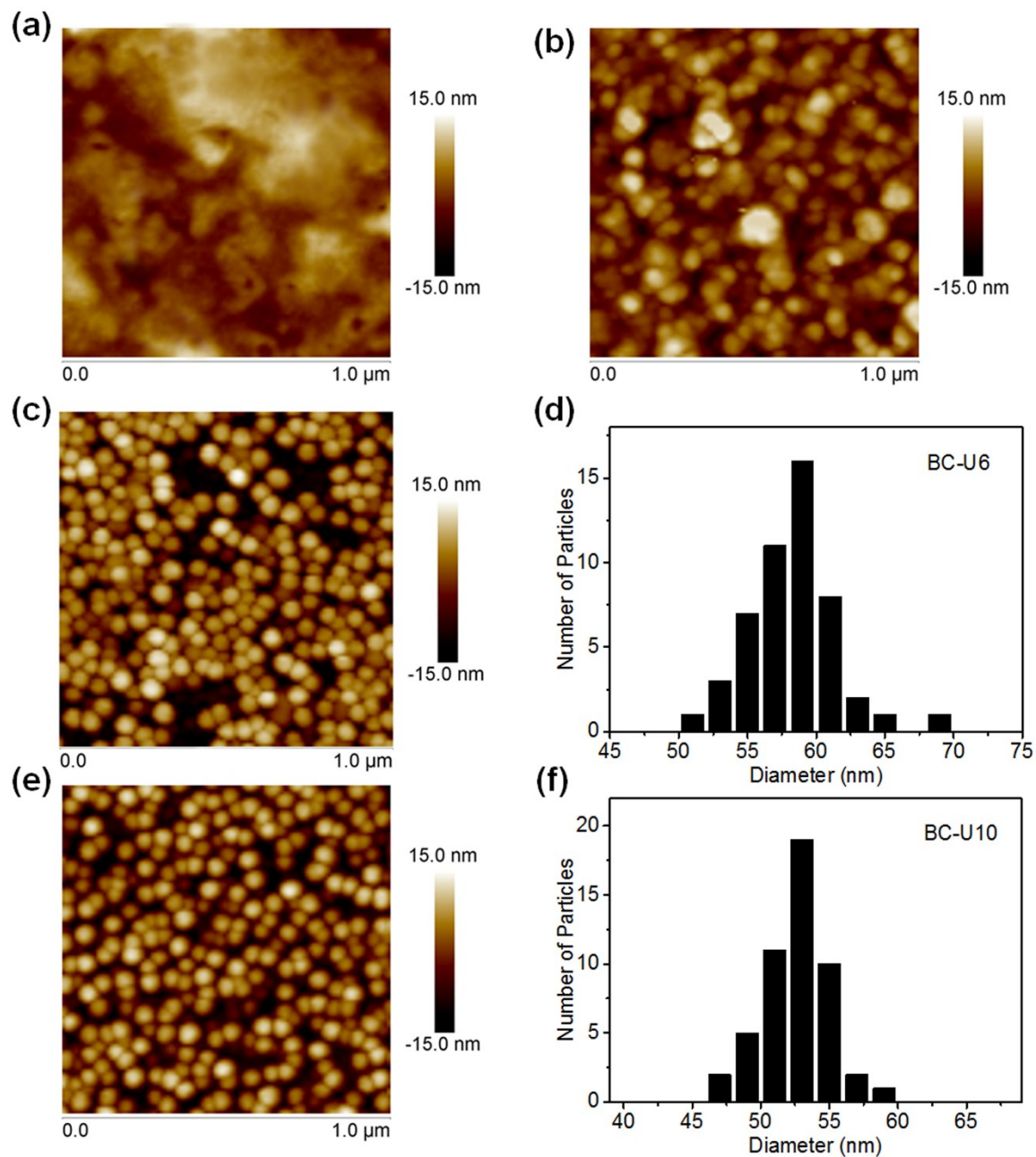
Figure 2.5. AFM topography images of (a) BC-U0 (b) BC-U3 (c) BC-U6 (e) BC-U10; and the corresponding diameter histograms of (d) BC-U6 (f) BC-U10.

The AFM images of surfaces obtained from the solutions of BC-U6 and BC-U10 show the appearance of spherical and uniform nanoparticles, which reveals the formation

of core cross-linked micelles. The number-average particle diameters of the micelles formed by BC-U6 and BC-U10 were generated from the sectional analysis of 50 particles, which were randomly picked from the analysis regions. According to the diameter histograms in **Figure 2.5d and Figure 2.5f**, the micelles prepared from BC-U6 and BC-U10 show sizes of 58.7±10.1 nm and 52.8±6.2 nm, respectively. Compared to DLS results, the larger particle size measured by AFM imaging is possibly due to the tip-induced deformation and the deformation of the soft micelles upon adsorption onto silica substrates. Although the measured particle sizes of the micelles are not accurate, the results can still reflect the characteristics of the polymer micelles. The smaller size of BC-U10 micelles is most likely due to the higher cross-link density with higher content of UPy moieties. These results are in excellent agreement with the corresponding hydrodynamic diameter distributions measured by DLS.

2.3.3 Thermo-Responsive Properties of the Core Cross-Linked Micelles

To investigate the thermo-responsive properties of the core cross-linked micelles, DLS was utilized to investigate the size and polydispersity of the UPy-containing polymers in water at different temperatures between 10 and 40 °C. **Figure 2.6a** shows the temperature dependence of polydispersity index (PDI) of polymers with different fractions of UPy groups. The aqueous solutions of BC-U6 and BC-U10 show relatively low PDI values (PDI<0.1) from 10 to 40 °C, which indicates that the polymers assemble into micelles over the selected temperature range. However, the PDI of polymers with 3 mol% UPy groups increases rapidly when the temperature decreases below 30 °C, which is a result of the dissociation of the polymeric micelles. The intensity-average hydrodynamic diameters of BC-U6 and BC-U10 as a function of temperature were

further characterized. As shown in **Figure 2.6b**, when the temperature increases from 10 to 40 °C, the average diameter of micelles formed by BC-U6 decreases from 49.5 nm to 40.3 nm, while the change of micelles of BC-U10 is less than 2 nm (from 40.1 nm to 38.2 nm). The above results demonstrate the swelling/shrinking processes of the polymeric micelles occur over a wide temperature range and the swelling capacity of the micelles decreases with increasing the content of UPy moieties on the block polymers. Besides, it has been clearly verified that the thermally triggered swelling/shrinking processes of the core cross-linked micelles are fully reversible as evident from the changes of hydrodynamic diameters detected during cyclic heating-cooling tests (**Figure 2.7**).
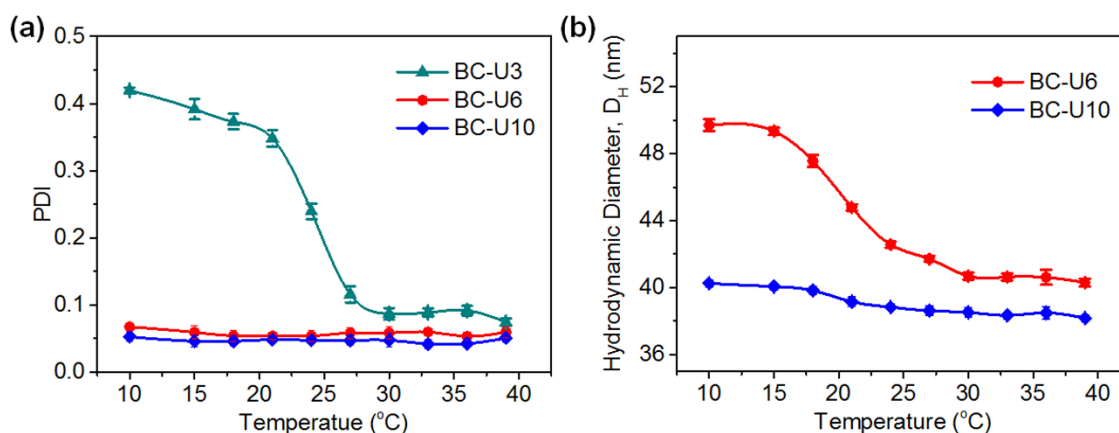
Figure 2.6. Temperature dependence of (a) polydispersity index (PDI) and (b) hydrodynamic diameters measured by DLS for micelles prepared from UPy-containing block copolymers.
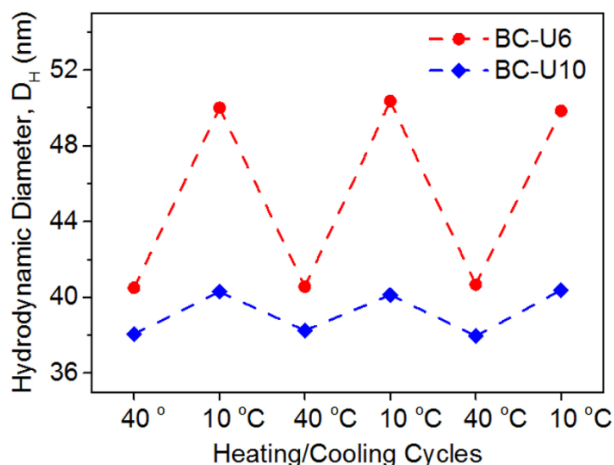
Figure 2.7. Hydrodynamic diameter changes of core cross-linked micelles during heating (40 °C) and cooling (10 °C) cycles.

Low critical solution temperature (LCST) is a basic physical property of thermo-responsive block copolymers and can be tuned by regulating the copolymer composition.[174] In this study, the effect of hydrogen-bonding groups on the LCST of the polymers was characterized by fluorescence probe technique. The variation of fluorescence intensity ratio (I_1/I_3) of pyrene is used to illustrate the polarity of the microenvironment surrounding pyrene molecules. **Figure 2.8** displays the temperature dependence of I_1/I_3 in aqueous solutions with the presence of functionalized block copolymers. Above 35 °C, all the samples show I_1/I_3 values around 1.3, revealing the formation of micelles due to the hydrophobic interactions of PNIPAm blocks above LCST. However, when temperature decreases below LCST, the PNIPAm cores become hydrophilic and the micelles tend to swell or dissociate, thus the polymers would release the encapsulated pyrene, and the fluorescence intensity ratios tend to increase as pyrene molecules are exposed to a relatively polar environment. As expected, the change of fluorescence intensity ratio is more significant with lower percentage of UPy groups,

since the strength of the network in the cores is weaker and the stability of micelles decreases. The LCSTs of BC-U0, BC-U3 and BC-U6 are determined to be 31 °C 24 °C and 20 °C, respectively. But the LCST of BC-U10 cannot be determined. The transition temperatures of the polymers are different from the LCST of PNIPAm, which is related with the amounts of incorporated functional groups. As the HEMA-UPy is relatively hydrophobic, the LCST of PNIPAm copolymer will decrease with its incorporation, which is consistent with DLS measurements and the results from the previous researches.[135,175,176] Due to its very low water solubility, pyrene could be used as a model chemical for hydrophobic drug. The thermo-responsive loading and release of pyrene reveal a potential application of the synthesized core cross-linked micelles in controlled drug delivery. To realize drug release in human physiological environments, the LCST of the copolymers can be facilely tuned to a desired temperature by incorporating hydrophilic comonomers such as poly (ethylene glycol) methacrylate (PEGMA) or acrylic acid (AA).[177]
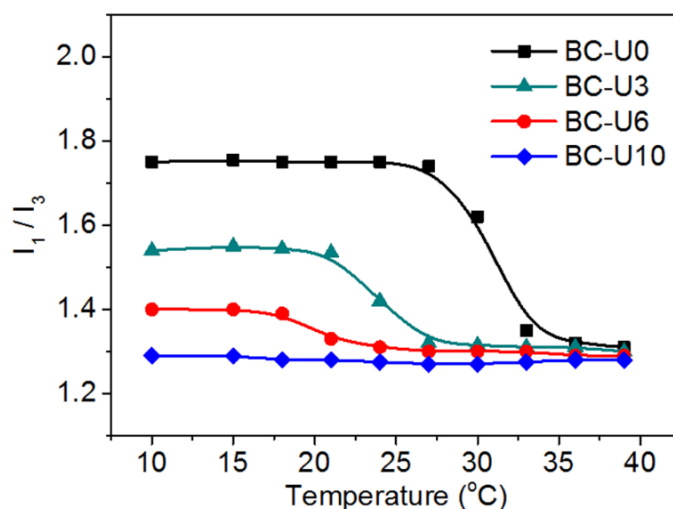
Figure 2.8. Fluorescence intensity ratios (I_1/I_3) of pyrene as a function of temperature in solutions of block copolymers with different functionalities.

2.4 Conclusions

In summary, we have successfully synthesized double hydrophilic block copolymers PEG-b-P(NIPAm-co-UPy), in which the thermo-responsive PNIPAm block was functionalized with varying content of self-complementary multiple hydrogen-bonding group 2-ureido-4[1H]-pyrimidinone (UPy) via RAFT copolymerization. Non-covalently core cross-linked micelles were self-assembled in water through dimerization of the self-complementary hydrogen-bonding UPy groups. The hydrogen-bonded micelles show excellent structural stability even with relatively low cross-linker fractions (e.g. 6 mol%) over a wide temperature range, which demonstrates that the hydrogen-bonding interactions of UPy are strong enough to hold the copolymer chains together even in hydrophilic aqueous environment. Besides, the PNIPAm core of the cross-linked micelles exhibits fully reversible thermo-responsive swelling/shrinking behavior, as evident from the hydrodynamic diameter changes detected during cyclic heating-cooling tests. The stability, size and thermo-responsive properties of these polymer micelles can be readily tuned by the incorporated content of hydrogen-bonding UPy groups. The thermo-responsive loading and release of pyrene molecules as a model hydrophobic drug reveal a potential application of the synthesized core cross-linked micelles in controlled drug delivery. The facile preparation of the core cross-linked micelles from double hydrophilic block polymers PEG-b-P(NIPAm-co-UPy) provides new insights into designing stable and stimuli-responsive polymer micelles with a wide range of applications in drug delivery, diagnosis and sensing.

CHAPTER 3   Polypyrrole-Doped   Conductive   Supramolecular   Elastomer   with   Stretchable,   Rapid   Self-Healing,   and   Adhesive   Properties for Flexible Electronic Sensors

3.1 Introduction

The development of electronic materials with flexible, stretchable and sensory features have attracted increasing attention in recent years,[178-180] which expands electronic devices to a broad range of applications such as artificial skin,[181-183] wearable electronics,[184,185] implantable biomedical devices,[186] and soft robotics.[187] Due to the rigidity of conventional electrical chips based on semiconductor wafers and metal foils, tremendous efforts have been dedicated to coupling electroconductive components with elastic polymers as the support material to accommodate the flexibility and stretchability of the soft electronics.[188-190] Although various attempts have been made to locate the conductors with micro- or nano-patterns on the surfaces of elastomeric substrates such as polydimethylsiloxane (PDMS) for the fabrication of skin-like electronics,[191,192] this strategy suffers from the high cost and complexity of microfabrication, as well as limited extensibility.[193] A facile and promising route toward the development of elastic conducting sensors is incorporating conductive fillers into the flexible polymer matrix, which complies with traditional processing methods such as solution casting and injection moulding.[194-196] Metallic particles,[197,198] carbon back,[199] carbon nanotubes,[200,201] and graphene[202] have been exploited as conducting nanofillers, however, the weak interaction between conductors and elastomers tend to result in aggregation and inhomogeneous distribution of the particles,[203,204] which is detrimental to the mechanical

46

properties of the material. Due to the versatile solubility of their corresponding monomers,[205] conductive polymers such as polypyrrole, polyaniline and polythiophene can form in situ within a soft polymer matrix, showing flexibility in processing and compatibility with the elastomeric polymers,[206-209] which makes them promising candidates for the fabrication of mechanically soft and electrically conducive sensing platform.

Inspired by the self-healable capability of human skin, it is highly desirable to endow conductive sensors with self-healing ability, which can undergo autonomous and repeatable repair processes when exposed to environmental or mechanical damages, leading to enhanced robustness and durability of the electronic devices with extended service lifetime for practical applications.[55,210,211] Several design strategies have been applied to achieve healing ability in flexible and stretchable electronics. For example, Xu et al. reported a conductive ternary polymer composite showing high stretchability and self-healing property, but the healing process required a relatively long time (24 h) and humidity assistance.[212] Bao and coworkers developed a self-healing electronic sensor based on a hydrogen-bonded supramolecular polymer with embedded nickel microparticles,[198] and Yu et al. prepared a conductive hybrid gel by incorporating metal-ligand supramolecules within a nanostructured polypyrrole matrix.[213] In spite of their self-healing ability under ambient conditions, the composite materials suffer from low stretchability due to the high content of rigid conductive components. Generally speaking, adhesive tapes are needed for attaching wearable sensors to the contacted substrates, and a conductive platform with self-adhesive behavior is favorable to simplify the operation process as well as facilitate the stability of the signal detection.[214] Therefore, the

development of multifunctional electronics with excellent stretchability, adhesiveness and fast self-healing ability still remains a challenge.

In this work, for the first time, we have demonstrated a facile solution casting method for the fabrication of novel polypyrrole (PPy)-doped conductive polymer composites from hydrogen-bonded elastomers, which exhibit highly stretchable, fast self-healing, adhesive and sensing abilities. The supramolecular elastomers were prepared by incorporating 2-ureido-4[1H]-pyrimidinone (UPy) groups into fully water-soluble poly(ethylene glycol) methyl ether methacrylate (PEGMA)-based polymers via free radical polymerization of PEGMA and UPy-modified 2-hydroxyethyl methacrylate (HEMA-UPy), and then the conductive composites were constructed by triggering the in situ polymerization of pyrrole within the polymer matrix. The uniformly dispersed PPy particles construct conductive pathways in the elastic network, which promotes the transport of electrons as well as provides mechanical reinforcement to the hybrid system. The self-complementary quadruple hydrogen bonding between UPy units serves as cross-linking sites for the formation of flexible elastomers, and the reversibility of the linkages render the composite materials fast self-healing property.[215-218] Moreover, the presence of dynamic hydrogen bonds contributes to the excellent and repeatable adhesiveness of the materials to various substrates including glass, metal and polymeric substrates.[95,219] The as-prepared strain sensor from the elastomer composite possesses low detection limit and high sensitivity to monitor both large and subtle human motions, which is capable to maintain its mechanical and electrical properties after several cutting/healing cycles. The facile strategy reported in this study provides new insights and opportunities for the

fabrication of multifunctional strain sensors with diverse applications in flexible electronic devices.

3.2 Experimental Methods

3.2.1 Materials

Hexamethylene diisocyanate (98%, Fluka), 2-Amino-4-hydroxy-6-methylpyrimidine (98%, Aldrich), dibutyltin dilaurate (95%, Aldrich), 2,2′-Azobis(2-methylpropionitrile) (AIBN, 98%, Aldrich), copper phthalocyanine-3,4′,4″,4‴-tetrasulfonic acid tetrasodium salt (CuPcTs, 85%, Aldrich), ammonium persulfate (APS, 98%, Aldrich), N,N-dimethylformamide (DMF, 99%, Aldrich) were used as received. Chloroform ($CHCl_3$) was dried over calcium hydride (CaH_2) and distilled before use. 2-Hydroxyethyl methacrylate (HEMA, 97%, Aldrich) and poly(ethylene glycol) methyl ether methacrylate (PEGMA, Mn=500, Aldrich) were destabilized through aluminum oxide columns before polymerization. Pyrrole (98%, Alfa Aesar) was purified by passing it over a silica gel column. All other reagents and solvents were used as received.

3.2.2 Synthesis

2-(6-isocyanatohexylaminocarbonylamino)-6-methyl-4[1H]-pyrimidinone (OCN-UPy). OCN-UPy was synthesized according to a typical method.[166] 2-amino-4-hydroxy-6-methylpyrimidine (5.00 g, 0.04 mol) was added into excess hexamethylene diisocyanate (40.32 g, 0.24 mol) and then the mixture was reacted at 100 ºC for 20 h under argon atmosphere. After 50 mL pentane was added into the flask, the resulting precipitate was filtered and then washed with pentane for 3 times. The white powder was then dried under vacuum overnight. ^{1}H NMR ($CDCl_3$, 400 MHz): δ_H (ppm) = 13.1 (s, 1H,

49

CH₃CNH̲), 11.9 (s, 1H, CH₂NH(C=O)NH̲), 10.2 (s, 1H, CH₂NH̲(C=O)NH), 5.8 (s, 1H, CH̲=CCH₃), 3.3 (m, 4H, NH(C=O)NHCH̲₂ + CH̲₂NCO), 2.2 (s, 3H, CH̲₃C=CH), 1.6 (m, 4H, NCH₂CH̲₂), 1.4 (m, 4H, CH₂CH₂CH̲₂CH₂CH₂).

UPy-based methacrylate monomer (HEMA-UPy). The preparation of HEMA-UPy monomer was carried out by following a procedure reported previously.[220] Freshly distilled HEMA (6.5 g, 50 mmol) and synthesized OCN-UPy (7.325 g, 25 mol) were dispersed in 200 mL chloroform, where 2 drops of dibutyltin dilaurate were added as a catalyst. The mixture was then heated at 60 °C with reflux for 20 h, and the resultant solution was filtered to remove the remaining solids. The filtrate was then concentrated to 50 mL by rotation evaporation and dropped into excess ethyl ether, where the precipitated monomers were collected, washed, and dried under vacuum overnight. ¹H NMR (CDCl₃, 400 MHz): δ$_H$ (ppm) = 13.2 (s, 1H, CH₃CNH̲), 11.9 (s, 1H, CH₂NH(C=O)NH̲), 10.2 (s, 1H, CH₂NH̲(C=O)NH), 6.1+5.6 (s, 2H, C=CH̲₂), 5.9 (s, 1H, CH̲=CCH₃), 5.0 (s, 1H, NH̲(C=O)O), 4.3 (m, 4H, CH̲₂O(C=O)), 3.3-3.2 (m, 4H, NH(C=O)NHCH̲₂ + CH̲₂NH(C=O)O), 2.2 (s, 3H, CH̲₃C=CH), 1.9 (s, 3H, (C=O)CCH̲₃), 1.7-1.2 (m, 8H, CH₂CH̲₂CH₂).

Copolymer P(PEGMA-co-UPy). Polymers with different contents of PEGMA and HEMA-UPy were prepared by free radical copolymerization as follows. A representative example of the synthesis of P(PEGMA-co-UPy) with 5 mol% HEMA-UPy, referred as PEG-5UPy, is given as follows. First, PEGMA (7.125 g, 14.25 mmol), HEMA-UPy (0.317 g, 0.75 mmol) and AIBN (12.3 mg, 0.075 mmol) were dissolved in 25 mL DMF. Afterwards, the flask was sealed and purged with continuous argon for 30 min to remove

oxygen, and the solution was then stirred at 60 ºC for 24 h. The resultant product was dialyzed against water for one week and freeze-dried to yield the purified copolymer.

3.2.3 Preparation of PPy/PEG-5UPy Composites

A series of PPy/PEG-5UPy nanocomposites were developed by a solution casting method with various amounts of pyrrole. In a typical process, 0.3 g PEG-5UPy and 22.5 mg pyrrole (23.2 μL, 0.34 mmol) were dissolved in 1.5 mL ethanol as solution A. Meanwhile, solution B was prepared by dissolving APS (77.5 mg, 0.34 mmol) and CuPcTs (8.4 mg, 0.0085 mmol) in 1 mL Milli-Q water. The polymerization of pyrrole was induced by adding solution B dropwise into solution A in an ice bath under vigorous stirring, followed by a further reaction at 4 °C for 24 h. After dialysis against water, the polymer solution was cast into a polytetrafluoroethylene (PTFE) mold and dried under vacuum to render an elastomer composite.

3.2.4 Characterization of the As-Synthesized Polymers

^{1}H NMR spectra were recorded in deuterated chloroform (CDCl$_3$) solutions at 25 °C on an Agilent 400-MR DD2 System (Agilent Technologies, USA). The Fourier transform infrared spectroscopy (FTIR) analysis of the polymers and nanocomposites were performed on a Nicolet iS50 FTIR spectrometer (Thermo Scientific, USA) over a range of 500–4000 cm^{-1} with a resolution of 4 cm^{-1}. The molecular weight (Mn) and polydispersity index (PDI) of the polymers were measured by gel permeation chromatography (GPC, Waters 1515 system, USA) using THF as the eluent at a flow rate of 1 mL/min. The thermal stability of the prepared composites with different PPy contents was investigated by thermogravimetric analysis (Discovery TGA, TA Instruments, USA) from 25 to 800 °C at a heating rate of 10 °C/min under N$_2$

atmosphere. Rheological characterizations were performed on an AR-G2 stress-controlled rheometer (TA Instruments, USA) with a 40-mm parallel-plate configuration and 1 mm gap. Oscillatory frequency sweep tests were performed at a strain of 1% with shear rates ranging from 0.1 to 100 rad/s. The morphologies of the composites were examined using a Zeiss EVO M10 scanning electron microscopy (SEM) at an acceleration voltage of 5 kV.

All mechanical tensile tests were conducted at room temperature using a AGS-X universal tensile testing machine (Shimadzu, Japan) equipped with a 50 N load cell. For each PPy fraction, three rectangular specimens with the dimension of 12 mm (length) $\times$ 8 mm (width) $\times$ 1.5 mm (thickness) were prepared and the uniaxial tensile tests were performed at a constant stretching rate at 10 mm/min. Healing tests were carried out by cutting the original sample into two halves with a blade and bringing the two separated interfaces into contact without applied stress for a certain time at room temperature. After self-healing, the mechanical properties of the sample were also measured by the uniaxial tensile test for the evaluation of healing efficiency. The adhesive strengths of the nanocomposites on a variety of substrates, including glass, stainless steel, copper, polycarbonate (PC), PTFE and porcine skin, were characterized via a lap shear testing method. Porcine skin was employed to mimic the human skin tissue. The samples were sandwiched between the surfaces of the substrates with a bonded area of 10 mm $\times$ 10 mm and compressed with a pressure of 5 kPa for 2 min. The adhered plates were mounted on the tensile tester and then pulled at a speed of 10 mm/min until separation. The adhesion strength was calculated by the measured maximum load divided by the initial bonded

area. Detachment/reattachment cyclic tests were conducted to evaluate the repeatability of adhesion.

The electrical conductivities of composite films with 6 mm diameter and 300 μm thickness were determined by a four-point probe tester (Lucas Labs Pro4, USA). To detect the resistance change during stretching, the samples were fixed on a self-made stretching stage with different strains applied. The real-time I-t (current versus time) curves of the strain sensors were recorded on an electrochemical workstation (CHI920, CH Instruments, USA) with a constant voltage of 1.5 V.

3.3 Results and Discussion

3.3.1 Preparation of Hydrogen-Bonded Elastomer

As illustrated in **Figure 3.1**, the conductive composite was developed based on a supramolecular polymer as the support matrix which is crosslinked by self-complementary, quadruple hydrogen-bonding groups. The copolymers were prepared by free radical copolymerization of PEGMA with varying amounts of HEMA-UPy, and were abbreviated as PEG-nUPy, where n presented the molar fraction of UPy-containing monomer in the feed (0, 3, 5, 8 mol%). The detailed synthesis process of the copolymers was depicted in **Figure 3.2**, and their molecular weights and polydispersities obtained by GPC were summarized in **Table 3.1**. ^{1}H NMR characterization of HEMA-UPy and PEG-5UPy were shown in **Figure S3.1-S3.2** in **Appendix B**, in which the characteristic peaks located in the range of 14.0~10.0 ppm were assigned to the urea NH protons of UPy groups, suggesting successful incorporation of UPy functionality in the prepared copolymers. The actual molar fraction of the UPy units in each polymer was determined

from the integral values of the characteristic signals in the corresponding spectrum, which was close to the feed molar content (**Table 3.1**).
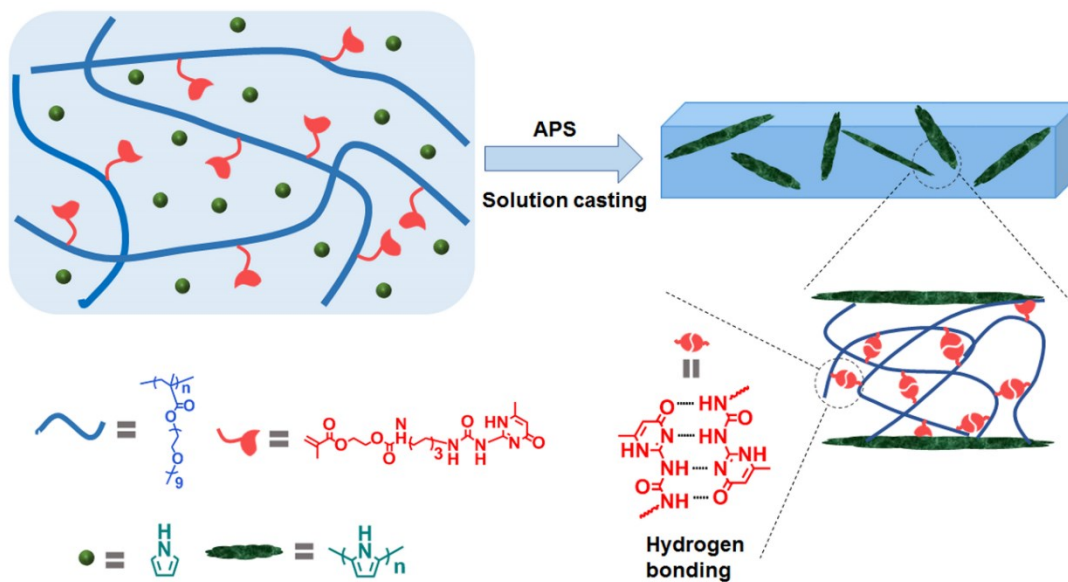
Figure 3.1. Schematic illustration of the fabrication process of the PPy-doped composite from hydrogen-bonded supramolecular elastomer.
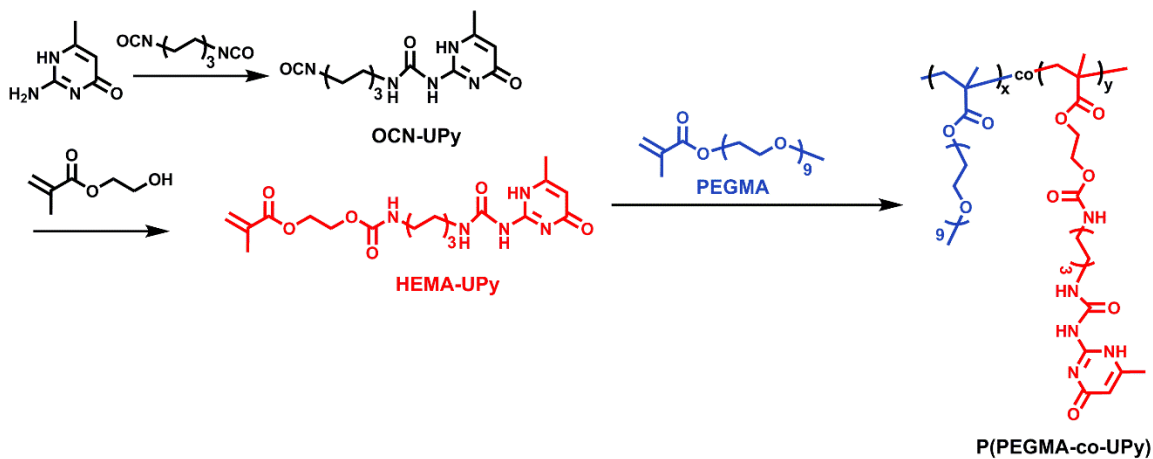
Figure 3.2. Synthesis route of supramolecular copolymer P(PEGMA-co-UPy).

Table 3.1. Summary of molecular characterizations of synthesized PEG-nUPy copolymers.

Polymer	UPy fraction (mol%)		Mn (kDa) [b]	Polydispersity [b]
	Feed	Product [a]		
PEG-0UPy	0	0	119	1.68
PEG-3UPy	3	3.2	108	1.91
PEG-5UPy	5	5.1	110	1.80
PEG-8UPy	8	7.6	121	1.79

[a] Molar fractions of the monomers were measured by ^{1}H NMR spectroscopy. [b] Mn and PDI were determined by GPC.

Macroscopically, PEG-0UPy without multiple hydrogen-bonding functionalities behaved as a viscous liquid under ambient conditions, while the introduction of UPy groups turned the PEG-based copolymers into an elastic state, which is ascribed to the formation of cross-linking sites via the intermolecular multiple hydrogen bonds. The mechanical properties of the PEG-based copolymers were evaluated by rheological study and the results were exhibited in **Figure 3.3a**. With the increasing amount of UPy moieties from 3 mol% to 8 mol%, both the storage modulus (G') and loss modulus (G'') of the copolymers were enhanced obviously, indicating a higher cross-linking density and stronger hydrogen-bonded network. Due to the strong dimerization of the UPy groups,[221] even when the content of hydrogen-bonding moieties was as low as 5 mol%, the G' of PEG-5UPy could reach a plateau around 1.0×10^5 Pa at a frequency of 10 rad/s. The transparent PEG-5UPy exhibited outstanding flexibility and elasticity (**Figure 3.3b**),

which could be stretched more than 10 times its original length without breaking. It is attributed to the automatic breaking and recombining of the hydrogen bonds upon strain, which facilitated energy dissipation. Besides, the supramolecular hydrogen-bonding network could undergo reversible association/dissociation at room temperature,[90,92] and this dynamic nature endowed the elastomer excellent self-healing ability as shown in **Figure 3.3c**. The specimens were stained with different colors for easy visual inspection and each of them was cut into halves with a blade, followed by bringing the freshly cut surfaces into contact immediately. After healing for 5 min in ambient environment, the two halves of the elastomer merged into a single piece which could withstand stretching without showing fracture at the damaged interface. The fatigue properties of both as-prepared and self-healed PEG-5UPy elastomers were investigated by applying 50 successive loading-unloading cycles with 100% strain (**Figure S3.3** in **Appendix B**), where the strength is only slightly compromised after 50 cycles of stretching. The mechanical properties of the self-healed sample were comparable to the original one, indicating efficient healing of the polymer network. The repeatable self-healing of the polymer was demonstrated by rheological characterization, with alternate frequency steps cycling between 100 rad/s and 0.1 rad/s, as presented in **Figure S3.4** in **Appendix B**. The elastic behavior, reversible network formation, as well as excellent stretchability and fast self-healing capability of the PEG-5UPy suggest its superiority to serve as the polymer matrix for the fabrication of elastomer composites, and it was utilized for preparing conductive composites in this work.
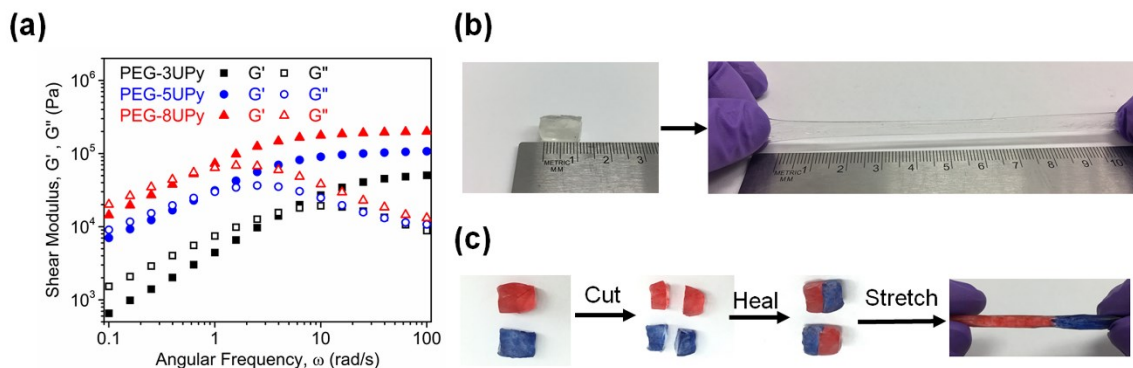
Figure 3.3. (a) Rheological frequency sweep measurements of PEG-based copolymers with different contents of UPy. (b, c) Optical images of PEG-5UPy showing (b) high stretchability and (c) autonomous self-healing ability (healing for 5 min after cut and contact) in ambient environment.

3.3.2 Fabrication of the PPy-Doped Elastomer Composites

The conductive nanocomposite was developed via a facile mixing and solution casting method by triggering pyrrole polymerization inside the PEG-5UPy elastomer network (**Figure 3.1**). Firstly, a homogenous solution was prepared by mixing pyrrole molecules with PEG-5UPy in ethanol owning to their good miscibility, followed by in situ polymerization of pyrrole induced with the addition of APS as the oxidant and CuPcTs as the dopant.[222] After 24 h reaction and dialysis, the color of the viscous solution changed from blue to black, and it was poured into a flat PTFE mold for the removal of water under reduced pressure, leading to an elastic composite material. A series of PPy/PEG-5UPy composites were prepared with the incorporated pyrrole fractions ranging from 2.5 to 10 wt%, and all the specimens were examined by thermogravimetric analysis (TGA) as shown in **Figure S3.5** in **Appendix B**. The elastic

polymer PEG-5UPy was thermally stable up to 300 °C and experienced a complete

decomposition when the temperature reached 450 °C. The weight loss of the composite

materials started around 200 °C ascribed to the degradation of PPy element,[223] and the

remaining residues at 800 °C increased with a higher content of PPy. The TGA results

indicated that PEG-5UPy served as the main component in the composites, and the actual

weight fractions of PPy were calculated to be 2.4 wt%, 4.7 wt%, 7.2 wt% and 9.5 wt%

for samples with 2.5 wt%, 5 wt%, 7.5 wt %, 10 wt% pyrrole in feed, respectively, which

were determined by the final residual weights of PPy at 800 °C. **Figure 3.4a** shows the

morphologies and microstructures of the four PPy-doped composites obtained by

scanning electron microscope (SEM). With an increasing amount of pyrrole addition, the

density of PPy particles dispersed in the continuous soft matrix was enhanced

significantly, and the PPy phase displayed a rough and irregular shape resulted from the

interconnection of small sphere-like nanoparticles.[204] Compared to the severe aggregation

of PPy particles generated by the direct mixing of polymerized PPy with PEG-5UPy

(**Figure S3.6** in **Appendix B**), the much more uniform distribution of PPy particles

displayed in **Figure 3.4a** was ascribed to the in situ polymerization of pyrrole molecules,

during which the PPy particles provided intermolecular hydrogen bonding sites to the

elastomer network,[224] and the resultant rough PPy surface facilitated the wetting by the

soft polymer matrix.[225] The chemical structure of the prepared composites was

investigated by Fourier transform infrared spectroscopy (FTIR), and **Figure 3.4b** displays

the FTIR spectra of PEG-5UPy matrix, PPy and polymer composite with 7.5 wt% PPy. In

the spectrum of PEG-5UPy, two absorption peaks appeared at 1662 and 1589 cm^{-1}

corresponding to the C=O (-CO-NH- bond) and in-ring C=C stretching of UPy units,

respectively.[216] The characteristic peak located at 1560 cm^{-1} in the spectrum of PPy was attributed to the in-plane bending of C=N bonds in the pyrrole rings.[222] These characteristic peaks could be observed in the spectrum of the prepared composite, suggesting that the hydrogen bonding between UPy groups still remained with a successful introduction of PPy in the PEG-5UPy network. Besides, the bending of C=N bonds shifted from 1560 cm^{-1} for pure PPy to 1550 cm^{-1} for the 7.5 wt% PPy composite, and the red shift was mainly attributed to the delocalization of π-electrons in PPy, indicating interactions between PPy fillers and the elastomer matrix.[213,226,227] The conductivities of the composites with varying content of PPy were characterized by a four-point probe and depicted in **Figure 3.4c**. Pure PEG-5UPy is non-conductive, and with increasing incorporated PPy content from 2.5 wt% to 10 wt%, the conductivity of the composites was improved by three orders of magnitude from 1.6×10^{-3} S/m to 1.48 S/m. It should be noted that the enhancement of electrical conductivity was nonlinear as a function of the PPy weight fraction, where the conductivity experienced a rapid increase with the amount of PPy changing from 5 wt% to 7.5 wt%. This phenomenon is most likely originated from the formation of the continuous PPy network[206] which acted as the transporting path for electrons in the composite material. The conductivity of the soft composites with relatively low PPy content ($\leq$10 wt%) is close to that of the pure PPy hydrogel (1.7 S/m),[228] suggesting the potential of the composites for sensing and conducting applications.
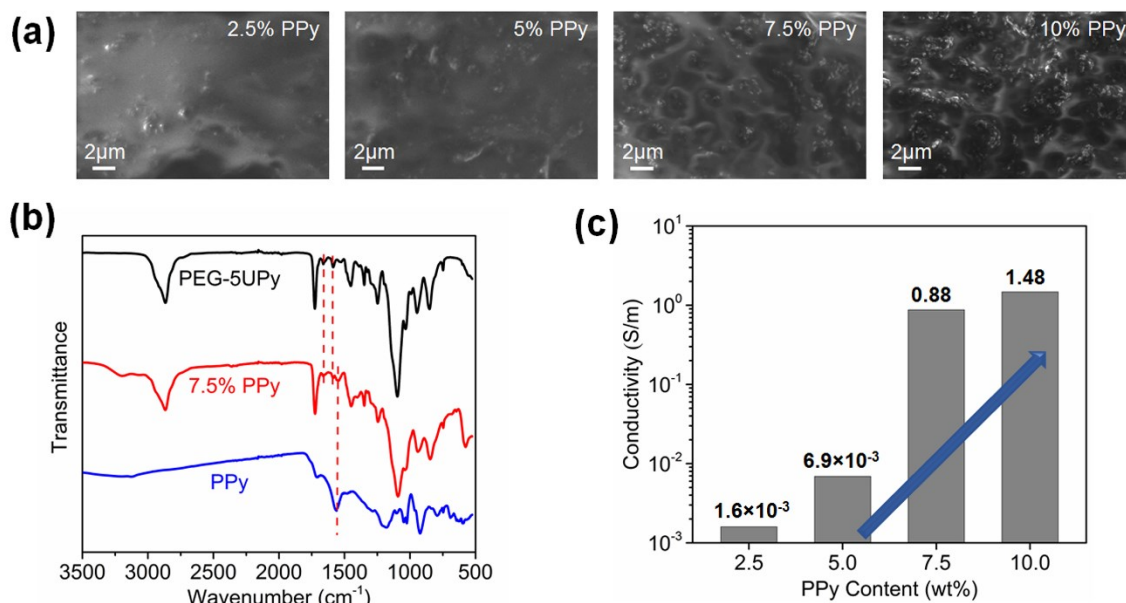
Figure 3.4. (a) SEM images of PPy/PEG-5UPy composites with incorporated PPy content of 2.5 wt%, 5 wt%, 7.5 wt % and 10 wt%, respectively. (b) FTIR spectra of PEG-5UPy, PPy and the polymer composite with 7.5 wt% PPy. (c) Electrical conductivity of PPy/PEG-5UPy composites with different fractions of PPy.

3.3.3 Mechanical Properties

The mechanical properties of the obtained nanocomposites were characterized by uniaxial tensile tests and **Figure 3.5a** presents the stress-strain curves of PEG-5UPy elastomer and composite materials containing different contents of PPy. Without the presence of conductive PPy fillers, the PEG-5UPy elastomer exhibited a high stretchability with a fracture strain more than 1000%, but the strength of the polymer was relatively low (<0.1 MPa). It can be observed that the introduction of PPy into the elastic matrix would significantly improve the tensile fracture stress of the composites from 0.11 MPa (2.5 wt% PPy) to 0.93 MPa (10 wt% PPy), while compromise the strain at breaking

point from 740% (2.5 wt% PPy) to 190% (10 wt% PPy), demonstrating that the formation of PPy particles could endow effective mechanical reinforcement to the composite materials. However, a high PPy content tended to impair the stretchability of the composites due to the rigidity of PPy.[229] It is worth mentioning that when the fraction of PPy increased from 5 wt% to 7.5 wt%, the fracture stress was greatly improved 2.4 times (from 0.30 MPa to 0.72 MPa), while the stretchability was slightly decreased by 18% (from 500% to 410%). The stretchability of the composite with 7.5 wt% PPy is also shown in **Figure 3.5b**. Due to its excellent mechanical properties as well as high conductivity, the composite was exploited for further characterizations involving self-healing, adhesive and sensory abilities.
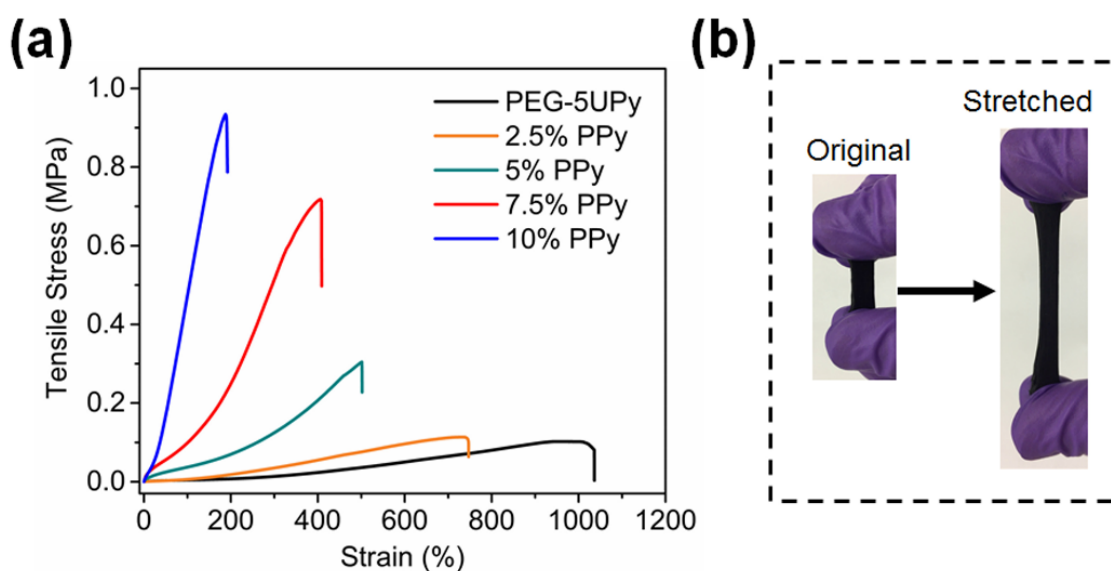
Figure 3.5. (a) Typical stress-strain curves of PEG-5UPy and PPy/PEG-5UPy composite materials with various PPy contents characterized by tensile tests. (b) Optical images of 7.5 wt% PPy composite before and after stretching.

3.3.4 Self-Healing and Adhesive Performances

The dynamic hydrogen bonds maintained in the elastomer matrix were expected to enable autonomous self-healing ability in the composite. As demonstrated in **Figure 3.6a**, the composite with 7.5 wt% PPy was cut into three pieces and the separated parts could be cured into a complete piece by attaching the freshly cut interfaces together without imposing any pressure or stimuli. Within 5 min, the interfaces were well-bonded, and the self-healed sample was strong enough to sustain stretching without breaking. The self-healing ability of the composite was further evaluated by tensile tests of the self-healed samples with different prescribed healing time, where the stress-strain curves and calculated healing efficiency are presented in **Figure 3.6b-c**. Both healing efficiencies of the strength and elongation were examined, which were defined as the proportions of ultimate stress and elongation recovered in the healed specimens compared to the original one. It is observed that the composite could display fast self-healing under ambient condition, and only after 2 min of contact, the stress-strain curve of the healed sample could restore 48% of its original ultimate stress and 63% of the original elongation. At the early stage of self-healing, the mechanical properties of the healed composite were remarkably improved with increasing healing time. When the healing time extended to 3 min, the healing efficiency enhanced to 81% of strength and 85% of elongation. After healing for a longer time, the healing process reached equilibrium and the stress-strain curves of the specimens overlapped with the curve of the pristine sample, where the calculated healing efficiencies were up to 98% (4 min) and 100% (5 min) of strength, while 96% (4 min) and 100% (5 min) of elongation. The fast self-healing capability of the composite was contributed by the rapid and reversible reconstruction of the physical

crosslinking in the elastomer network, taking advantage of the reversible nature of the dynamic hydrogen bonding interactions at room temperature as well as the mobility of PEG-based polymer chain.[215] With a higher content of PPy particles, the movement of the polymer chains in the matrix were restricted, and the composite with 10 wt% PPy could be healed after 30 min of contact (**Figure S3.7** in **Appendix B**). Compared to previously reported composite elastomers which either lack stretchability (<50%) [198,230] or require relatively long time for healing process (> 24h),[196,212] the prominent combination of satisfied mechanica property with rapid self-healing ability offers the as-prepared composite material advantages for numerous practical applications involving flexible electronics.
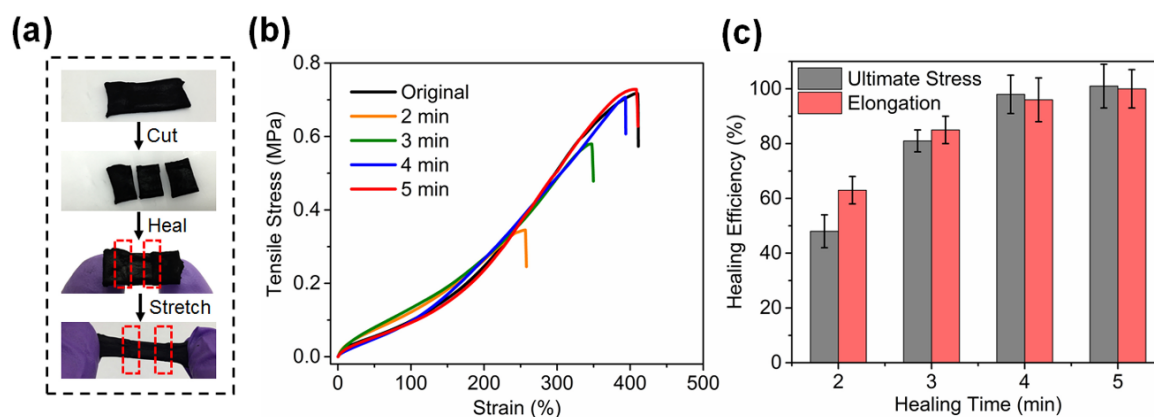
Figure 3.6. Self-healing ability of the composite with 7.5 wt% PPy. (a) A composite is cut into three pieces and recombined to self-heal into a complete piece that can sustain stretching. The red rectangles indicate the healing interfaces of the composite. (b) Typical stress-strain curves of the original and self-healed composites with different healing time under ambient condition. (c) Healing efficiency of the strength and elongation of the composites as a function of healing time.

The hydrogen-bonding moieties in the polymer matrix provided the composite self-adhesiveness to a broad range of substrates, where the adhesion was generated from several possible physical interactions including hydrogen bonding (with -OH, -NH$_2$ groups and N, O, F components),[231] metal coordination (with metal ions on the solid surfaces)[232] and van der Waals interactions.[219] As indicated in **Figure 3.7a**, the composite with 7.5 wt% PPy could firmly adhere two weights together and easily support a mass of 500 g. The adhesive strength of the composite to a variety of inorganic and organic substrates were quantitatively evaluated by lap shear measurements, and the results were summarized in **Figure 3.7b**. The adhesive strength between the composite and metal surfaces such as stainless steel and copper were the highest (53 kPa on steel and 48 kPa on copper) among the substrates, which was ascribed to the synergetic interactions of hydrogen bonding and metal complexation. Hydrogen bonding, together with van der Waals interactions, played an important role in the adhesion of the composite with glass, polycarbonate (PC) and polytetrafluoroethylene (PTFE), where the adhesive strengths were determined to be 44 kPa, 46 kPa and 17 kPa, respectively. Porcine skin was employed to imitate the human skin tissue, and the hydrogen bonds formed on the interface of the composite and porcine skin resulted in an adhesion of 29 kPa. The sample containing 10 wt% PPy could also adhere to the abovementioned substrates, where the adhesive strength was lower than that of the composite with 7.5 wt% PPy, which was mainly ascribed to the reduced mobility of the polymer chains (**Figure S3.8** in **Appendix B**). Adhesiveness were rarely reported in conductive elastomer systems due to the lack of noncovalent interactions, and the adhesion strength of the as-prepared composite to skin preceded that of fibrin glue (<10 kPa), a commercialized tissue adhesive, as well as the

reported conductive adhesive hydrogels (5~20 kPa).[214,223,233]. The strong self-adhesiveness of the composite material to skin tissue suggested its superiority for the applications in wearable electronic devices. Due to the reversibility of the physical interactions, the composite exhibited repeatable adhesion to the substrates. As shown in **Figure 3.7c**, the adhesive strengths of the composite to glass and stainless steel were completely maintained during five detachment/reattachment cycles, suggesting the excellent reusability of the composite for practical applications.
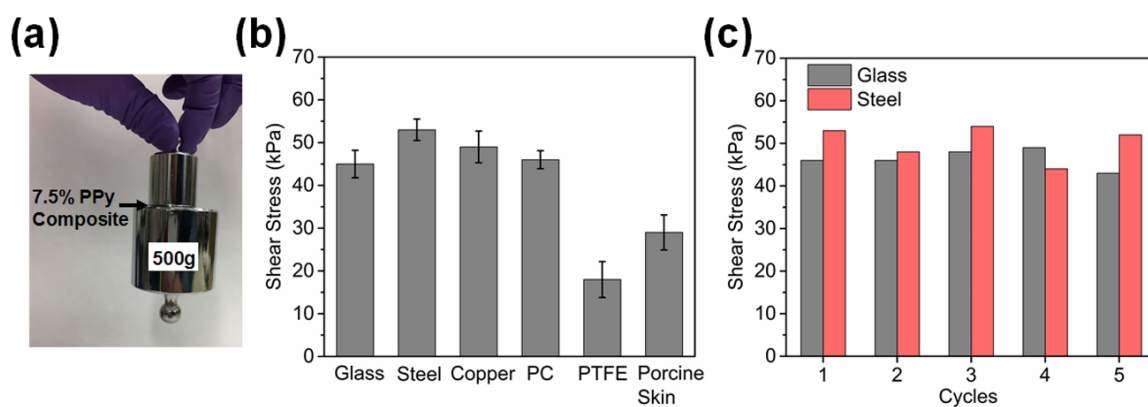
Figure 3.7. Adhesive property of the composite with 7.5 wt% PPy. (a) An optical image showing a composite attached to the metal surfaces can completely support 500 g mass. (b) Adhesive strengths of the composite to different substrates examined by lap shear tests. (c) Repeatable adhesive behaviors of the composite during several detachment/reattachment cycles.

3.3.5 Electrical Behaviors of the Strain Sensor

Taking advantage of its elasticity and conductivity, the composite material shows great potential application for fabrication as a strain sensor, and a representative plot of relative resistance change ($\Delta R/R_0$, where R_0 and ΔR denote the pristine resistance and

variation in resistance after being stretched) as a function of strain is presented in **Figure 3.8a**. It is observed that resistance of the composite experiences a monotonic increase with the applied stain up to 300%, and the strain sensitivity of the material was further evaluated by the gauge factor (GF), which is defined as the ratio of $\Delta R/R_0$ to the applied strain and presented as the slope of the curve in **Figure 3.8a**. Within 180% strain, the GF was found to be 4.5, which increased to 10.8 with strains in the range of 180~230%, and it was significantly enhanced to 30.8 for strains exceeding 230%. During the stretching process, the increasing strain would lead to the deformation and breakage of the formed PPy network, and the increased gap between the conductive particles resulted in a higher resistance of the composite.[234] Simultaneously, some rearrangements and network reconstruction of the dispersed PPy particles also took place, and this process tended to compensate for the increase in resistance, especially at low elongation.[235] The sensing repeatability of the composite was demonstrated in **Figure 3.8b**. During 15 stretching/releasing cyclic tests with strain varying between 0% and 150%, the resistance change of the composite was completely reversible, and the electrical property remained stable even after 1000 loading-unloading cycles (**Figure S3.9** in **Appendix B**), indicating the durability of the material for practical applications. Since the composite possessed high sensitivity at both small and large strains, it could be exploited as wearable strain sensors to monitor diverse human activities, where the adhesiveness of the material enabled it to directly attach to skin or other substrates. As illustrated in **Figure 3.8c**, when the composite was mounted on a finger, the large motions of finger joint were detected with a stepwise increase in the relative resistance change, which corresponded to the bending angles of the finger from 0° to 120°. It should be noted that the electrical

response of the sensor to the finger bending was quite fast, and the resistance could return to the original value when the joint was straightened. The detection of subtle motions such as pulse beating was proved by adhering a composite film on the radial artery, where the frequency of cyclic resistance change of the sensor agreed well with the frequency of the human pulse (**Figure 3.8d**).

The electrical self-healing ability was further demonstrated in **Figure 3.8e-f**. An LED bulb could be illuminated using the composite as a conductor in the circuit, and it immediately went off when the composite was cut into two halves, where the current diminished with an open circuit. After a separation for 30 s, the surfaces of the two pieces were brought into contact with a gentle pressure and the bulb was lighted up again with a rapid increase in the current, suggesting a reestablishment of the conductor. During the following 3 min healing, the current gradually restored to the original value, indicating the self-healing of the hydrogen-bonded elastomer network facilitated the rearrangement of the PPy particles and the reconstruction of the conductive network.[198] Moreover, the self-healing in conductivity was repeatable, which was examined by multiple cut-healing cycles at the same location (**Figure 3.8f** and **Figure S3.10** in **Appendix B**), where the conductivity could be fully recovered to the initial value within 20 cycles of healing.
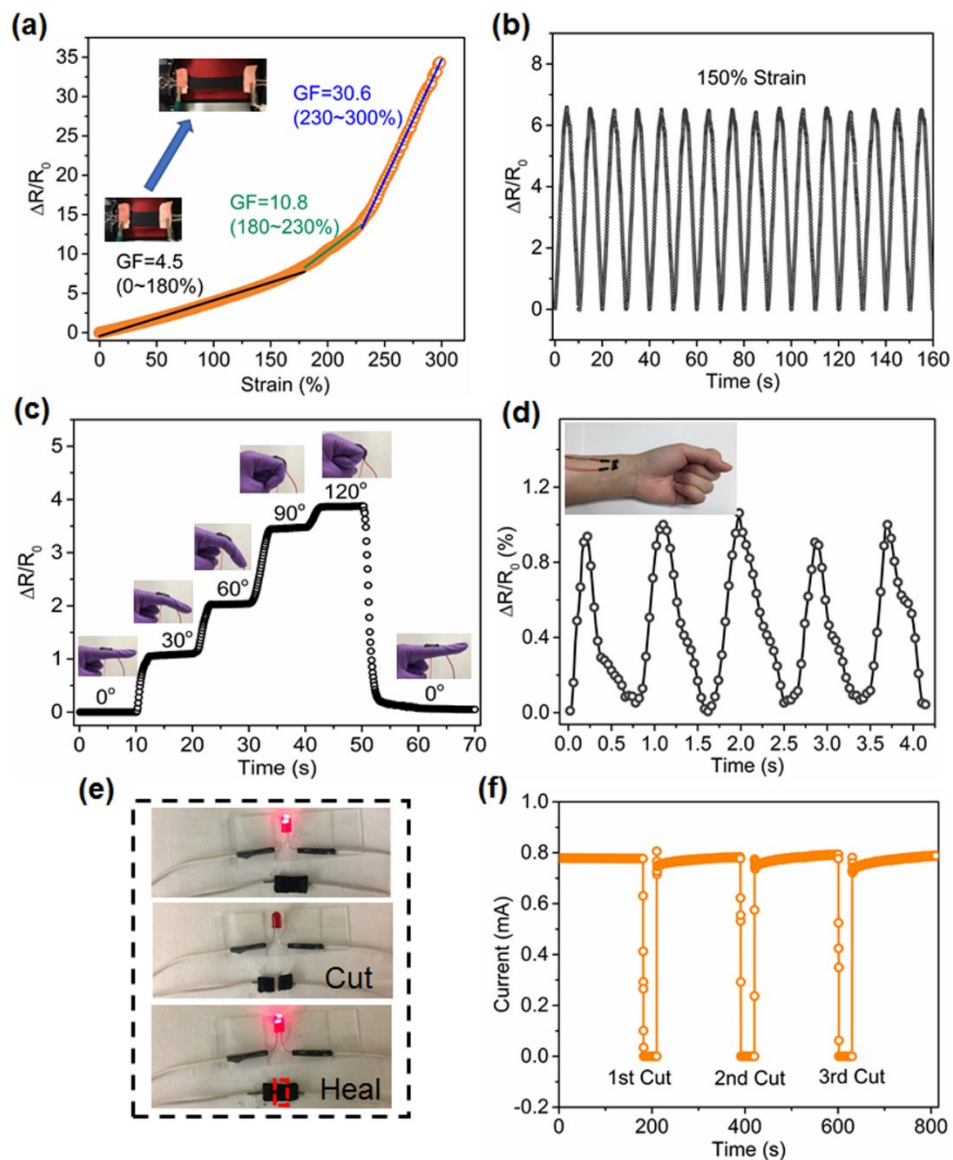
Figure 3.8. (a) Relative resistance change ($\Delta R/R_0$) of the composite with 7.5 wt% PPy under increasing strain. (b) Relative resistance change of the composite during multiple stretching/releasing cycles between 0% and 150% applied strain. (c, d) Demonstration of the composite as a wearable sensor for monitoring (c) finger bending and (d) pulse beating. (e) Demonstration of electrical self-healing ability of the composite with an LED bulb in the circuit. The red rectangle represents the contact interface of the cut composite. (f) Current change of the composite with three cut and healing processes.

3.4 Conclusions

In this work, we have developed a novel conductive composite by introducing in situ polymerization of pyrrole within a hydrogen-bonded supramolecular elastomer matrix through a facile solution casting method, which, for the first time, combines excellent stretchability, self-healing ability and adhesiveness of the UPy-functionalized elastomer with strain sensing capability resulted from the formation of conductive PPy network. The uniformly dispersed PPy particles not only provide high conductivity to the composite but also reinforce the polymer matrix, where the composite with 7.5 wt% PPy exhibits a conductivity of 0.88 S/m and mechanical strength of 0.72 MPa. Due to the dynamic nature of the quadruple hydrogen-bonding groups, the composite possesses a fast and repeated self-healing ability under ambient condition, achieving a complete recovery of both mechanical and electrical properties after 5 min of healing. Moreover, the composite has been demonstrated to display universal adhesiveness to various substrates including glass, metal and organic materials. The conductive elastomer possesses high strain sensitivity up to 300% elongation, and it can be successfully exploited as strain sensors for monitoring various human motions such as finger bending and pulse beating. Taking advantage of the unique features of supramolecular chemistry, the PPy-doped conductive elastomer can be readily integrated with the multifunctionality of the components, holding great promises for sensing applications, and the facial fabrication of the composite elastomer provides new inspirations for the development of advanced functional soft electronic devices.

CHAPTER 4 Stretchable, Injectable and Self-Healing Conductive Hydrogel Enabled by Multiple Hydrogen Bonding toward Wearable Electronics

4.1 Introduction

Hydrogels are three-dimensional (3D) cross-linked porous polymer networks containing high water content and have emerged as promising candidates for biological applications due to their resemblance to human tissues.[10,236] Conductive hydrogels, which combine the electronic properties of conductors with the soft nature of hydrogels,[223,229,237] can mimic the functions of human skin with mechanical and sensory properties,[212,238] and have drawn enormous attention in the past decade for the fabrication of flexible electronics with applications in wearable devices, implantable biosensors, and artificial skin for soft robotics.[239-244] Conductive hydrogels have been directly prepared by introducing conducting fillers such as metallic particles,[245,246] carbon nanotubes[247,248] and graphene[249] into polymer networks, but this blending method usually suffers from low loading amount and aggregation of the conducting components, resulting in either poor conductivity or compromised mechanical properties.[250,251] An alternate facile approach to imparting conductivity to hydrogels is triggering in situ polymerization of conjugated precursors for the generation of conducting polymers such as polythiophene, polyaniline and polypyrrole in hydrogel matrixes.[252-254] Due to the formation of mesh-like conducting networks which entangle with the soft primary networks, the hydrogels possess both fast electron transfer and enhanced mechanical strength.[204] As a widely studied conducting polymer with tunable electrical properties, polyaniline (PANI) has been employed for the

fabrication of various conductive hydrogels, with the utilization of phytic acid[255] or polyelectrolytes[250,256] as dopants. Despite the satisfying electrical conductivity, the relatively weak and brittle networks severely impede their practical applications.[257] One fascinating feature of human skin is its capability to self-repair the injuries inflicted by external force or stimuli,[198] thus it is highly desirable to endow conductive hydrogels with self-healing ability,[258,259] leading to "smart" and durable materials for real-world applications, which still remains a challenge.

An effective strategy toward autonomous self-healing hydrogels is based on the utilization of a variety of reversible molecular interactions including dynamic covalent bonds,[211] ionic interactions,[260,261] hydrogen bonding,[15] metal-ligand coordination,[25] host-guest interactions, and hydrophobic association.[262] Among them, hydrogen bonding interactions are of particular interest for the fabrication of self-healing hydrogels owing to their modulated strength, biocompatibility as well as the fast dissociation/association behavior.[2] Besides, the dynamics of the hydrogen bonds can be readily modulated by temperature and pH of the surrounding environment,[85,90,220] which renders the hydrogels stimuli-responsive properties. As a multiple hydrogen-bonding motif, 2-ureido-4[1H]-pyrimidinone (UPy) has been extensively exploited to direct self-assembly of molecules in supramolecular chemistry since it was introduced by Meijer and coworkers,[78] taking advantage of its easy accessibility and strong self-complementary dimerization ($>10^6$ M^{-1} in chloroform) via quadruple hydrogen bonds.[221,263,264] Several functional materials displaying self-healing abilities have been developed based on the dynamic interaction between UPy groups. Del Campo and coworkers reported an injectable and thermo-responsive hydrogel cross-linked by dimerized UPy pendants, where the self-healing

property could be tuned by temperature.[86] When UPy moieties were grafted onto the backbone of biocompatible dextran, a self-integrating and injectable hydrogel was developed, which was capable of sustainably releasing encapsulated biomolecules and facilitating the regeneration of bone tissues.[265] Cui and Vlassak et al. prepared an extremely stretchable hydrogel by protecting the dimerization of UPy groups in hydrophobic micelles, and the hydrogel could be stretched more than 100 times without fracture as well as exhibited fast self-healing property.[92] However, the multiple hydrogen-bonded moiety has not been extended to conducting polymer hydrogels to provide these systems self-healing ability and other functionalities.

In this work, we have developed a novel conductive polymer hydrogel that combines high conductivity with stretchability, injectability and rapid self-healing ability in one platform, by introducing UPy groups into fragile conducting PANI/poly(4-styrenesulfonate) (PSS) polymers. The hydrogel was primarily composed of a negatively charged PSS supramolecular network cross-linked by UPy groups, where an interpenetrating conducting PANI network was formed by in situ polymerization and electrostatically interacted with PSS chains.[256] The dynamic and reversible dissociation/association process of the hydrogen bonds contributed to the energy dissipation and network reconstruction in the hydrogel, which offered the hydrogel stretchable and self-healing properties. Meanwhile, the thermo-sensitive nature of the hydrogen-bonding interaction provided thermoplasticity of the material,[266] making it injectable and moldable. The hydrogel possessed excellent conductivity as well as high sensitivity to external strain due to the electronic conduction assisted by ionic transport, and it was successfully employed for the detection of various human activities with rapid

and repeatable response, holding great promise for applications in artificial skins and flexible intelligent sensors.

4.2 Experimental Methods

4.2.1 Materials

2-Amino-4-hydroxy-6-methylpyrimidine (98%, Aldrich), 2-isocyanatoethyl methacrylate (98%, TCI), dimethyl sulfoxide (DMSO, anhydrous, 99.9%, Aldrich), 4-styrenesulfonic acid sodium salt (NaSS, Aldrich), sodium hydroxide solution (NaOH, 50 wt% in H_2O, Aldrich), ammonium persulfate (APS, 98%, Aldrich), N,N,N′,N′-tetramethylethylenediamine (TEMED, 99%, Aldrich), hydrochloric acid (HCl, 37%, Aldrich), aniline (ANI, 99.5%, Aldrich), iron(III) chloride hexahydrate (FeCl$_3$·6H$_2$O, 97%, Aldrich) were used as received if not specified. Milli-Q water was utilized for preparing all the aqueous solutions.

4.2.2 Synthesis of UPy-Functionalized Methacrylate Monomer (UPyMA)

The methacrylate monomer functionalized with UPy moiety was synthesized via a previously reported method.[86] 2-amino-4-hydroxy-6-methylpyrimidine (2.0 g, 16 mmol) was dispersed into 50 mL DMSO and the mixture was stirred at 170 °C in an oil bath for 10 min until the solids were completely dissolved. Then the oil bath was removed and followed by the instant addition of 2.5 mL 2-isocyanatoethyl methacrylate (2.75g, 17.7 mmol) into the flask under vigorous stirring. After reaction for 3 min, the solution was quickly cooled to room temperature by immersing in a water bath with the appearance of fine white solids. After 6 h, the precipitate was filtered and washed with excess acetone for 3 times. The collected white power was dried under vacuum overnight. ^{1}H NMR

characterization was performed with an Agilent 400-MR DD2 system (Agilent Technologies, USA) at 25 °C, using deuterated chloroform (CDCl$_3$) as the solvent. δ_H (ppm) = 13.0 (s, 1H, CH$_3$CN$\underline{H}$), 12.0 (s, 1H, CH$_2$NH(C=O)N$\underline{H}$), 10.5 (s, 1H, CH$_2$N$\underline{H}$(C=O)NH), 6.2+5.6 (m, 2H, C=C$\underline{H}_2$), 5.8 (s, 1H, C$\underline{H}$=CCH$_3$), 4.3, (t, 2H, OC$\underline{H}_2$), 3.6 (m, 2H, NHC$\underline{H}_2$), 2.2 (s, 3H, C$\underline{H}_3$C=CH), 1.9 (s, 3H, (C=O)CC$\underline{H}_3$).

4.2.3 Formation of Hydrogen-Bonded PSS (PSS-nUPy) Hydrogels

Supramolecular hydrogels with different amounts of hydrogen-bonding moieties (UPyMA) were prepared by one-pot free radical polymerization, and the resultant products were named as PSS-nUPy, where n indicated the molar percentage of UPyMA with respect to NaSS in the feed. For example, a PSS-20UPy hydrogel was developed from 0.5 mL aqueous solution containing NaSS (0.5 mmol, 103 mg) and UPyMA (0.1 mmol, 28 mg), and the pH of the solution was adjusted to 10 by NaOH to facilitate the dissolution of UPyMA. After the addition of 5 μL TEMED and 5 μL APS stock solution (120 mg APS dissolved in 1mL Milli-Q water) as reaction initiator, the polymerization was conducted at 50 °C for 20 h in a sealed vial, yielding a viscous solution. At room temperature, by adjusting the pH back to 7 using HCl solution, a hydrogen-bonded PSS hydrogel was formed.

4.2.4 Preparation of PANI/PSS-20UPy Hybrid Hydrogels

A series of conductive hydrogels with the incorporated ANI concentration varying from 0.1 M to 0.4 M were prepared. In a typical process, the prepared PSS-20UPy hydrogel was heated to 50 °C resulting in a viscous solution, and a desired amount of ANI was added into the solution with an equivalent amount of HCl. After vigorous agitation for 5 min, ANI was uniformly dispersed in the solution and the mixture was

cooled to room temperature. The reformed hydrogel was immersed in an acidic (0.1 M HCl) solution containing 0.5 M FeCl$_3$ to initiate the polymerization of ANI at 4 °C for 48 h. The obtained dark green hydrogel was purified by immersing in Milli-Q water to remove the unreacted residues and excess ions. The resultant hybrid hydrogels were named as PANI/PSS-20UPy hydrogels with x M ANI, where x indicated the feed concentration of ANI in the hydrogels.

4.2.5 Characterizations of the Hydrogels

The water contents (Q) of the hydrogels were determined by the weight of the swollen hydrogel (W_s) and the corresponding weight of the freeze-dried polymer network (W_d) according to the following equation:

$$Q = \frac{(W_s - W_d)}{W_s} \qquad (4.1)$$

The weight fraction of PANI network in the hybrid hydrogel was characterized by UV-vis spectroscopy on an Evolution 300 UV-vis spectrophotometer (Thermo Scientific, USA). The concentration of ANI diffused into FeCl$_3$ solution during polymerization was determined by a calibration curve of absorbance at 440 nm versus the concentration of added ANI, showing a linear relationship of $A=1.184C-0.0214$, where A and C represented the absorbance and ANI concentration, respectively. The actual weight of PANI in the products was calculated by subtracting the diffused amount of ANI from the feed.

All Fourier transform infrared spectroscopy (FTIR) spectra of the freeze-dried hydrogels were recorded by a Nicolet iS50 FTIR spectrometer (Thermo Scientific, USA), over a range of 500~4000 cm^{-1} with a resolution of 4 cm^{-1}. The internal morphologies of

the hydrogels were investigated by a Zeiss EVO M10 scanning electron microscopy (SEM) operated at 5 kV acceleration voltage. Before observation, the as-prepared hydrogels were quenched in liquid nitrogen, and after freeze-drying, the samples were fractured using a scalpel, with a thin layer of gold sputtered on the fractured surface prior to imaging.

Stretchability of the hydrogels was characterized using a AGS-X universal tensile testing machine (Shimadzu, Japan) at a constant stretching rate of 10 mm/min with a 50 N load cell, and the rectangular hydrogel specimens were prepared with a dimension of 12 mm (length) × 8 mm (width) ×4 mm (thickness). Rheological behaviors and self-healing properties of the hydrogels were examined by oscillatory rheological measurements on an AR-G2 rheometer (TA Instruments, USA). All characterizations were carried out with a 20 mm, 2 ° cone configuration, and silicone oil was applied around the plate to prevent water loss from the hydrogels during the experiments. Oscillatory frequency sweep measurements were conducted at a strain of 1% with shear frequency in the range of 0.1 to 100 rad/s at 25 °C to determine the storage and loss moduli of the hydrogels, and temperature sweep measurements were performed from 10 °C to 50 °C with a heating rate of 2 °C/min. The strain amplitude sweep was performed with strain increasing from 0.1% to 1000% at a frequency of 10 rad/s to induce a failure of the hydrogen network, followed by an immediate return to 1% strain for the examination of network reconstruction. Self-healing performances in response to the applied shear force were also evaluated by cyclic tests, with strain steps shifting between 1% and 800%, and the procedure was programmed as follows: 1% (300 s) → 800% (60 s) → 1% (300 s) → 800% (60 s) → 1% (300 s) → 800% (60 s) → 1% (300 s).

Sheet resistance (R_s) values of the prepared hydrogel slabs were determined by a four-point probe tester (Lucas Labs Pro4, USA) with a linear probe head. The conductivity (σ) was calculated by the following equation:

$$\sigma = \frac{1}{R_s h} \qquad (4.2)$$

where h represents the thickness of the hydrogel. The strain sensing performances of the hydrogels were evaluated by an electrochemical workstation (CHI920, CH Instruments, USA), where the real-time I-t (current versus time) curves were recorded with a constant applied voltage (U) of 1.5 V and the resistance (R) change induced by stretching was calculated by Ohm's law ($R = \dfrac{U}{I}$). Various strains were introduced to the hydrogels by mounting the samples on an in-house prepared stretching stage, which could record the deformation during stretching and releasing. The electrical self-healing property of the hydrogels was detected by both the LED illumination and the current change during cutting and healing process. To evaluate the sensing performances of the hydrogels for diverse human activities, the hydrogels were mounted onto the finger, wrist, throat, and radial artery of a volunteer, and the real-time I-t curves were recorded during finger bending, wrist bending, swallowing, speaking and pulse beating.

4.3 Results and Discussion

4.3.1 Formation of Primary Hydrogen-Bonded PSS Networks

As presented in **Figure 4.1**, hydrogen-bonded anionic polyelectrolyte PSS served as the primary network for the preparation of the conductive hydrogels, which was developed by one-pot free radical polymerization of NaSS and UPyMA using APS as the

initiator. The synthesis route and ^{1}H NMR characterization of the UPy-functionalized monomer are shown in **Figure S4.1-S4.2** in **Appendix C**. A series of the PSS hydrogels with different amounts of incorporated UPyMA were prepared and referred to as PSS-nUPy, where n denoted the molar percentage of UPyMA with respect to NaSS in the feed. The copolymerization reactions were carried out under alkaline conditions (pH=10) to facilitate the dissolution of UPy groups in aqueous environment, since the deprotonation of the UPy groups would generate negatively charged enolate tautomers.[162] When the pH of the as-prepared viscous solutions was adjusted back to 7, the gelation of the copolymers were induced immediately, indicating that the protonation of UPy units led to the formation of hydrogen-bonded dimers and the construction of the 3D network.[90,161]
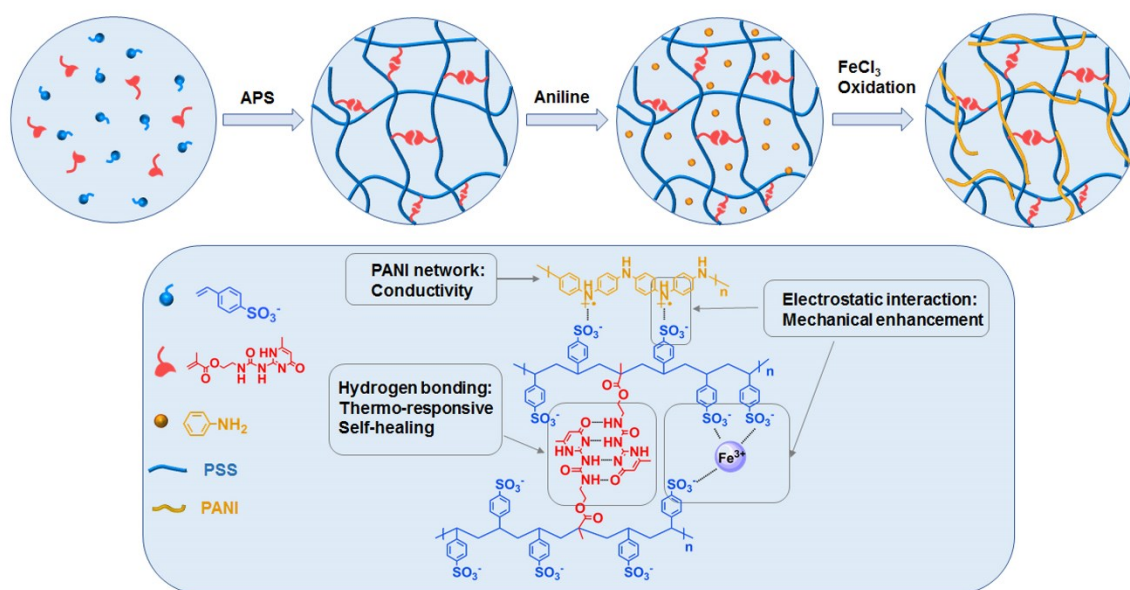
Figure 4.1. Schematic illustration of synthesis process of the supramolecular conductive PANI/PSS-UPy hydrogels and the formation mechanism.

The viscoelastic behaviors of the PSS-nUPy hydrogels were characterized by rheological measurements, where the evolution of storage modulus G' (elastic behavior)

and loss modulus G'' (viscous behavior) as a function of angular frequency was displayed in **Figure 4.2a**. Both G' and G'' were found to be significantly improved with the increasing amount of UPy addition, suggesting a higher cross-linking density resulted from the increment of intermolecular hydrogen bonds. It should be noted that the in each hydrogel, G' and G'' were strongly dependent on the frequency and presented a crossover within the range of 0.1~100 rad/s, which demonstrated the temporary character of the hydrogen-bonded network.[267] At low frequencies, $G'<G''$, indicating a quasi-liquid behavior, while $G'>G''$ at high frequencies, signifying an elastic gel. The crossovers of PSS-10UPy and PSS-15UPy were 63 rad/s and 25 rad/s, respectively, where the resultant materials could flow slowly, while PSS-20UPy and PSS-25UPy showed crossovers at 1.5 rad/s, yielding compliant yet solid-like gels. Polymerization of PSS-20UPy hydrogel was conducted at different temperatures (i.e., 20, 50, 70 °C) for 20 h, and at 50 °C for different times (i.e., 10, 20, 30 h). The viscoelastic behaviors of the hydrogels prepared at each temperature and reaction time are shown in **Figure S4.3** in **Appendix C**. At 20 °C, the polymerization rate is very low, and after 20 h, only a highly viscous solution was obtained. When the polymerization occurred at 70 °C, the initiator decomposed fast, leading to high polydispersity, and the strength of the prepared hydrogel was lower than that prepared at 50 °C. As indicated in **Figure S4.3b** in **Appendix C**, the shear moduli of the hydrogel were enhanced with longer reaction time, and the strengths of the hydrogels prepared for 20 h and 30 h were comparable. Therefore, the optimized reaction condition was determined to be 50 °C for 20 h.

Since hydrogen-bonding interactions tend to be weakened at elevated temperatures,[87] the hydrogels were expected to exhibit thermo-responsiveness, and the

thermosensitivity of PSS-20UPy hydrogel was examined by rheological tests over the range of 10 to 50 °C at a constant frequency of 10 rad/s (**Figure 4.2b**). The gel-sol transition temperature, defined as the crossover of G' and G'', was determined to be 32 °C, and the viscosity of the hydrogel was rapidly reduced with increasing temperature, which dropped below 1 Pa·s at 50 °C. The reversible thermo-induced gel-sol-gel transition was also demonstrated in **Figure 4.2c** and **Figure S4.4** in **Appendix C**, rendering the hydrogel moldability and injectability at moderately elevated temperatures. The performances of PSS-20UPy hydrogel upon applied external strain was characterized by strain sweep measurements (**Figure 4.2e**), where the G' and G'' remained stable up to ~700% strain, suggesting the hydrogel was capable of withstanding large deformation. When the strain was further increased, the hydrogel would collapse accompanied by a rapid decrease of the shear moduli. Notably, once the strain turned back to 1% after severe damage (2000% strain), the hydrogel could fully recover to the original strength without hesitation, which was attributed to the fast reassociation process of the multiple hydrogen bonds.[268] The rapid self-healing ability of the hydrogen-bonded hydrogel was also visually verified in **Figure 4.2d**, where the two separated pieces of the stained and dissected hydrogels could be easily attached to each other at the cut surfaces and healed into one integrated piece within seconds.
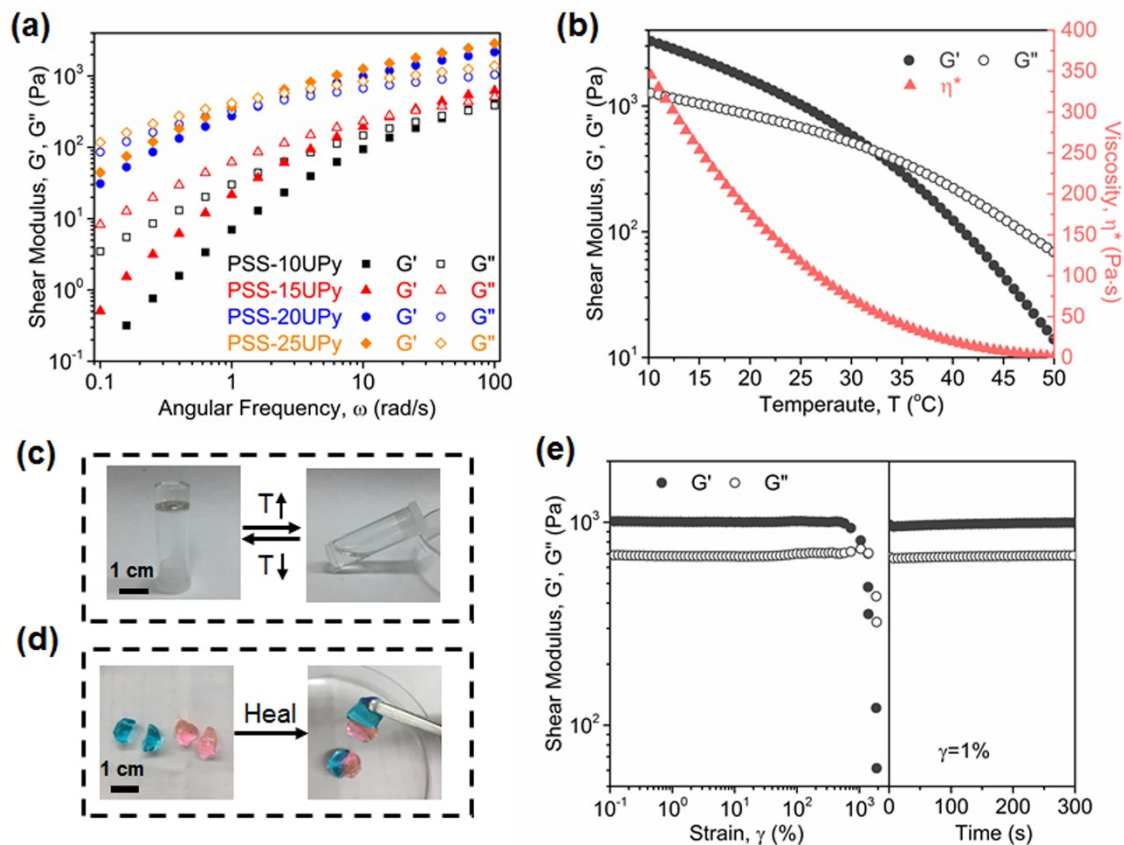
Figure 4.2. (a) Frequency-dependent rheological measurements of PSS hydrogels with different amounts of UPy as cross-linkers at 25 °C. (b) Changes of shear moduli and viscosity of PSS-20UPy hydrogel as a function of temperature at ω=10 rad/s. (c-d) Optical pictures showing (c) temperature-responsive property and (d) self-healing ability at room temperature of PSS-20UPy hydrogel. The scale bar is applied to all the images. (e) Strain sweep measurement (left) followed by immediate recovery from 2000% strain to 1% strain (right) of PSS-20UPy hydrogel at 25 °C.

4.3.2 Preparation of PANI/PSS-20UPy Hybrid Hydrogels

The PSS-20UPy hydrogel was employed for the fabrication of conductive hybrid hydrogels via triggering the in situ polymerization of the incorporated ANI in the

hydrogel frameworks using $FeCl_3$ as the oxidizing agent. (**Figure 4.1**). Different contents of ANI were loaded in the hydrogels by mixing the components at 50 °C, where the liquid state of the hydrogels promoted the uniform dispersion of ANI monomers. In acidic environment, cationic anilinium ions were generated due to the protonation of ANI, which were attracted by the negatively charged sulfonate groups in the hydrogel framework through Coulombic interactions, and the following oxidative polymerization would result in interpenetrating PANI/PSS network within the hydrogel.[229,269] The excess amount of Fe^{3+} ions also coordinated with the anionic PSS via electrostatic interaction and served as cross-linking points,[270] while the hydrogel polymerized in APS solution dissociated into fragments (**Figure S4.8a** in **Appendix C**). The resultant dark green hydrogels were purified by Milli-Q water for further characterization. **Figure 4.3a** shows the FTIR spectra of the hybrid hydrogels prepared with ANI concentrations ranging from 0~0.4 M. The adsorption peaks located at 1030 and 1001 cm^{-1} were ascribed to the asymmetric and symmetric S=O stretching, confirming the presence of PSS primary network in all samples.[256] With the introduction of ANI, the characteristic peaks of emeraldine PANI salt appeared at 1559, 1497 and 1339 cm^{-1}, which were assigned to quinoid and benzenoid ring deformation as well as C-N stretching of benzenediamine.[253,256] The intensities of these peaks increased with a higher content of ANI, suggesting the successful formation of PANI in the hydrogel networks. The water contents of the initial PSS-20UPy hydrogel and the PANI/PSS-20UPy hydrogels were evaluated, as shown in **Table S4.1** in **Appendix C**. After immersing into $FeCl_3$ solution, the hydrogels experienced a slight swelling and the swelling ratio decreased with a higher loading amount of ANI. The actual weight fraction of PANI network in each hybrid

hydrogel was examined by UV-vis spectroscopy, which was close to the feed ratio, indicating most ANI were polymerized in the hydrogel network (**Table S4.1** in **Appendix C**).The morphologies of the corresponding freeze-dried PANI/PSS-20UPy hydrogels were examined by SEM and presented in **Figure 4.3b-e**. Compared to the microstructure of pure PSS-20UPy hydrogel without the addition of ANI (**Figure S4.5** in **Appendix C**), all of the hydrogels loaded with different amounts of ANI displayed similar 3D porous networks, indicating the generation of interpenetrating networks due to the entanglement of PANI and PSS polymer chains, where PSS served as the template as well as dopant to stabilize the in situ formed PANI.[254,271] With increasing amount of PANI, the pore size of the hydrogels was gradually diminished, leading to a denser network.
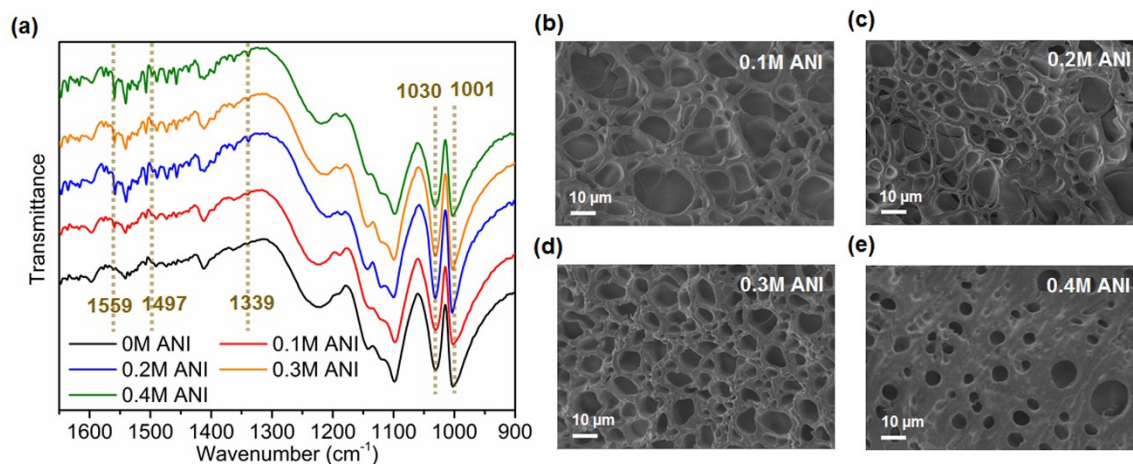
Figure 4.3. (a) FTIR spectra and (b-e) representative SEM images of PANI/PSS-20UPy hybrid hydrogels with different contents of ANI varying from 0.1 to 0.4 M.

4.3.3 Mechanical Properties and Self-Healing Behaviors of the Hydrogels

The viscoelastic mechanical properties of the prepared PANI/PSS-20UPy hybrid hydrogels with different ANI concentrations were evaluated by performing frequency sweep measurements at 1% strain, and the variations of shear moduli are depicted in **Figure 4.4a**. For all samples, G' was higher than G'' over the detection range of 0.1~100 rad/s even without the incorporation of PANI, implying that the sulfonate groups were coordinated with Fe^{3+} ions which served as cross-linkers of the networks and contributed to the elastic behavior of the hydrogels. In addition, both G' and G'' were significantly enhanced with a higher content of PANI, verifying an efficient mechanical reinforcement resulted from the establishment of the continuous PANI/PSS interpenetrating networks, which was in good accordance with the SEM images. The frequency dependence of the shear moduli also revealed the dynamic nature of the non-covalent interactions (e.g., hydrogen bonding between UPy groups, Fe^{3+} coordination) of the cross-linking points, which was further examined with thermo-responsiveness in (**Figure S4.6** in **Appendix C**). The results in **Figure S4.6** in **Appendix C** indicate that the formation of the hydrogel and the thermo-responsive property were mainly contributed by the dimerization between UPy groups, while the relatively weak Fe^{3+} coordination could further improve the elastic property of the hydrogel. **Figure 4.4b** illustrates the response of G' to applied strain. When 0.3 M or a lower amount of ANI were introduced into the hydrogel, G' remained unchanged within 300% strain, indicating their excellent stability upon large deformation, while the hydrogel with 0.4 M ANI started to break down over 30% strain due to the rupture of the densely cross-linked rigid PANI network. Therefore, the hybrid hydrogel

loaded with 0.3 M ANI exhibited an outstanding combination of mechanical strength and flexibility, which was exploited for further characterizations and applications.
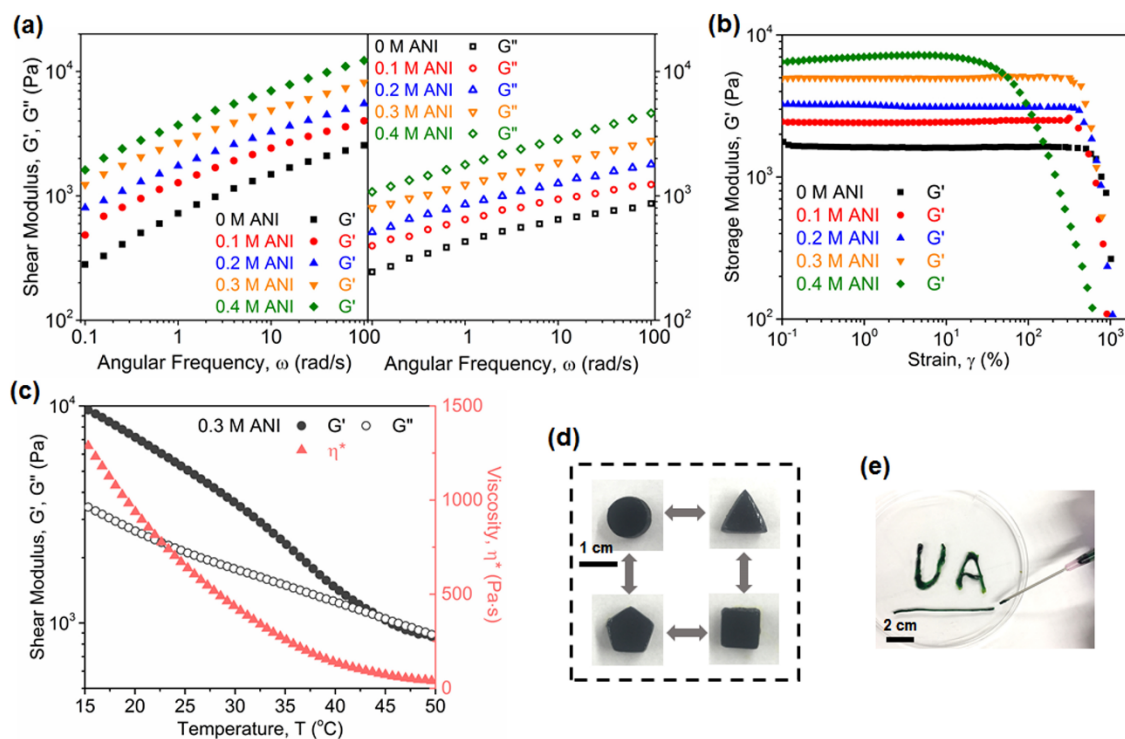
Figure 4.4. (a-b) Rheological measurements of PANI/PSS-20UPy hydrogels with different contents of ANI at 25 °C showing (a) frequency dependence of storage modulus G′ (left) and loss modulus G″ (right) at 1% strain and (b) strain dependence of G′ at ω=10 rad/s. (c) Temperature dependence of shear moduli and viscosity of the hybrid hydrogel with 0.3 M ANI. (d-e) Optical images of the hybrid hydrogels with 0.3 M ANI (d) molded into different shapes, the scale bar is applied to all the images, and (e) injected through an 18-gauge needle.

The thermal response of the hybrid hydrogel with 0.3 M ANI was investigated, where the shear moduli and viscosity were greatly reduced upon heating, leading to a liquid-like material above 45 °C (**Figure 4.4c**). This thermo-induced gel-sol transition

was mainly attributed to the reversible hydrogel bonding between the large amount of UPy groups in the hydrogel network, imparting the hybrid hydrogel thermoplasticity at moderate temperatures. As shown in **Figure 4.4d**, the hydrogel could be facilely molded into a variety of shapes (e.g., circle, triangle, square, and pentagon) by melting it at 50 °C in a particular mold followed by gelation at room temperature. The melting/solidification process was totally reversible and the hydrogel could be readily reshaped and reused. The injectability of the hydrogel was verified in **Figure 4.4e**, where a hydrogel preserved at 50 °C was injected through an 18-gauge needle into different characters due to the reduced viscosity at elevated temperatures, and the injected shapes could be fixed at room temperature. The injectable behavior of the hydrogel implies its great potential in 3D printing.

Strain sweep and cyclic step strain measurements were employed to characterize the self-healing performances of the hybrid hydrogel with 0.3 M ANI. As shown in **Figure 4.5a**, although G' experienced a decrease when the strain reached to 350%, the crossover of G' and G'', which denoted severe damage of the hydrogel network, appeared at 670% strain, suggesting the capability of the hydrogels to undergo large deformation. The excellent stretchability was macroscopically proved in **Figure 4.5b**, where the hybrid hydrogel was readily stretched beyond 6 times of its original length without any fracture, and a typical stress-strain curve is presented in **Figure S4.7** in **Appendix C**. Moreover, when the strain returned to 1% after the failure of the hydrogel at 1000% strain, the reconstruction of the network occurred immediately demonstrated by an instant restoration of the mechanical strength. Both G' and G'' were recovered to the initial values within 30 s. The spontaneous and reversible dissociation/association of the non-

covalent cross-linkers formed by UPy dimerization and Fe^{3+} coordination was responsible for the efficient energy dissipation upon elongation as well as the fast self-healing ability.[234,272] The effect of Fe^{3+} concentration on the viscoelastic behavior and self-healing property of the hydrogels is displayed in **Figure S4.8b-c** in **Appendix C**. The repeatability of the self-healing behavior was further studied by applying continuous strain steps cycling between large and small amplitude (**Figure 4.5c**). Upon 1% strain, G' and G'' of the hydrogel were found to be 5.1 kPa and 1.9 kPa, respectively, while the following 800% strain destroyed the network with a sudden decrease of G' (to 410 Pa) and G'' (to 820 Pa). With a continuous 1% strain step, the hydrogel was reformed rapidly with a healing efficiency of 100%, and this process could be repeated several times without any loss in mechanical properties. The cyclic step strain measurements were also performed at 5 °C and 40°C (**Figure S4.9** in **Appendix C**), and the fast self-healing ability of the hydrogel was demonstrated under both temperature conditions, suggesting its potential in practical applications. **Figure 4.5d** provides optical evidence of the self-healing ability. When an intact hybrid hydrogel was cut into two halves by a scalpel, the freshly-generated surfaces were brought into contact to allow autonomous healing. The two segments adhered to each other instantly, and only after a few seconds, they merged into one piece with a well-bonded interface that could withstand stretching.
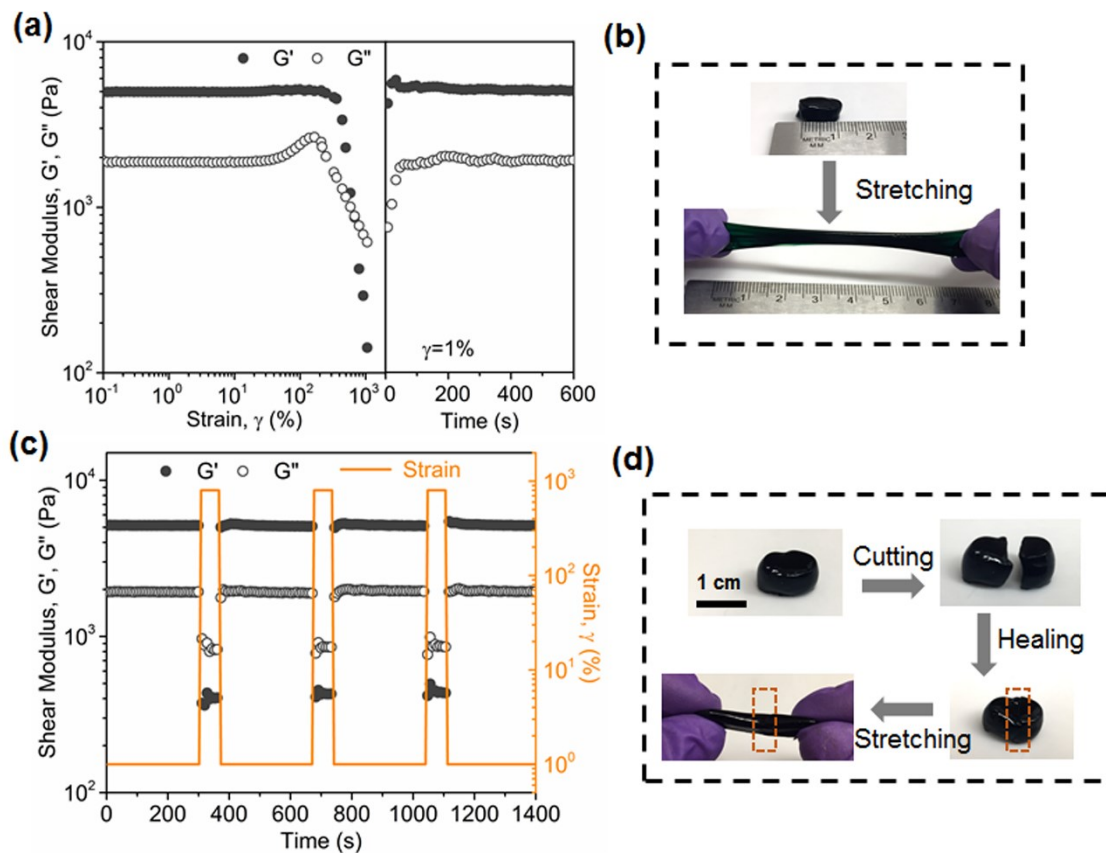
Figure 4.5. Stretchability and self-healing ability of PANI/PSS-20UPy hybrid hydrogel with 0.3 M ANI. (a) Strain sweep measurements (left) followed by time sweep measurement of recovery from 1000% strain to 1% strain (right). (b) Optical demonstration of the stretchability. (c) Variation of the shear moduli during cyclic steps with strain shifting between 1% and 800%. (d) Two separated parts of the hybrid hydrogel merge into one piece after healing for 30 s and withstand stretching. The orange rectangles indicate the contact interface and the scale bar is applied to all the images.

4.3.4 Strain Sensing Performances of the Conductive Hydrogels

Due to the formation of interpenetrating PANI/PSS network which was cross-linked by hydrogen bonding and electrostatic interactions, the conductivity of the hybrid

hydrogels was contributed by two factors: electronic conduction offered by conjugated PANI and ionic conduction due to the existence of Fe^{3+} and PSS.[253,258] The conductivities of the as-prepared hydrogels with various ANI concentrations were detected by a four-point probe and summarized in **Figure 4.6a**. In the absence of ANI, the conductivity of the hydrogel was found to be 1.1 S/m, which was solely dependent on the ion conduction, and this value was notably enhanced to 7.4 S/m with the addition of 0.1 M ANI, suggesting the establishment of efficient electron transfer pathways due to the formation of the PANI network, The conductivity was further improved to 14.2 S/m with 0.4 M ANI loaded in the hydrogel matrix, which was mainly contributed by electronic transport and higher than that of the fragile pure PANI hydrogel (11 S/m).[59] Compared to previously reported hydrogels involving conducting polymers (**Table S4.2**), the integration of high conductivity, stretchability and fast self-healing ability in the developed hybrid hydrogel indicates its promising applications for the fabrication of flexible electronics, especially strain sensors. **Figure 4.6b** displays the relative variation of resistance ($\Delta R/R_0$) of the hybrid hydrogel with 0.3 M ANI in response to applied strain, calculated by $\Delta R/R_0 = (R-R_0)/R_0$, where R_0 and R represent the initial resistance and real-time resistance upon stretching, respectively. Within 300% elongation, the hydrogel exhibited a linear increase in resistance under external strain, and the linearity was most likely attributed to the uniform deformation of the network upon stretching.[271] The slope of the curve, which was referred as gauge factor (GF), was employed to assess the strain sensitivity and determined to be 3.4 within the whole detection range. It is worth mentioning that the previously reported conductive hydrogels generally either lack self-healing ability[241,271] or suffer from low sensitivity (GF<0.5) at small strains,[214,233,273]

therefore, the high sensitivity over the wide strain range of the developed self-healing hydrogel suggests its superiority for the detection of both large and subtle deformations. Cyclic loading/unloading tests were carried out on the hydrogel to evaluate the reliability and repeatability of the sensing performances. As shown in **Figure 4.6c**, when the applied strain varied between 0% and 100%, the relative resistance change of the hydrogel was identical in each cycle and the sensitivity was well preserved after 20 cyclic measurements, demonstrating its excellent stability and reproducibility for practical applications. The reversible sensing ability was also illustrated in the inset photos, displaying the luminance variation of an LED bulb in the circuit upon stretching and releasing of the hydrogel. The self-healing ability of the electrical performance was investigated by recording the current change during cut/healing process (**Figure 4.6d**) with an optical demonstration (**Figure 4.6e**). When the original hydrogel employed as the conductor in a closed loop was cut into two parts, the resultant open circuit would lead to a sudden drop of the current to zero and an immediate extinction of the illuminated LED bulb. After a certain time of separation, the two fractured surfaces were brought into contact, and the LED bulb was turned on instantly along with a complete recovery of the current to the initial value. The slight fluctuation of current in the initial stage of self-healing resulted from the viscoelastic nature of the hydrogel,[198] and the efficient reconstruction of the conductive network was ascribed to the fast reassociation of the non-covalent cross-links. Successive cut and healing steps were carried out on the hydrogel at the same location, and the rapid restoration of electrical performance in each cycle verified the repeatable self-healing of conductivity in the hybrid hydrogel.
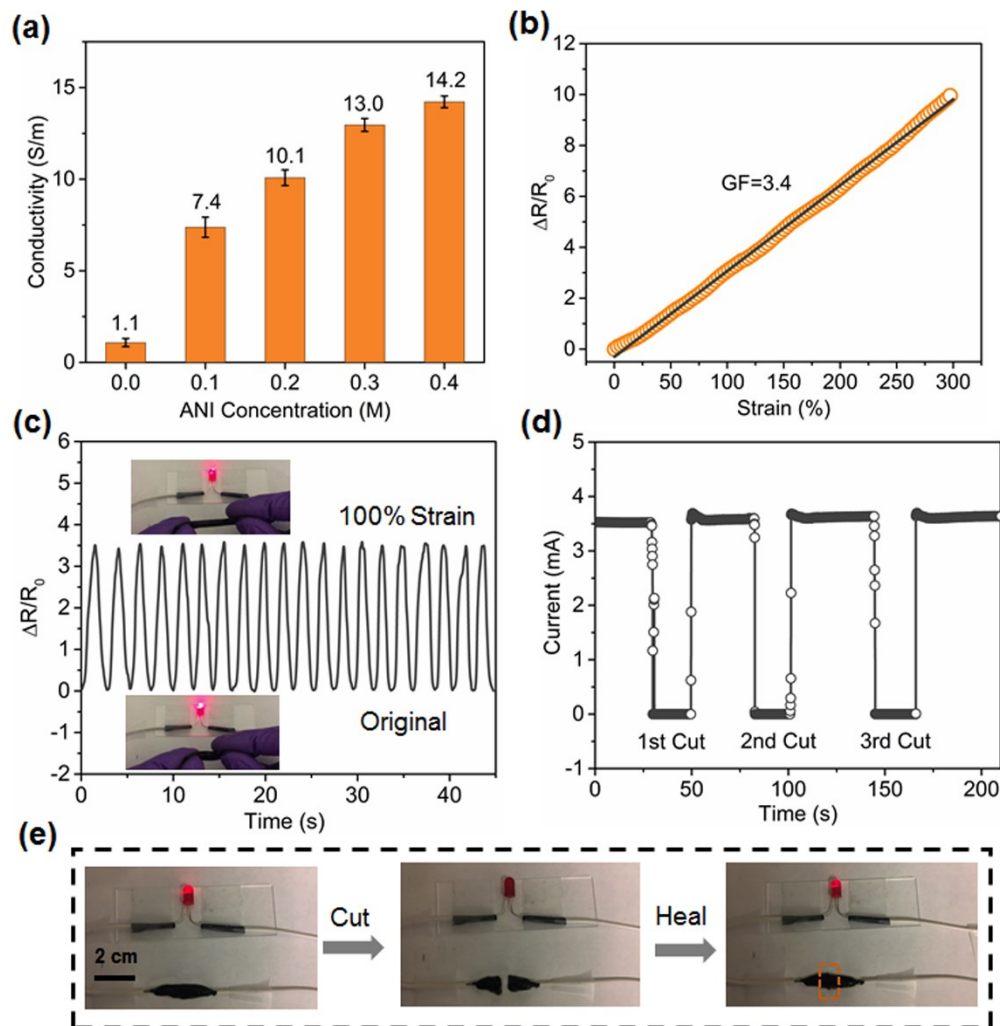
Figure 4.6. (a) Conductivity of PANI/PSS-20UPy hydrogels with different incorporated concentrations of ANI. (b) Relative resistance change ($\Delta R/R_0$) of the hybrid hydrogel with 0.3 M ANI as a function of applied strain. (c) Relative resistance change of the hybrid hydrogel during cyclic loading/unloading tests with strain varying between 0% and 100%. The insets show the luminance variation of an LED bulb in the circuit with different applied strains. (d-e) Electrical self-healing ability of the hybrid hydrogel showing (d) current change and (e) illuminance variation of an LED bulb during cut/healing process. The orange rectangle highlights the contact interface and the scale bar is applied to all the images.
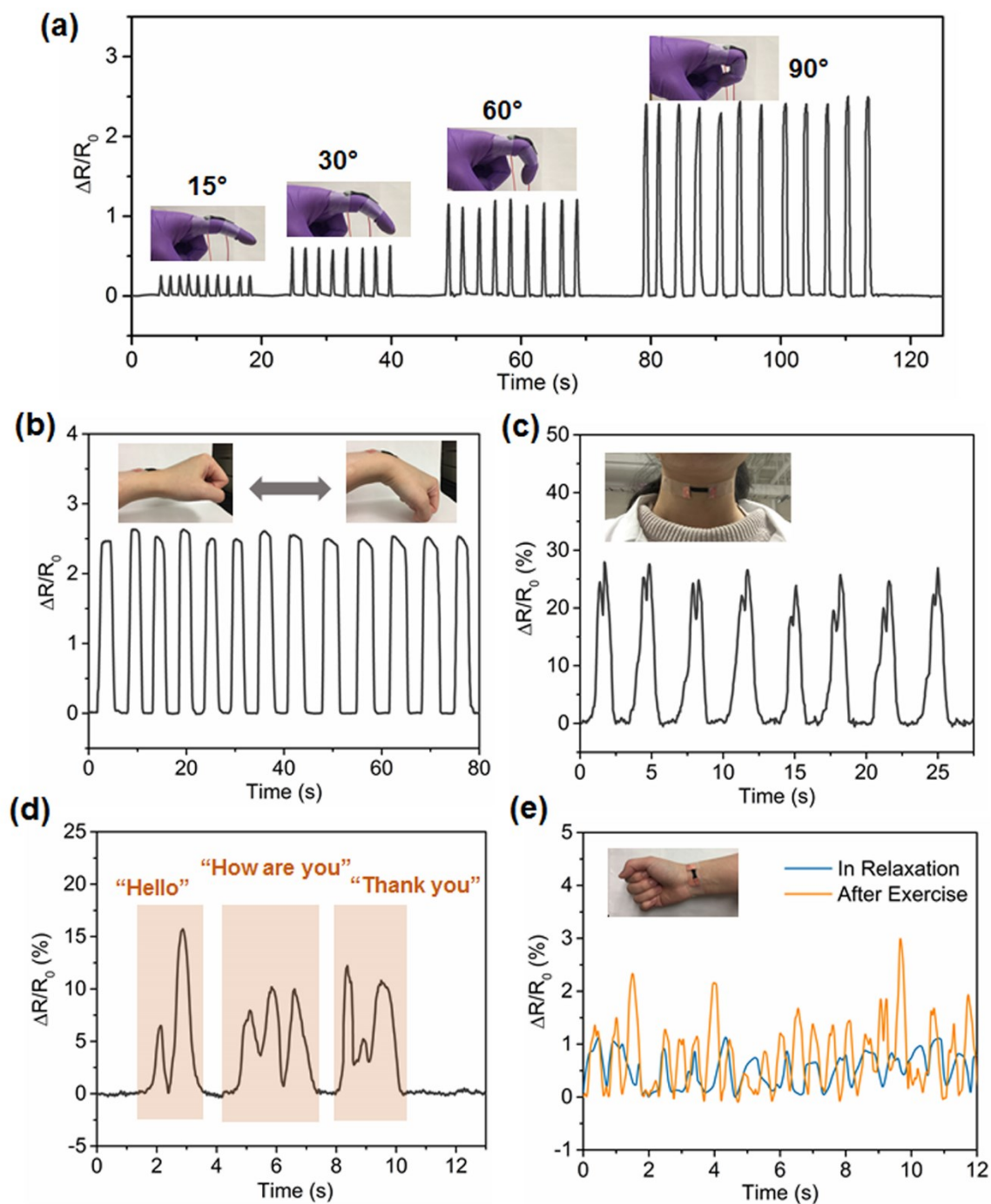
Figure 4.7. Real-time relative resistance change of the hybrid hydrogel with 0.3 M ANI used as wearable strain sensors for monitoring various human activities including (a) finger bending, (b) wrist bending, (c) swallowing, (d) speaking and (e) pulse beating.

Taking advantage of its flexibility and high sensitivity in response to deformation, the hybrid hydrogel with 0.3 M ANI was directly exploited as strain sensors to monitor diverse human activities in real time. As illustrated in **Figure 4.7a**, when a finger attached with the hydrogel was bent from the straightened state to 15 °, 30 °, 60 ° and 90 °, the stretching of the hydrogel would generate a corresponding increase in the relative resistance change to 0.25, 0.60, 1.15 and 2.35, respectively. Moreover, at each certain bending angle, the variation of resistance was founded to be repeatable and reliable during the cyclic bending and straightening process, showing excellent reversibility along with fast response. Similarly, the hydrogel mounted on the wrist also distinguished the bending activity repeatedly with stable resistance change (**Figure 4.7b**).

In addition to the successful detection of the abovementioned large motions, the capability of the hydrogel to monitor subtle motions was further demonstrated. By attaching the hydrogel to the neck, the movement of throat caused by repetitive swallowing was clearly reflected by the change of resistance with two associated peaks (**Figure 4.7c**). When the tester pronounced different phrases such as "Hello", "How are you" and Thank you" in sequence, the diverse vibrations of the vocal cords could be recorded accordingly and these phrases were readily differentiated by the distinct patterns of the signals (**Figure 4.7d**). As displayed in **Figure 4.7e**, the hybrid hydrogel was placed over the radial artery to detect pulse beating, where the frequency of the blood pulse was determined by the frequency of resistance change. Under relaxation condition, it was calculated to be 80 beats/min, while after exercise, both frequency and amplitude of the signals were clearly enhanced, indicating an increased pulse frequency of 115 beats/min. Based on the above demonstrations of human motion monitoring, the hybrid hydrogel

shows great potential to be explored as wearable devices for the detection of full-range human activities with high sensitivity and reliability.

4.4 Conclusions

In this study, we have developed a multifunctional conductive hydrogel which integrates high conductivity with stretchability, injectability and rapid self-healing ability by triggering in situ polymerization of ANI in a hydrogen-bonded PSS network. Taking advantages of the dynamic and reversible nature of the non-covalent cross-links (i.e. multiple hydrogen bonding, Fe^{3+} coordination), the hybrid hydrogel exhibits an excellent stretchability along with an autonomous self-healing ability, showing complete and repeatable recovery of both mechanical properties and electrical conductivity within 30 s. The thermo-responsive dissociation/association of the quadruple hydrogen-bonding groups offers the hydrogel thermoplasticity and injectability, which can be facilely molded into different shapes and injected from a needle. The formation of PANI/PSS interpenetrating network not only provides mechanical enhancement but also endows electronic conduction assisted by ionic transport, where the hybrid hydrogel with 0.3 M ANI displays a superior conductivity of 13 S/m with a linear and sensitive response to a wide range of applied strains. The prepared hydrogel has been successfully employed as strain sensors to monitor diverse human activities with accuracy and reliability, including large motions of human body (e.g., finger and wrist bending) and subtle movements of muscles (e.g., swallowing, speaking, pulse beating), suggesting their great potential to be used as wearable devices. The combination of supramolecular chemistry and conductive polymers has been demonstrated an effective approach toward the fabrication of flexible electronics with multifunctionalities.

CHAPTER 5   Mechanistic Understanding and Nanomechanics of Multiple Hydrogen-Bonding Interactions in Aqueous Environment

5.1 Introduction

Hydrogen bonding interaction has become one of the most commonly used approaches for directing self-assembly of molecules and generating self-organized structures in supramolecular chemistry,[2] owing to their modulated strength, directionality and biocompatibility.[15] Although a variety of supramolecular polymers such as polymer glasses,[274] elastomers,[66,77] micelles[218,275] and hydrogels[85,276] have been prepared via hydrogen bonding interactions, it still remains a challenge to use hydrogen bonds as the sole driving interaction for the formation of supramolecular architectures stable in aqueous environment, due to the competition of intermolecular hydrogen bonds by polar water molecules.[277-279] Inspired by biological self-assembly systems, such as DNA double helix and secondary structures of proteins (α-helix and β-sheet),[12,280] hydrophobic domains have been exploited to provide nonpolar microenvironments[281,282] to shield the hydrogen bonding groups from water and enhance their interactions, leading to stabilized supramolecular structures.[220,283-285]

As a preeminent multiple hydrogen bonding motif, self-complementary 2-ureido-4[1H]-pyrimidinone (UPy) unit has been successfully applied to direct the formation of a variety of supramolecular polymer networks due to the strong dimerization via quadruple hydrogen bonding,[81,159,264,286] but the association constant and lifetime of the dimers are greatly diminished in polar solvents,[89,221] leading to weak hydrogen-bonded hydrogels.[86,287] Hence, UPy-based hydrogels with high water content and enhanced

mechanical performance were developed by generating hydrophobic pockets to protect hydrogen bonding moieties, such as incorporation of long alkyl-urea spacers,[87,90] structure modification with adamantyl substituent,[91] and formation of sodium dodecyl sulfate (SDS) micelles.[92] In spite of considerable progress in developing various materials with tunable mechanical properties based on "protected" hydrogen-bonding groups, there is still a lack of fundamental understanding of the corresponding intermolecular forces from the molecular perspective, which is crucial for directing self-assembly pathways and developing stable hydrogen-bonded structures.

Over the past two decades, atomic force microscopy (AFM)-based single-molecule force spectroscopy (SMFS) has evolved as a powerful technique for directly measuring inter/intramolecular interaction forces at the single-molecular level with pico-newton resolution,[100,104,288] providing useful information about the underlying unbinding energy landscapes and molecular interaction mechanisms.[289-291] Vansco et al. first detected the rupture forces of individual supramolecular polymer chains bonded by UPy dimers in hexadecane using SMFS, in which the binding strength and kinetic parameters were comparable to the results probed by NMR measurements.[292-294] Recently, single-chain polymeric nanoparticles[295] and biomimetic modular polymers[296] carrying UPy functionalities were also investigated by SMFS, where a complete potential energy profile of binding and unbinding of the hydrogen-bonded dimer was constructed and correlated to their bulk mechanical behaviors. However, the previous SMFS studies on the interactions of UPy groups were all conducted in nonpolar solvents, where the dimerization is favorable. As the polarity of solvent plays an important role in the interaction of hydrogen-bonded arrays,[88,297] it is of great significance to understand the

binding behaviors of the dimeric complexes in aqueous solutions,[298,299] which contribute to numerous self-assembling systems including synthetic hydrogels, colloids and various biological structures.[15,300]

Herein, we present the first attempt to quantitatively characterize the pairwise interactions between hydrogen-bonded UPy dimers in water using AFM-based SMFS. To study the effects of hydrophobic interactions on the intermolecular hydrogen bonding, alkylene spacers of varying lengths are incorporated between the multiple hydrogen-bonding group and the water-soluble poly (ethylene glycol) (PEG) linkers. By conducting dynamic force spectroscopy, we unveil the dynamics and free energy landscapes on dissociation of different alkylene-functionalized UPy dimers. Moreover, complementary molecular dynamics (MD) simulation is performed to obtain the free energies of corresponding UPy dimers as a function of distance in water by umbrella sampling method. Our results provide a fundamental understanding of hydrogen-bonding interactions in aqueous environment at the single-molecular level, which is of significance in directing the self-assembly of molecules based on multiple hydrogen bonds.

5.2 Experimental Methods

5.2.1 Materials

2-Amino-4-hydroxy-6-methylpyrimidine (98%, Aldrich), hexamethylene diisocyanate (98%, Fluka), 1,12-diisocyanatododecane (97%, Aldrich), 1,1′-carbonyldiimidazole (CDI, 97%, Aldrich), polyethylene glycol 1500 (PEG1500, Alfa Aesar), thioctic acid (TA, 98%, Alfa Aesar), N,N'-dicyclohexylcarbodiimide (DCC, 99%, Alfa Aesar), 4-dimethylaminopyridine (DMAP, 99%, ACROS), poly(ethylene glycol)

bis(3-aminopropyl) terminated (NH$_2$-PEG-NH$_2$, Mw~1,500, Aldrich), dibutyltin dilaurate (95%, Aldrich), heptanoic acid (99%, Aldrich), tridecanoic acid (98%, Aldrich), dimethyl sulfoxide (DMSO, anhydrous, 99.9%, Aldrich), methylene chloride (DCM, 99.9%, Fisher)were used as received. Chloroform (CHCl$_3$) was dried over calcium hydride (CaH$_2$) and distilled before use.

5.2.2 Synthesis of Functional PEG Linkers

The synthesis routes of PEG linkers with Cn-UPy (n=3, 6 and 12, which denotes the number of carbon atoms) functionalities were illustrated in **Figure 5.1**. Firstly, PEGs with averaged molecular weight of 1500 Da were attached to thioctic acid via esterification or amidation reaction, and then the 1,2-dithiolane-3-pentyl-derivatized PEGs (TA-PEG-OH and TA-PEG-NH$_2$) reacted with the prepared pyrimidinone-containing molecules (OCN-C6-UPy, OCN-C12-UPy and Im-Py), leading to PEG linkers end-functionalized with hydrophobic and hydrogen-bonding moieties (PEG-Cn-UPy). For comparison, PEG linkers without hydrogen-bonding groups (PEG-C6 and PEG-C12) were also prepared by performing reactions between TA-PEG-OH and heptanoic acid / tridecanoic acid instead of pyrimidinone-containing molecules. The detailed synthesis procedures and ^{1}H NMR characterization of the products are described in **Appendix D**.
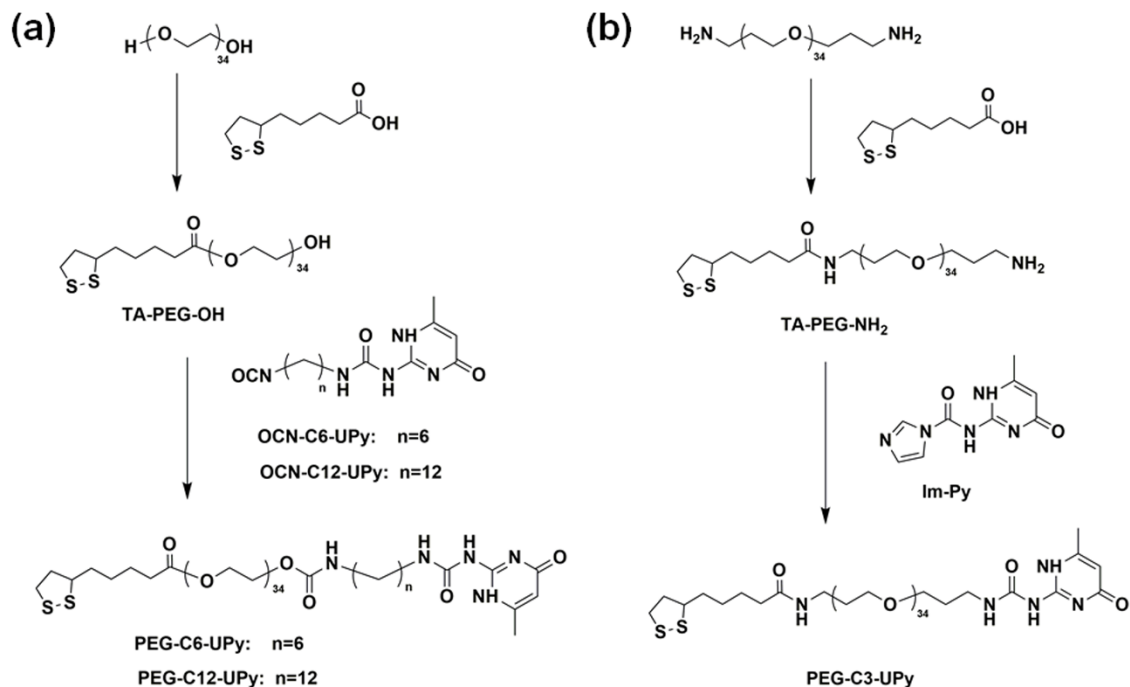
Figure 5.1. Synthesis routes of UPy terminated PEG linkers with different lengths of hydrophobic spacers (a) PEG-C6-UPy, PEG-C12-UPy and (b) PEG-C3-UPy.

5.2.3 Sample Preparation

For all AFM-based SMFS experiments, gold coated silicon nitride cantilevers (NPG-10, spring constant = 0.06~0.35 N/m, Bruker), and gold coated silicon wafers (1×1 cm^2, 100-nm-thick gold, Aldrich) were used. Prior to use, each surface and tip were pre-cleaned by UV/Ozone treatment for 30 min in a UV-ozone chamber (Bioforce Nanosciences). Upon removal, they were rinsed with large amounts of Milli-Q water and ethanol thoroughly, and then dried with high-purity N$_2$ before further modification.

The modification of the gold surfaces was realized by the chemisorption of thioctic-functionalized PEG linkers, where the other end of PEG was functionalized with UPy groups (PEG-C3-UPy, PEG-C6-UPy and PEG-C12-UPy) or alkanes (PEG-C6 and

PEG-C12). A representative example of modification with PEG-C12-UPy is given. PEG-C12-UPy and TA-PEG-OH were dissolved at a molar ratio of PEG-C12-UPy: TA-PEG-OH = 1:8 in anhydrous DMSO at a total concentration of 1 mM, and then the solution was passed through 0.45 μm pore size filters. The high polarity of DMSO would prevent the dimerization of UPy. The hydroxy terminated TA-PEG-OH was used to dilute the number of functional groups (UPy or alkanes). The substrates and tips were immersed in 10 ml of the solution at room temperature for 16 h. Surface modification with PEG-C6-UPy, PEG-C3-UPy, PEG-C6 and PEG-C12 were performed by following the same procedures. The samples were washed thoroughly with DMSO and excessive Milli-Q water, dried in N_2 stream and immediately mounted into the AFM.

5.2.4 Force Measurements.

AFM-based force spectroscopy measurements were carried out with an MFP-3D AFM (Asylum Research) using the chemically modified probes and substrates described above. All the experiments were performed in Milli-Q water (18.2 MΩ·cm, Thermo Scientific) at room temperature. The spring constant of each tip was calibrated by the built-in thermal noise analysis method and was found around 130 pN/nm.

Force-extension curves were obtained by controlling the movement of the piezo tube of the AFM tip approaching to and retracting from the modified substrates. In each detection, the tip was retracted immediately after being in contact with the substrate, and the contact force between the tip and substrate was as low as 2 nN to avoid the physical entanglement of the PEG linkers. In loading rate-dependent force spectroscopy experiments, the probe retract velocity was varied between 400, 800, 1400, 2000 and 2600 nm/s, and more than 2000 force curves were accumulated at different points for

each velocity by scanning over the sample's surface. Igor Pro software (Wave Metrics) was used for the data processing analysis.

5.2.5 Data Analysis

The Force-Extension curves with specific rupture events were fitted with the modified freely-jointed chain (M-FJC) model to characterize the polymer chain by extracting contour length and Kuhn length parameters. The equation of M-FJC model correlates the extension of polymer chain $E(F)$ with applied force F.

$$E(F) \ = \ L_{\mathrm{c}} \left[\coth(\frac{F \cdot l_{\mathrm{k}}}{k_{\mathrm{B}}T} - \frac{k_{\mathrm{B}}T}{F \cdot l_{\mathrm{k}}}) \right] + N \cdot \frac{F}{K_{\mathrm{s}}} \qquad (5.1)$$

where L_{c}, l_{k}, N, K_{s}, k_{B} and T represent contour length, Kuhn length, total number of segments, segment elasticity, Boltzmann constant and temperature, respectively. **Equation 5.1** indicates that the extension of PEG chain is dominated by either l_{k} in the low-force regime or K_{s} in the high-force regime.[301]

In aqueous solutions, both planar and helical conformations could be retained in PEG chains, and the applied force would induce a conformation transition from shorter helical state to elongated planer state. Therefore, contour length L_{c} is dependent on F, and the polymer extension is given by **equation 5.2**.

$$E(F) \ = \ N \cdot \left(\frac{L_{\mathrm{planar}}}{e^{\Delta G(F)/k_{\mathrm{B}}T} + 1} + \frac{L_{\mathrm{helical}}}{e^{-\Delta G(F)/k_{\mathrm{B}}T} + 1} \right) \left[\coth(\frac{F \cdot l_{\mathrm{k}}}{k_{\mathrm{B}}T} - \frac{k_{\mathrm{B}}T}{F \cdot l_{\mathrm{k}}}) \right] + N \cdot \frac{F}{K_{\mathrm{s}}} \qquad (5.2)$$

$$\Delta G(F) = \Delta G_0 - F(L_{\mathrm{planar}} - L_{\mathrm{helical}}) \qquad (5.3)$$

Here, L_{planar} and L_{helical} are the monomer lengths in planar and helical conformations, and are fixed to 3.58 Å and 2.8 Å respectively as reported previously.[103] $\Delta G(F)$ is the

difference in free energy of the two states, and at zero applied force, ΔG_0 is fixed to 3

$k_{\mathrm{B}}T$.[103] The PEG force-extension curves measured in Milli-Q water were fitted with

three parameters: Kuhn length l_{k}, number of segments N, and segment elasticity K_{s}.

These parameters were varied to obtain a close fit to the data near the rupture point.

Dynamic force spectroscopy was carried out to determine the dissociation kinetics

of the complexes, where the loading rates were determined by the pulling velocity of the

probe and the measured spring constant. The most probable rupture forces were obtained

by fitting histograms of rupture forces with Gaussian distributions.

5.2.6 Molecular Dynamics Simulation

All-atom molecular dynamics (MD) simulations were carried out using

GROMACS with GROMOS force field (54A7)[302] for the all-atom models of Cn-UPy

(n=3, 6, 12) dimers. Each pair of the dimers was immersed in an explicit water box with

SPC water molecules. The energy minimization of each system was performed and

followed by NPT equilibration (constant number of particles, pressure and temperature)

at a temperature of 298 K and a pressure of 1 atm for 100 ps. For all the simulations,

electrostatic energy was evaluated by particle mesh Ewald (PME) method[303] with a cut-

off distance of 1.4 nm, and the cut-off distance for van der Waals interactions was also

taken to 1.4 nm.

To conduct umbrella sampling, for each system, a series of configurations were

generated along a reaction coordinate. For each system, 5 ns simulations per window

were performed with a biasing harmonic potential with a spring constant of

$1000 \, \mathrm{kJ/(nm^2 mol)}$. The potential of mean force (PMF) was calculated using the weighted

histogram analysis method (WHAM).[304] The free energy for the unbinding process is the difference between the highest and lowest value of the PMF curve which tends to converge to a stable value with increasing distance.

5.3 Results and Discussion

5.3.1 Single-Molecule Force Spectroscopy

The SMFS experimental setup for measuring interaction forces of hydrogen-bonded dimers is schematically depicted in **Figure 5.2**. The hydrogen-bonding moieties UPy were immobilized on a smooth gold substrate as well as a gold-coated AFM tip via a widely used PEG linker strategy, where the chemisorption of molecules was induced by thioctic acid group linked to one end of the PEG chain. The flexible PEG linker could not only suppress the nonspecific tip-surface interaction but also identify single molecule stretching with well-defined length.[305] To study the hydrophobic effects on hydrogen-bonding groups, alkylene segments of different lengths were tethered between PEG and UPy moieties, and the functionalized groups were named as Cn-UPy (n=3, 6 and 12), where n indicated the number of carbon atoms of the alkylene spacers. The symmetric force measurements were conducted in aqueous medium by bringing Cn-UPy modified AFM tip into contact with the surface functionalized with the same group, and a contact force of 2 nN was applied to facilitate the formation of molecular bonds between two hydrogen-bonding moieties. Upon retracting the AFM probe at a constant force loading rate (R_f) of $1.8 \times 10^5 \, \text{pN/s}$, the stretching of PEG bridges and unbinding forces of molecular dimers were recorded.
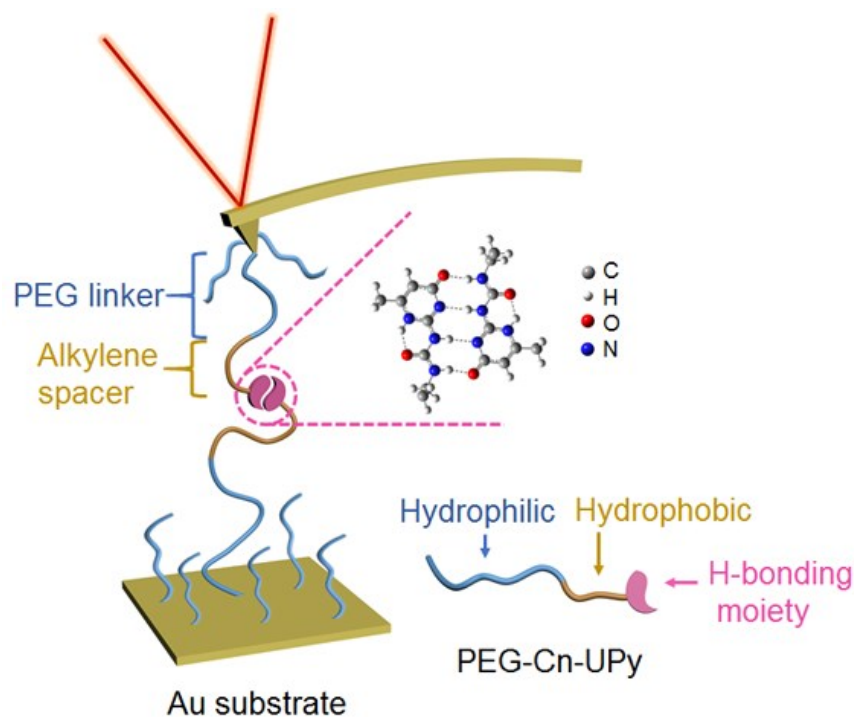
Figure 5.2. Schematic representation of SMFS setup for quantifying the interactions of multiple hydrogen-bonding dimers with hydrophobic alkylene spacers.

Typical force-extension curves exhibiting single molecular bond rupture events are presented in **Figure 5.3a**, in which the blue and black curves represent the force signal of AFM tip approaching to and withdrawing from the surface, respectively. Upon retraction, the initial attractive force within 2 nm separation corresponded to nonspecific interaction of AFM tip with the modified surface. To differentiate the specific molecular binding between Cn-UPy end-capped molecule pairs, the force measurements of "empty tethered" PEG chains which were terminated by hydroxyl groups were performed as control experiments, and a typical force-extension curve between PEG-OH was displayed as the bottom trace in **Figure 5.3a**. In most cases, no specific rupture events could be measured between PEG linkers with a detection probability less than 0.5%, and the

negligible adhesion also revealed extremely weak interactions between the hydrophilic chains.[306] When the flexible PEG linkers were grafted with hydrogen-bonding moieties and hydrophobic spacers, ~10% force profiles with specific rupture events around 20 nm were detected by SMFS. The consistent extension length corresponded to twice the length of PEG linkers used in the surface modification (PEG$_{1500}$ is about 9.5 nm[292]), and it served as an essential signature to identify desired dimer dissociation events from the interference of initial adhesion and other interactions of impurities showing rupture events at random distances.[307] The characteristic stretching events preceded before bond rupture were fitted by modified freely-jointed chain (M-FJC) model taking into account the conformation transition of PEG linkers in water (**Equation 5.2** and **5.3**).[103] From the superimposed traces (red curves in **Figure 5.3a**), the Kuhn length of the flexible linker was obtained as 7 Å and the segment elasticity was found to be around 4 nN/nm, which were in good accordance with the reported mechanical parameters of PEG[292] and thus further confirmed the successful stretching of single PEG chains. The values of rupture forces measured between Cn-UPy dimers are in the range of tens of pN and increase with longer alkylene spacers. Despite the low surface density of UPy groups which were diluted by the utilization of excess hydroxyl-ended PEG linkers, on some rare occasions, multiple rupture events appeared in force profiles indicated multiple binding sites between the two opposite surfaces, and the effect of multiple attachments were eliminated from the following statistical process. **Figure 5.3b-d** display the statistical histograms of rupture forces (F_R) with different functional moieties, and in each case about 200 force profiles showing a single specific rupture event with extensions between 10 and 30 nm were collected, in consideration of the polydispersity of the PEG chains

and different anchoring locations of linkers on AFM tip.[301] By fitting the unimodal histograms with Gaussian distribution, the most probable rupture forces of each dimer could be determined with a distribution width around 15 pN, which is consistent with the force resolution of AFM-based SMFS.[308] When the length of hydrophobic spacer increases from 3 carbon atoms to 6 carbon atoms, the rupture force of UPy-functionalized dimer is only slightly increased from 24 pN to 41 pN. However, with a longer alkylene spacer, the unbinding force of C12-UPy dimer is considerably enhanced to 109 pN, and this value is almost 5 times higher than that of C3-UPy dimer, indicating that the hydrophobic spacer adjacent to the hydrogen bonding group plays a critical role in the interaction of UPy-based dimers in aqueous media and can provide additional binding strength to the dimers. To further evaluate the interaction between hydrophobic segments, SMFS measurements between alkanes in the absence of hydrogen-bonding moiety were conducted, where PEG linkers were tethered with hexane (C6) or dodecane (C12). The rupture forces measured between C6 and C12 dimers were rather low and both within 30 pN (**Figure S5.1** in **Appendix D**). It is worth mentioning that the unbinding force of C12-UPy dimer is much larger than the sum of C3-UPy and C12 dimers, providing direct evidence of synergetic effect between hydrogen bonding and hydrophobic interactions.
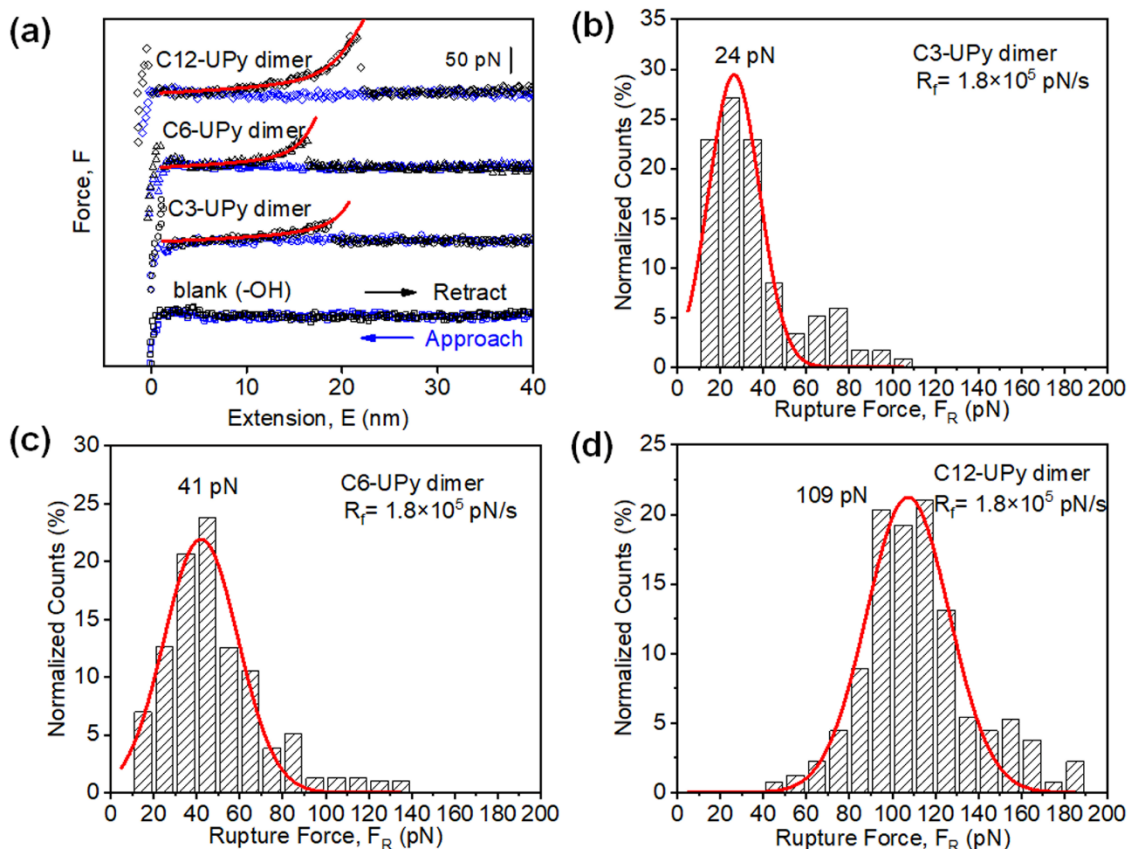
Figure 5.3. (a) Representative force-extension curves measured between PEG-OH or PEG-Cn-UPy (n=3, 6 and 12) dimers by symmetric SMFS at $R_f = 1.8 \times 10^5 \, \text{pN/s}$. The red curves correspond to modified freely-jointed chain (M-FJC) fitting to the rupture events. (b-d) Normalized histograms of rupture forces for individual Cn-UPy (n=3, 6 and 12) dimers. The red curves are Gaussian fits to the corresponding histograms.

Simply comparing the bond dissociation forces at a given pulling speed is not sufficient to fully characterize the binding strength of molecular interactions.[309] To decipher the binding mechanism of Cn-UPy dimers, dynamic force spectroscopy was carried out to evaluate the dissociation kinetics and establish the free energy landscapes of the unbinding processes. The most probable rupture forces of each dimer were systematically determined at five different loading rates, over a range from 4.4×10^4 to

3.4×10^5 pN/s , and the associated histograms with unimodal distributions were summarized in **Figure S5.2-S5.4** in **Appendix D**. **Figure 5.4a** compares the dynamic force spectra of Cn-UPy dimers, presenting the evolution of the most probable rupture force with the corresponding loading rate. It is found that the unbinding forces of both C6-UPy and C12-UPy dimers respond linearly with the logarithm of the loading rate, and the rupture force of C12-UPy dimer is about 4 times higher than that of C6-UPy dimer at each specific loading rate. However, with shorter hydrophobic spacers, the loading rate dependence of the C3-UPy dimer displays two distinct regimes with a clear transition at a pulling speed around 1.8×10^5 pN/s . As reported by Friddle et al., when natural dissociation/association rate of the detected interaction is comparable to or faster than the timescale of the experiments, the thermal equilibrium state of the bond is reached during detection and not affected by the duration of the applied force, leading to a plateau of unbinding force.[310,311] Therefore, at low loading rates, the force required for bond breaking of C3-UPy dimer is insensitive to the loading rate and converges to a constant value of about 25 pN, presenting a typical characteristic of near-equilibrium regime and suggesting the relatively fast kinetics of the bonded structure. While in the range of high loading rates, the logarithmic increase of rupture force with respect to loading rate is similar to the change of C6-UPy and C12-UPy dimers, indicating that the dynamic unbinding processes are kept far from equilibrium, where the bond re-forming is neglected. According to the Bell-Evans theory,[112,113] which describes the deformation of the energy landscape under an externally applied force, we can extract structure information and dynamics of molecular unbinding process by fitting the loading rate-dependent rupture forces using the following equation:

$$F_R = \frac{k_B T}{x_B} \ln\left(\frac{R_f \cdot x_B}{k_B T \cdot k_{off}}\right) \qquad\qquad (5.4)$$

Where F_R is the most probable rupture force, R_f is the loading rate, k_B is the Boltzmann

constant, T and is the absolute temperature. The slope of linear fitting on F_R versus

$\ln R_f$ provides a characteristic dissociation distance x_B, over which the dimer goes from

the bound state to the transition energy barrier; and the dissociation rate k_{off}, which

denotes the thermal off rate in the absence of external force, can be extrapolated from the

interception on the x-axis. Both x_B and k_{off} serve as important measures for the stability

of interactions,[221] and the height of the energy barrier ΔG along the dissociative pathway

is estimated by

$$\Delta G = -k_B T \left(\frac{k_{off}}{A}\right) \qquad\qquad (5.5)$$

A is the Arrhenius prefactor and is kept at 10^7 s^{-1} in our calculation in accordance with

previous studies on hydrophobic alkane pairs in water.[306] The dynamic and energetic

parameters during the unbinding processes of Cn-UPy dimers are summarized in **Figure**

5.4b, and all of the values fall into the range of hydrogen bonding interactions. The

forced unbinding of C3-UPy dimer in water shows a dissociation distance of

$x_B = 0.31$ nm and thermal off rate of $k_{off} = 2,086$ s^{-1}, yielding an energy barrier with the

height of $\Delta G = 21.0$ kJ/mol . Since previous UPy-based SMFS studies conducted in

nonpolar solvents usually gives an energy barrier around 50 kJ/mol,[293,295,296] the much

higher k_{off} and lower ΔG measured in aqueous medium in our experiments indicate that

the hydrogen bonding interaction between UPy groups greatly depends on the local

environment and would be weakened by solvent with high polarity. With increasing

length of the hydrophobic spacer, x_B is found to be reduced to 0.29 nm of C6-UPy and 0.24 nm of C12-UPy, characterizing the corresponding width of energy barriers, and the decreasing distance suggests an extra binding affinity. It should be noted that k_{off} measured in the rupture of C12-UPy dimer is reduced to 21 s^{-1}, which is almost two orders of magnitude lower than that of C3-UPy dimer. The significant difference of k_{off} reveals that when longer hydrophobic segment was tethered to UPy moiety, the molecules would bind to each other more tightly with higher stability. ΔG of C6-UPy and C12-UPy are calculated to be 23.7 kJ/mol and 32.4 kJ/mol, respectively. With longer alkylene spacers, the energy landscape of Cn-UPy becomes steeper and narrower, and it is most likely ascribed to the synergetic effect of hydrophobic spacers. The incorporation of hydrophobic segments tends to supress the solvent-solute interactions between water molecules and UPy groups, which would facilitate the formation of UPy dimers via self-complementary hydrogen bonding with enhanced bonding strength.[88] To differentiate the hydrophobic interactions, dynamic force spectroscopy was also conducted on C6 and C12 dimers (**Figure S5.5 and S5.6** in **Appendix D**), and no increase of the rupture force was observed over the entire range of loading rates (**Figure 5.4c**). The low values of rupture force and the persistence of near-equilibrium regime to high loading rates demonstrate very fast dynamics of the pairwise interaction between the hydrophobic species, and ΔG of C6 and C12 dimers are both expected to be lower than 20 kJ/mol. Therefore, hydrogen bonding interaction between UPy moieties is critical for the formation of dimers, and the presence of long hydrophobic spacers remarkably improves the strength of the dimerization in water. It should be noted that although ΔG is commonly used to denote the binding free energy, they are not identical.[312] Binding

energy is the equilibrium free energy difference between bound state and dissociated state, while in SMFS experiments, ΔG is the barrier height of the rupture transition state, which depends on dissociation pathway.[111,312]
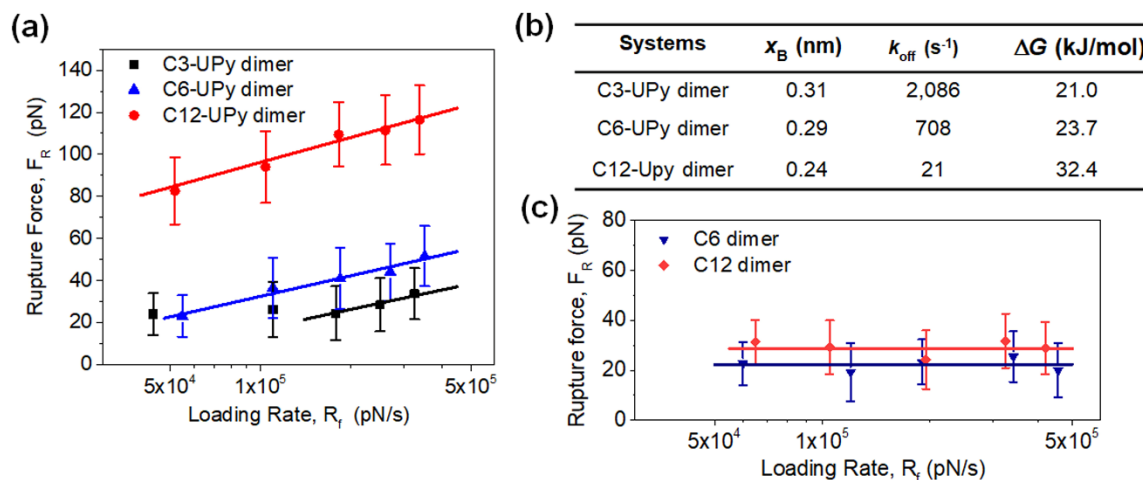
Figure 5.4. (a) Loading rate dependence of the most probable rupture forces for Cn-UPy (n=3, 6 and 12) dimers. (b) Summary of dissociation kinetics and energetic parameters based on the Bell−Evans theory for the unbinding processes of Cn-UPy (n=3, 6 and 12) dimers. (c) Loading rate dependence of the most probable rupture forces for C6 and C12 dimers. In (a) and (c), the error bars present standard deviations of the most probable unbinding forces determined from Gaussian curve fits, and the solid lines correspond to the far-from-equilibrium linear fits by the Bell−Evans model.

5.3.2. Molecular Dynamics Calculations

To gain insight into molecular mechanics and confirm the synergetic effect between hydrogen bonding and hydrophobic interactions revealed by SMFS results, umbrella sampling molecular dynamics simulations were conducted on Cn-UPy (n=3, 6 and 12) dimers without consideration of PEG linkers, where alkanes of different lengths

were tethered to UPy groups. The potential of mean force (PMF) of each dimer was calculated by pulling one molecule from another in an explicit water box (**Figure S5.7 in Appendix D**) and a biasing potential was introduced to the system as a function of the reaction coordinate between two Cn-UPy molecules. The PMF curves were obtained via the weighted histogram analysis method (WHAM).[303] As shown in **Figure 5.5**, the PMF depicts free energy variations versus center-of-mass distance between the two molecules, where notable attractive interactions were detected at the short range. Each curve exhibited an energy minimum starting around 5 Å, which was usually expected to be interactions between nonpolar atoms.[313] However, in our study, the distance is defined based on the center-of-mass between the two molecules, hence short range polar interactions likely contribute to the total free energy variation. The minimum free energy represents the stability of each dimer in equilibrium with water. We can notice that C3-UPy and C6-UPy dimers exhibit shallow energy barriers with free energies of $0.72\,\mathrm{kJ/mol}$ and $1.89\,\mathrm{kJ/mol}$, respectively; but when the length of hydrophobic alkane increases to 12 carbon atoms, the slope of potential becomes quite steep and the binding free energy is rapidly enhanced to $7.37\,\mathrm{kJ/mol}$. The typical configurations of each dimer at three different separating distances were presented in **Figure S5.8** in **Appendix D**. At separations with free energy minima, both of C6-UPy and C12-UPy dimers showed configurations that can form intermolecular hydrogen bonds with short range distance, while the two C3-UPy molecules did not display bonded structure. The results indicate that longer hydrophobic chain adjacent to UPy group would contribute to the stability of hydrogen-bonded dimerization and improve the binding free energy. It should be noted that the binding energies of Cn-UPy dimers calculated from MD simulation are lower

than the SMFS results. One possible reason for the discrepancy is that MD simulations were conducted in equilibrium and reversible free energies were directly calculated, while in non-equilibrium SMFS experiments, the soft PEG linkers would lead to deflected loading rates and an overestimation of the extrapolated equilibrium binding energies.[314,315] Besides, in GROMOS force field exploited in simulation, aliphatic hydrogens are not explicitly modeled, which may lead to a certain deviation.[316] Despite the differences, the values of free energy change with the increasing length of hydrophobic spacers obtained from the two methods are similar. To be specific, the difference of free energy between C6-UPy and C12-UPy dimer was estimated as 8.7 kJ/mol from the experiment, which compares well with the simulation result of 5.5 kJ/mol, and both clearly confirm the enhanced binding strength of the hydrogen-bonded dimers with the assist of hydrophobic interactions at the single-molecular level, where the hydrogen bonding units are not "completely shielded" from the surrounding water.
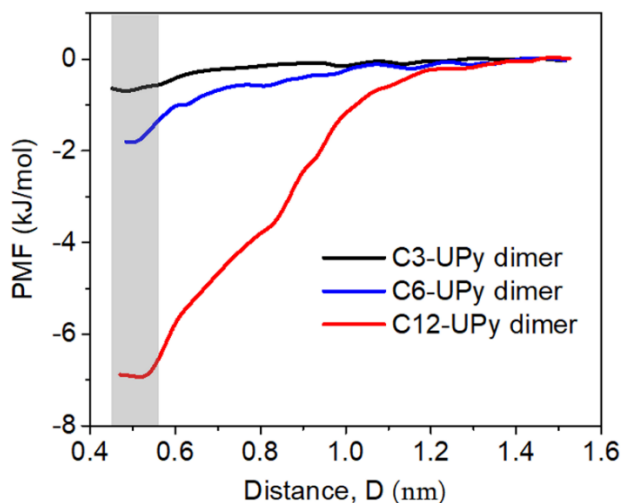
Figure 5.5. PMF plots of free energy change for Cn-UPy (n=3, 6, 12) dimers in bulk water as a function of center-of-mass distance.

5.4 Conclusions

By combining SMFS experimental measurements and MD simulation, we have quantitatively determined the kinetic parameters and nanomechanical strength of multiple hydrogen-bonding interaction between UPy-based dimers in aqueous environment, and the influence of hydrophobic interactions on hydrogen bonds was investigated by tethering different lengths of alkylene spacers to UPy moieties. In SMFS experiments, although the dimerization of UPy was disrupted by water to some extent, the rupture forces and binding energies were found to increase with the spacer length. In good agreement, the complementary MD simulations of UPy dimers also indicated higher structural stability with increasing length of the adjacent hydrophobic segment. Specifically, when the number of carbon atoms of hydrophobic fragment increased from 6 to 12, the binding free energy was enhanced by 8.7 kJ/mol from the experiment, which is in good accordance with the simulation result, revealing synergetic effect between hydrogen bonding and hydrophobic interactions. Our results elucidate the effects of surrounding environment on hydrogen-bonding interactions at the single-molecular level and demonstrate the validity of using hydrophobic interactions to stabilize hydrogen-bonded structures in aqueous environment. This work provides fundamental and practical insights into the design of functional molecular machines, novel self-assembled structures and advanced soft materials based on multiple hydrogen-bonding interactions.

CHAPTER 6   Conclusions and Future Work

6.1 Major Conclusions and Contributions

In this thesis work, the multiple hydrogen-bonding motif 2-ureido-4[1H]-pyrimidinone (UPy) has been applied into various polymeric systems (e.g., micelles, elastomers, hydrogels) for the development of novel supramolecular materials with multifunctionalities, and the interaction mechanism of the hydrogen-bonding groups has been investigated at the single-molecule level. The major conclusions and original contributions are presented as below.

(1) Thermo-responsive core cross-linked polymeric micelles have been prepared from double hydrophilic block copolymers PEG-b-P(NIPAm-co-UPy), where the strong dimerization of the quadruple hydrogen-bonding UPy groups induces non-covalent interactions between the copolymer chains and serves as core cross-linking sites. The stability, size and thermo-responsive properties of the polymer micelles can be readily tuned by the incorporated content of hydrogen-bonding UPy groups. The thermo-responsive loading and release of pyrene molecules (as a model hydrophobic drug) demonstrate a potential application of the synthesized core cross-linked micelles in controlled drug delivery, and the facile fabrication strategy provides new insights into the design of stable and stimuli-responsive polymer micelles with a wide range of applications in drug delivery, diagnosis and sensing.

(2) By triggering in situ polymerization of pyrrole in a UPy-cross-linked supramolecular elastomer matrix, an electrically conductive polymer composite, which combines stretchability, self-healing ability, adhesiveness and sensing capability, has

been readily fabricated via solution casting method. The polypyrrole particles are uniformly dispersed and impart the composite desirable conductive properties (0.88 S/m), while the reversible nature of the dynamic multiple hydrogen bonds in the polymer matrix leads to excellent stretchability (>300%), fast self-healing ability (~5 min) under ambient condition, and universal adhesiveness to a broad range of inorganic and organic substrates. The composite has been successfully exploited as strain sensors for monitoring various human motions such as finger bending and pulse beating, suggesting its great potential in sensing applications and providing a promising approach to the development of flexible electronic materials with multifunctionalities by combining conductive components with supramolecular polymers.

(3) A multifunctional conductive polymer hydrogel with the integration of high conductivity, stretchability, injectability and rapid self-healing ability has been developed via introducing UPy groups as cross-linking points into a brittle PANI/PSS conducting network. The formation of interpenetrating PANI/PSS network offers the hydrogel unique electronic/ionic conduction with a superior conductivity of 13 S/m and a linear response (gauge factor=3.4) to external strain (≈300%). Both large and subtle human motions (e.g., finger bending, throat movement and pulse beating) have been successfully distinguished by employing the hydrogel as wearable sensors, demonstrating its accuracy and reliability for monitoring diverse human activities. Taking advantage of the reversibility of the non-covalent cross-links, the hydrogels can be facilely molded into different shapes and injected from a needle, as well as demonstrate a complete self-healing within 30 s upon damage. The combination of supramolecular chemistry with conducting polymers enables multifunctionalities in the novel type of conductive polymer

hydrogel with inspirations into the design of advanced functional materials with applications in 3D printing, wearable devices (e.g., intelligent skins) and flexible electronics.

(4) The pairwise interactions between hydrogen-bonded UPy dimers and the effects of hydrophobic interactions on the intermolecular hydrogen bonding have been investigated by AFM-based SMFS in aqueous environment in combination with molecular dynamics (MD) simulations. The rupture force and unbinding energy of self-complementary UPy-UPy dimers are found to be remarkably enhanced with increasing spacer length, which reveals cooperative effect between hydrogen bonding and hydrophobic interactions. In good agreement, the MD simulations on interactions of UPy-UPy dimers also indicate higher structural stability with longer hydrophobic spacers. Our results provide quantitative information and fundamental insights into the understanding of the multiple hydrogen-bonding interactions in aqueous environment, with important implications on the design of hydrogen-bonded assemblies for various bioengineering and engineering applications, such as functional molecular machines, novel self-organized structures and advanced soft materials.

6.2 Future Work

In this study, we have introduced the hydrogen-bonding UPy group into micelles, elastomer composites and conducting hydrogels to explore the potential of hydrogen-bonding motifs in the preparation of functional materials and pave the way to applications in diverse fields. However, there are still challenges regarding practical applications, and some recommendations for future research are presented.

117

(1) In biological systems, the changes of physiological conditions (e.g., temperate, pH) are generally subtle; thus, it is desirable to develop stimuli-responsive materials which show sensitive response to the surrounding environment within the range of physiological fluctuations. Besides, different stimuli-responsiveness can be integrated into one system for the development of versatile drug delivery vehicles.

(2) For flexible electronics, high conductivity is still limited in elastic polymeric materials, since the soft polymer matrix are generally non-conductive. By employing deformable highly-conductive additives or forming continuous conductive networks within supramolecular materials, excellent conductivity can be combined with stretchable, adhesive, self-healing properties and other functionalities for the fabrication of high-performance electronic devices.

(3) Robust mechanical properties and self-healing ability has been regarded as a dilemma in materials science. The combination of hydrogen bonding with other interactions (covalent bonds, non-covalent bonds, phase aggregation) in one system can induce synergetic effect and lead to materials with superior properties. The fundamental study in Chapter 5 provides a principle to prepare materials based on hydrogen bonding and hydrophobic interactions, and this technique can be applied to study the mechanism of other interactions, which further facilitates the development and optimization of supramolecular materials.

Bibliography

(1)   Lehn, J. M. Supramolecular polymer chemistry-scope and perspectives. *Polym. Int.* **2002,** *51*, 825-839.

(2)   Brunsveld, L.; Folmer, B.; Meijer, E.; Sijbesma, R. Supramolecular polymers. *Chem. Rev.* **2001,** *101*, 4071-4098.

(3)   Yang, L.; Tan, X.; Wang, Z.; Zhang, X. Supramolecular polymers: historical development, preparation, characterization, and functions. *Chem. Rev.* **2015,** *115*, 7196-7239.

(4)   Seiffert, S.; Sprakel, J. Physical chemistry of supramolecular polymer networks. *Chem. Soc. Rev.* **2012,** *41*, 909-930.

(5)   Rossow, T.; Seiffert, S., Supramolecular polymer networks: Preparation, properties, and potential. *Supramolecular Polymer Networks and Gels*, Springer: Switzerland, 2015.

(6)   Steed, J. W.; Atwood, J. L. *Supramolecular chemistry;* John Wiley & Sons, United Kingdom, 2013.

(7)   Dong, R.; Zhou, Y.; Huang, X.; Zhu, X.; Lu, Y.; Shen, J. Functional supramolecular polymers for biomedical applications. *Adv. Mater.* **2015,** *27*, 498-526.

(8)   Lehn, J. M. Towards complex matter: supramolecular chemistry and self-organization. *Eur. Rev.* **2009,** *17*, 263-280.

(9)   Yan, X.; Wang, F.; Zheng, B.; Huang, F. Stimuli-responsive supramolecular polymeric materials. *Chem. Soc. Rev.* **2012,** *41*, 6042-6065.

(10)   Appel, E. A.; del Barrio, J.; Loh, X. J.; Scherman, O. A. Supramolecular polymeric hydrogels. *Chem. Soc. Rev.* **2012,** *41*, 6195-6214.

(11)   Liu, Y.; Wang, Z.; Zhang, X. Characterization of supramolecular polymers. *Chem. Soc. Rev.* **2012,** *41*, 5922-5932.

(12)   Kellis, J. T.; Nyberg, K.; Fersht, A. R. Contribution of hydrophobic interactions to protein stability. *Nature* **1988,** *333*, 784-786.

(13)   Armstrong, G.; Buggy, M. Hydrogen-bonded supramolecular polymers: A literature review. *J. Mater. Sci.* **2005,** *40*, 547-559.

(14)   Krische, M. J.; Lehn, J.-M., The utilization of persistent H-bonding motifs in the self-assembly of supramolecular architectures. *Molecular Self-Assembly Organic Versus Inorganic Approaches*, Springer: Berlin, 2000.

(15)   Sherrington, D. C.; Taskinen, K. A. Self-assembly in synthetic macromolecular systems via multiple hydrogen bonding interactions. *Chem. Soc. Rev.* **2001,** *30*, 83-93.

(16)   Binder, W. H.; Bernstorff, S.; Kluger, C.; Petraru, L.; Kunz, M. J. Tunable materials from hydrogen-bonded pseudo block copolymers. *Adv. Mater.* **2005,** *17*, 2824-2828.

(17)   Djurdjevic, S.; Leigh, D. A.; McNab, H.; Parsons, S.; Teobaldi, G.; Zerbetto, F. Extremely strong and readily accessible AAA-DDD triple hydrogen bond complexes. *J. Am. Chem. Soc.* **2007,** *129*, 476-477.

(18)   Beijer, F. H.; Kooijman, H.; Spek, A. L.; Sijbesma, R. P.; Meijer, E. Self-complementarity achieved through quadruple hydrogen bonding. *Angew. Chem. Int. Ed.* **1998,** *37*, 75-78.

(19)   Corbin, P. S.; Lawless, L. J.; Li, Z.; Ma, Y.; Witmer, M. J.; Zimmerman, S. C. Discrete and polymeric self-assembled dendrimers: Hydrogen bond-mediated assembly with high stability and high fidelity. *Proc. Natl. Acad. Sci. U.S.A.* **2002,** *99*, 5099-5104.

(20)   Leong, W. L.; Vittal, J. J. One-dimensional coordination polymers: complexity and diversity in structures, properties, and applications. *Chem. Rev.* **2010,** *111*, 688-764.

(21)   Kersey, F. R.; Loveless, D. M.; Craig, S. L. A hybrid polymer gel with controlled rates of cross-link rupture and self-repair. *J. Royal Soc. Interface* **2007,** *4*, 373-380.

(22)   Beck, J. B.; Ineman, J. M.; Rowan, S. J. Metal/ligand-induced formation of metallo-supramolecular polymers. *Macromolecules* **2005,** *38*, 5060-5068.

(23)   Burnworth, M.; Tang, L.; Kumpfer, J. R.; Duncan, A. J.; Beyer, F. L.; Fiore, G. L.; Rowan, S. J.; Weder, C. Optically healable supramolecular polymers. *Nature* **2011,** *472*, 334-337.

(24)   Hofmeier, H.; Schubert, U. S. Recent developments in the supramolecular chemistry of terpyridine-metal complexes. *Chem. Soc. Rev.* **2004,** *33*, 373-399.

(25)   Holten-Andersen, N.; Harrington, M. J.; Birkedal, H.; Lee, B. P.; Messersmith, P. B.; Lee, K. Y. C.; Waite, J. H. pH-induced metal-ligand cross-links inspired by mussel yield self-healing polymer networks with near-covalent elastic moduli. *Proc. Natl. Acad. Sci. U.S.A.* **2011,** *108*, 2651-2655.

(26)   Eisenberg, A.; Rinaudo, M. Polyelectrolytes and ionomers. *Polym. Bull.* **1990,** *24*, 671-671.

(27)   Kim, J.-S.; Jackman, R. J.; Eisenberg, A. Filler and percolation behavior of ionic aggregates in styrene-sodium methacrylate ionomers. *Macromolecules* **1994,** *27*, 2789-2803.

(28)   Tant, M. R.; Mauritz, K. A.; Wilkes, G. L. *Ionomers: synthesis, structure, properties and applications;* Chapman & Hall, New York, 1997.

(29)   Kalista, S. J.; Pflug, J. R.; Varley, R. J. Effect of ionic content on ballistic self-healing in EMAA copolymers and ionomers. *Polym. Chem.* **2013,** *4*, 4910-4926.

(30)   Kim, H. J.; Yang, B.; Park, T. Y.; Lim, S.; Cha, H. J. Complex coacervates based on recombinant mussel adhesive proteins: their characterization and applications. *Soft matter* **2017,** *13*, 7704-7716.

(31)   Chen, Y.; Liu, Y. Cyclodextrin-based bioactive supramolecular assemblies. *Chem. Soc. Rev.* **2010,** *39*, 495-505.

(32)   Kim, K.; Selvapalam, N.; Ko, Y. H.; Park, K. M.; Kim, D.; Kim, J. Functionalized cucurbiturils and their applications. *Chem. Soc. Rev.* **2007,** *36*, 267-279.

(33)   Szejtli, J. Introduction and general overview of cyclodextrin chemistry. *Chem. Rev.* **1998,** *98*, 1743-1754.

(34)   Kretschmann, O.; Choi, S. W.; Miyauchi, M.; Tomatsu, I.; Harada, A.; Ritter, H. Switchable hydrogels obtained by supramolecular cross-linking of adamantyl-containing LCST copolymers with cyclodextrin dimers. *Angew. Chem. Int. Ed.* **2006,** *45*, 4361-4365.

(35)   Liu, S.; Ruspic, C.; Mukhopadhyay, P.; Chakrabarti, S.; Zavalij, P. Y.; Isaacs, L. The cucurbit[n]uril family: prime components for self-sorting systems. *J. Am. Chem. Soc.* **2005,** *127*, 15959-15967.

(36)   Kim, J.; Jung, I. S.; Kim, S. Y.; Lee, E.; Kang, J. K.; Sakamoto, S.; Yamaguchi, K.; Kim, K. New cucurbituril homologues: syntheses, isolation, characterization, and X-ray crystal structures of cucurbit[n]uril (n= 5, 7, and 8). *J. Am. Chem. Soc.* **2000,** *122*, 540-541.

(37)   Fang, L.; Olson, M. A.; Benítez, D.; Tkatchouk, E.; Goddard III, W. A.; Stoddart, J. F. Mechanically bonded macromolecules. *Chem. Soc. Rev.* **2010,** *39*, 17-29.

(38)   Zhu, Z.; Cardin, C. J.; Gan, Y.; Murray, C. A.; White, A. J.; Williams, D. J.; Colquhoun, H. M. Conformational modulation of sequence recognition in synthetic macromolecules. *J. Am. Chem. Soc.* **2011,** *133*, 19442-19447.

(39)   Burattini, S.; Greenland, B. W.; Merino, D. H.; Weng, W.; Seppala, J.; Colquhoun, H. M.; Hayes, W.; Mackay, M. E.; Hamley, I. W.; Rowan, S. J. A healable supramolecular polymer blend based on aromatic π-π stacking and hydrogen-bonding interactions. *J. Am. Chem. Soc.* **2010,** *132*, 12051-12058.

(40)   Berl, V.; Schmutz, M.; Krische, M. J.; Khoury, R. G.; Lehn, J. M. Supramolecular polymers generated from heterocomplementary monomers linked through multiple hydrogen-bonding arrays-formation, characterization, and properties. *Chem. Eur. J.* **2002,** *8*, 1227-1244.

(41)   Yang, S. K.; Ambade, A. V.; Weck, M. Main-chain supramolecular block copolymers. *Chem. Soc. Rev.* **2011,** *40*, 129-137.

(42)   Martin, R. B. Comparisons of indefinite self-association models. *Chem. Rev.* **1996,** *96*, 3043-3064.

(43)   Vallerien, S.; Werth, M.; Kremer, F.; Spiess, H. Molecular dynamics and the glass transition in a columnar liquid crystal formed by a chiral discotic mesogen. *Liq. Cryst.* **1990,** *8*, 889-893.

(44)   Dong, R.; Zhou, Y.; Zhu, X. Supramolecular dendritic polymers: from synthesis to applications. *Acc. Chem. Res.* **2014,** *47*, 2006-2016.

(45)   Tian, W.; Li, X.; Wang, J. Supramolecular hyperbranched polymers. *Chem. Commun.* **2017,** *53*, 2531-2542.

(46)   Voorhaar, L.; Hoogenboom, R. Supramolecular polymer networks: hydrogels and bulk materials. *Chem. Soc. Rev.* **2016,** *45*, 4013-4031.

(47)   Fox, J. D.; Rowan, S. J. Supramolecular polymerizations and main-chain supramolecular polymers. *Macromolecules* **2009,** *42*, 6823-6835.

(48)   Dankers, P. Y.; Hermans, T. M.; Baughman, T. W.; Kamikawa, Y.; Kieltyka, R. E.; Bastings, M.; Janssen, H. M.; Sommerdijk, N. A.; Larsen, A.; van Luyn, M. J. Hierarchical formation of supramolecular transient networks in water: A modular injectable delivery system. *Adv. Mater.* **2012,** *24*, 2703-2709.

(49)   Li, J.; Viveros, J. A.; Wrue, M. H.; Anthamatten, M. Shape-memory effects in polymer networks containing reversibly associating side-groups. *Adv. Mater.* **2007,** *19*, 2851-2855.

(50)   Appel, E. A.; Biedermann, F.; Rauwald, U.; Jones, S. T.; Zayed, J. M.; Scherman, O. A. Supramolecular cross-linked networks via host-guest complexation with cucurbit[8]uril. *J. Am. Chem. Soc.* **2010,** *132*, 14251-14260.

(51)   Zhang, Q.; Qu, D.-H.; Wu, J.; Ma, X.; Wang, Q.; Tian, H. A dual-modality photoswitchable supramolecular polymer. *Langmuir* **2013,** *29*, 5345-5350.

(52)   Nakahata, M.; Mori, S.; Takashima, Y.; Hashidzume, A.; Yamaguchi, H.; Harada, A. pH- and sugar-responsive gel assemblies based on boronate-catechol interactions. *ACS Macro Lett.* **2014,** *3*, 337-340.

(53)   Shan, M.; Gong, C.; Li, B.; Wu, G. A pH, glucose, and dopamine triple-responsive, self-healable adhesive hydrogel formed by phenylborate-catechol complexation. *Polym. Chem.* **2017,** *8*, 2997-3005.

(54)   Miller, A. K.; Li, Z.; Streletzky, K. A.; Jamieson, A. M.; Rowan, S. J. Redox-induced polymerisation/depolymerisation of metallo-supramolecular polymers. *Polym. Chem.* **2012,** *3*, 3132-3138.

(55)   Syrett, J. A.; Becer, C. R.; Haddleton, D. M. Self-healing and self-mendable polymers. *Polym. Chem.* **2010,** *1*, 978-987.

(56)   Murphy, E. B.; Wudl, F. The world of smart healable materials. *Prog. Polym. Sci.* **2010,** *35*, 223-251.

(57)   Liu, F.; Urban, M. W. Recent advances and challenges in designing stimuli-responsive polymers. *Prog. Polym. Sci.* **2010,** *35*, 3-23.

(58)   Blaiszik, B.; Kramer, S.; Olugebefola, S.; Moore, J. S.; Sottos, N. R.; White, S. R. Self-healing polymers and composites. *Annu. Rev. Mater. Res.* **2010,** *40*, 179-211.

(59)   Wu, D. Y.; Meure, S.; Solomon, D. Self-healing polymeric materials: a review of recent developments. *Prog. Polym. Sci.* **2008,** *33*, 479-522.

(60)   Yang, Y.; Urban, M. W. Self-healing polymeric materials. *Chem. Soc. Rev.* **2013,** *42*, 7446-7467.

(61)   Hayes, W.; Greenland, B. W. *Healable Polymer Systems;* Royal Society of Chemistry, United Kingdom, 2013.

(62)   Wei, Z.; He, J.; Liang, T.; Oh, H.; Athas, J.; Tong, Z.; Wang, C.; Nie, Z. Autonomous self-healing of poly (acrylic acid) hydrogels induced by the migration of ferric ions. *Polym. Chem.* **2013,** *4*, 4601-4605.

(63)   Holten-Andersen, N.; Jaishankar, A.; Harrington, M. J.; Fullenkamp, D. E.; DiMarco, G.; He, L.; McKinley, G. H.; Messersmith, P. B.; Lee, K. Y. C. Metal-coordination: using one of nature's tricks to control soft material mechanics. *J. Mater. Chem. B* **2014,** *2*, 2467-2472.

(64)   Ahn, B. K.; Lee, D. W.; Israelachvili, J. N.; Waite, J. H. Surface-initiated self-healing of polymers in aqueous media. *Nat. Mater.* **2014,** *13*, 867.

(65)   Li, L.; Yan, B.; Yang, J.; Chen, L.; Zeng, H. Novel mussel-inspired injectable self-healing hydrogel with anti-biofouling property. *Adv. Mater.* **2015,** *27*, 1294-1299.

(66)   Chen, Y.; Kushner, A. M.; Williams, G. A.; Guan, Z. Multiphase design of autonomic self-healing thermoplastic elastomers. *Nat. Chem.* **2012,** *4*, 467-472.

(67)   Tee, B. C.; Wang, C.; Allen, R.; Bao, Z. An electrically and mechanically self-healing composite with pressure-and flexion-sensitive properties for electronic skin applications. *Nat. Nanotechnol.* **2012,** *7*, 825-832.

(68)   Vaiyapuri, R.; Greenland, B. W.; Rowan, S. J.; Colquhoun, H. M.; Elliott, J. M.; Hayes, W. Thermoresponsive supramolecular polymer network comprising pyrene-functionalized gold nanoparticles and a chain-folding polydiimide. *Macromolecules* **2012,** *45*, 5567-5574.

(69)   Yan, T.; Schröter, K.; Herbst, F.; Binder, W. H.; Thurn-Albrecht, T. Nanostructure and rheology of hydrogen-bonding telechelic polymers in the melt: From micellar liquids and solids to supramolecular gels. *Macromolecules* **2014,** *47*, 2122-2130.

(70)   Sivakova, S.; Bohnsack, D. A.; Mackay, M. E.; Suwanmala, P.; Rowan, S. J. Utilization of a combination of weak hydrogen-bonding interactions and phase segregation to yield highly thermosensitive supramolecular polymers. *J. Am. Chem. Soc.* **2005,** *127*, 18202-18211.

(71)   Versteegen, R. M.; Kleppinger, R.; Sijbesma, R. P.; Meijer, E. Properties and morphology of segmented copoly (ether urea) s with uniform hard segments. *Macromolecules* **2006,** *39*, 772-783.

(72)   Wisse, E.; Govaert, L.; Meijer, H.; Meijer, E. Unusual tuning of mechanical properties of thermoplastic elastomers using supramolecular fillers. *Macromolecules* **2006,** *39*, 7425-7432.

(73)   Wisse, E.; Spiering, A.; Pfeifer, F.; Portale, G.; Siesler, H.; Meijer, E. Segmental orientation in well-defined thermoplastic elastomers containing supramolecular fillers. *Macromolecules* **2008,** *42*, 524-530.

(74)   Besenius, P.; Portale, G.; Bomans, P. H.; Janssen, H. M.; Palmans, A. R.; Meijer, E. Controlling the growth and shape of chiral supramolecular polymers in water. *Proc. Natl. Acad. Sci. U.S.A.* **2010,** *107*, 17888-17893.

(75)   Jeffrey, G. A.; Saenger, W. *Hydrogen bonding in biological structures;* Springer, Berlin, 2012.

(76)   Smulders, M. M.; Schenning, A. P.; Meijer, E. Insight into the mechanisms of cooperative self-assembly: The "sergeants-and-soldiers" principle of chiral and achiral C3-symmetrical discotic triamides. *J. Am. Chem. Soc.* **2008,** *130*, 606-611.

(77)   Cordier, P.; Tournilhac, F.; Soulié-Ziakovic, C.; Leibler, L. Self-healing and thermoreversible rubber from supramolecular assembly. *Nature* **2008,** *451*, 977-980.

(78)   Sijbesma, R. P.; Beijer, F. H.; Brunsveld, L.; Folmer, B. J.; Hirschberg, J. K.; Lange, R. F.; Lowe, J. K.; Meijer, E. Reversible polymers formed from self-complementary monomers using quadruple hydrogen bonding. *Science* **1997,** *278*, 1601-1604.

(79)   Dankers, P. Y.; van Leeuwen, E. N.; van Gemert, G. M.; Spiering, A.; Harmsen, M. C.; Brouwer, L. A.; Janssen, H. M.; Bosman, A. W.; van Luyn, M. J.; Meijer, E. Chemical and biological properties of supramolecular polymer systems based on oligocaprolactones. *Biomaterials* **2006,** *27*, 5490-5501.

(80)   Colquhoun, H.; Klumperman, B. Self-healing polymers. *Polym. Chem.* **2013,** *4*, 4832-4833.

(81)   Bosman, A. W.; Sijbesma, R. P.; Meijer, E. Supramolecular polymers at work. *Mater. Today* **2004,** *7*, 34-39.

(82)   van Gemert, G. M.; Peeters, J. W.; Söntjens, S. H.; Janssen, H. M.; Bosman, A. W. Self-healing supramolecular polymers in action. *Macromol. Chem. Phys.* **2012,** *213*, 234-242.

(83)   Feldman, K. E.; Kade, M. J.; de Greef, T. F.; Meijer, E.; Kramer, E. J.; Hawker, C. J. Polymers with multiple hydrogen-bonded end groups and their blends. *Macromolecules* **2008,** *41*, 4694-4700.

(84)   Hentschel, J.; Kushner, A. M.; Ziller, J.; Guan, Z. Self-healing supramolecular block copolymers. *Angew. Chem.* **2012,** *124*, 10713-10717.

(85)   Phadke, A.; Zhang, C.; Arman, B.; Hsu, C. C.; Mashelkar, R. A.; Lele, A. K.; Tauber, M. J.; Arya, G.; Varghese, S. Rapid self-healing hydrogels. *Proc. Natl. Acad. Sci. U.S.A.* **2012,** *109*, 4383-4388.

(86)   Cui, J.; del Campo, A. Multivalent H-bonds for self-healing hydrogels. *Chem. Commun.* **2012,** *48*, 9302-9304.

(87)   Guo, M.; Pitet, L. M.; Wyss, H. M.; Vos, M.; Dankers, P. Y.; Meijer, E. Tough stimuli-responsive supramolecular hydrogels with hydrogen-bonding network junctions. *J. Am. Chem. Soc.* **2014,** *136*, 6969-6977.

(88)   Hunter, C. A. Quantifying intermolecular interactions: guidelines for the molecular recognition toolbox. *Angew. Chem. Int. Ed.* **2004,** *43*, 5310-5324.

(89)   Sun, H.; Lee, H. H.; Blakey, I.; Dargaville, B.; Chirila, T. V.; Whittaker, A. K.; Smith, S. C. Multiple hydrogen-bonded complexes based on 2-ureido-4[1H]-pyrimidinone: a theoretical study. *J. Phys. Chem. B* **2011,** *115*, 11053-11062.

(90)   Bastings, M.; Koudstaal, S.; Kieltyka, R. E.; Nakano, Y.; Pape, A.; Feyen, D. A.; Van Slochteren, F. J.; Doevendans, P. A.; Sluijter, J. P.; Meijer, E. A fast pH-switchable and self-healing supramolecular hydrogel carrier for guided, local catheter injection in the infarcted myocardium. *Adv. Healthc. Mater.* **2014,** *3*, 70-78.

(91)   Chirila, T. V.; Lee, H. H.; Oddon, M.; Nieuwenhuizen, M. M.; Blakey, I.; Nicholson, T. M. Hydrogen-bonded supramolecular polymers as self-healing hydrogels: effect of a bulky adamantyl substituent in the ureido-pyrimidinone monomer. *J. Appl. Polym. Sci.* **2014,** *131*, No. 39932.

(92)   Jeon, I.; Cui, J.; Illeperuma, W. R.; Aizenberg, J.; Vlassak, J. J. Extremely stretchable and fast self-healing hydrogels. *Adv. Mater.* **2016,** *28*, 4678-4683.

(93)   Maes, F.; Montarnal, D.; Cantournet, S.; Tournilhac, F.; Corté, L.; Leibler, L. Activation and deactivation of self-healing in supramolecular rubbers. *Soft Matter* **2012,** *8*, 1681-1687.

(94)   Zhang, R.; Yan, T.; Lechner, B.-D.; Schröter, K.; Liang, Y.; Li, B.; Furtado, F.; Sun, P.; Saalwächter, K. Heterogeneity, segmental and hydrogen bond dynamics, and aging of supramolecular self-healing bubber. *Macromolecules* **2013,** *46*, 1841-1850.

(95)   Faghihnejad, A.; Feldman, K. E.; Yu, J.; Tirrell, M. V.; Israelachvili, J. N.; Hawker, C. J.; Kramer, E. J.; Zeng, H. Adhesion and surface interactions of a self-healing polymer with multiple hydrogen-bonding groups. *Adv. Funct. Mater.* **2013,** *24*, 2322-2333.

(96)   Giannotti, M. I.; Vancso, G. J. Interrogation of single synthetic polymer chains and polysaccharides by AFM-based force spectroscopy. *Chemphyschem* **2007,** *8*, 2290-2307.

(97)   Clausen-Schaumann, H.; Seitz, M.; Krautbauer, R.; Gaub, H. E. Force spectroscopy with single bio-molecules. *Curr. Opin. Chem. Biol.* **2000,** *4*, 524-530.

(98)   Binnig, G.; Quate, C. F.; Gerber, C. Atomic force microscope. *Phys. Rev. Lett.* **1986,** *56*, 930-933.

(99)   Puntheeranurak, T.; Neundlinger, I.; Kinne, R. K.; Hinterdorfer, P. Single-molecule recognition force spectroscopy of transmembrane transporters on living cells. *Nat. Protoc.* **2011,** *6*, 1443-1452.

(100)   Hinterdorfer, P.; Dufrêne, Y. F. Detection and localization of single molecular recognition events using atomic force microscopy. *Nat. Methods* **2006,** *3*, 347-355.

(101)   Hugel, T.; Seitz, M. The study of molecular interactions by AFM force spectroscopy. *Macromol. Rapid Commun.* **2001,** *22*, 989-1016.

(102)   Janshoff, A.; Neitzert, M.; Oberdörfer, Y.; Fuchs, H. Force spectroscopy of molecular systems-single molecule spectroscopy of polymers and biomolecules. *Angew. Chem. Int. Ed.* **2000,** *39*, 3212-3237.

(103)   Oesterhelt, F.; Rief, M.; Gaub, H. Single molecule force spectroscopy by AFM indicates helical structure of poly (ethylene-glycol) in water. *New J. Phys.* **1999,** *1*, 6.

(104)   Zhang, W.; Zhang, X. Single molecule mechanochemistry of macromolecules. *Prog. Polym. Sci.* **2003,** *28*, 1271-1295.

(105)   Smith, S. B.; Finzi, L.; Bustamante, C. Direct mechanical measurements of the elasticity of single DNA molecules by using magnetic beads. *Science* **1992,** *258*, 1122-1126.

(106)   Marko, J. F.; Siggia, E. D. Stretching DNA. *Macromolecules* **1995,** *28*, 8759-8770.

(107)   Ortiz, C.; Hadziioannou, G. Entropic elasticity of single polymer chains of poly (methacrylic acid) measured by atomic force microscopy. *Macromolecules* **1999,** *32*, 780-787.

(108)   Smith, S. B.; Cui, Y.; Bustamante, C. Overstretching B-DNA: the elastic response of individual double-stranded and single-stranded DNA molecules. *Science* **1996,** *271*, 795-799.

(109)   Strick, T.; Dessinges, M.; Charvin, G.; Dekker, N.; Allemand, J.; Bensimon, D.; Croquette, V. Stretching of macromolecules and proteins. *Rep. Prog. Phys.* **2002,** *66*, 1-45.

(110)   Carrion-Vazquez, M.; Oberhauser, A. F.; Fisher, T. E.; Marszalek, P. E.; Li, H.; Fernandez, J. M. Mechanical design of proteins studied by single-molecule force spectroscopy and protein engineering. *Prog. Biophys. Mol. Biol.* **2000,** *74*, 63-91.

(111)   Strunz, T.; Oroszlan, K.; Schumakovitch, I.; Güntherodt, H.-J.; Hegner, M. Model energy landscapes and the force-induced dissociation of ligand-receptor bonds. *Biophys. J.* **2000,** *79*, 1206-1212.

(112)   Merkel, R.; Nassoy, P.; Leung, A.; Ritchie, K.; Evans, E. Energy landscapes of receptor-ligand bonds explored with dynamic force spectroscopy. *Nature* **1999,** *397*, 50-53.

(113)   Evans, E. Probing the relation between force-lifetime-and chemistry in single molecular bonds. *Annu. Rev. Biophys. Biomol. Struct.* **2001,** *30*, 105-128.

(114)   Evans, E.; Ritchie, K. Dynamic strength of molecular adhesion bonds. *Biophys. J.* **1997,** *72*, 1541-1555.

(115)   Rösler, A.; Vandermeulen, G. W.; Klok, H.-A. Advanced drug delivery devices via self-assembly of amphiphilic block copolymers. *Adv. Drug Deliv. Rev.* **2012,** *64*, 270-279.

(116)   Cheng, Y.; Hao, J.; Lee, L. A.; Biewer, M. C.; Wang, Q.; Stefan, M. C. Thermally controlled release of anticancer drug from self-assembled γ-substituted amphiphilic poly (ε-caprolactone) micellar nanoparticles. *Biomacromolecules* **2012,** *13*, 2163-2173.

(117)   Hao, J.; Cheng, Y.; Ranatunga, R. U.; Senevirathne, S.; Biewer, M. C.; Nielsen, S. O.; Wang, Q.; Stefan, M. C. A combined experimental and computational study of the substituent effect on micellar behavior of γ-substituted thermoresponsive amphiphilic poly (ε-caprolactone)s. *Macromolecules* **2013,** *46*, 4829-4838.

(118)   Trubetskoy, V. S. Polymeric micelles as carriers of diagnostic agents. *Adv. Drug Deliv. Rev.* **1999,** *37*, 81-88.

(119)   Gao, G. H.; Li, Y.; Lee, D. S. Environmental pH-sensitive polymeric micelles for cancer diagnosis and targeted therapy. *J. Control. Release* **2013,** *169*, 180-184.

(120)   Ma, B.; Wu, S.; Zeng, F.; Luo, Y.; Zhao, J.; Tong, Z. Nanosized diblock copolymer micelles as a scaffold for constructing a ratiometric fluorescent sensor for metal ion detection in aqueous media. *Nanotechnology* **2010,** *21*, No. 195501.

(121)   Hu, J.; Liu, S. Responsive polymers for detection and sensing applications: current status and future developments. *Macromolecules* **2010,** *43*, 8315-8330.

(122)   Menezes, W.; Zielasek, V.; Thiel, K.; Hartwig, A.; Bäumer, M. Effects of particle size, composition, and support on catalytic activity of AuAg nanoparticles prepared in reverse block copolymer micelles as nanoreactors. *J. Catal.* **2013,** *299*, 222-231.

(123)   Cölfen, H. Double-hydrophilic block copolymers: synthesis and application as novel surfactants and crystal growth modifiers. *Macromol. Rapid Commun.* **2001,** *22*, 219-252.

(124)   Bütün, V.; Liu, S.; Weaver, J.; Bories-Azeau, X.; Cai, Y.; Armes, S. A brief review of 'schizophrenic' block copolymers. *React. Funct. Polym.* **2006,** *66*, 157-165.

(125)   Wang, L.; Liu, G.; Wang, X.; Hu, J.; Zhang, G.; Liu, S. Acid-disintegratable polymersomes of pH-responsive amphiphilic diblock copolymers for intracellular drug delivery. *Macromolecules* **2015,** *48*, 7262-7272.

(126)   Zhou, Y.; Jiang, K.; Song, Q.; Liu, S. Thermo-induced formation of unimolecular and multimolecular micelles from novel double hydrophilic multiblock copolymers of N, N-dimethylacrylamide and N-isopropylacrylamide. *Langmuir* **2007,** *23*, 13076-13084.

(127)   Zhang, X.; Li, J.; Li, W.; Zhang, A. Synthesis and characterization of thermo- and pH-responsive double-hydrophilic diblock copolypeptides. *Biomacromolecules* **2007,** *8*, 3557-3567.

(128)   Mountrichas, G.; Pispas, S. Synthesis and pH responsive self-assembly of new double hydrophilic block copolymers. *Macromolecules* **2006,** *39*, 4767-4774.

(129)   Wang, D.; Wu, T.; Wan, X.; Wang, X.; Liu, S. Purely salt-responsive micelle formation and inversion based on a novel schizophrenic sulfobetaine block copolymer: structure and kinetics of micellization. *Langmuir* **2007,** *23*, 11866-11874.

(130)   Cheng, C.; Wei, H.; Shi, B. X.; Cheng, H.; Li, C.; Gu, Z. W.; Cheng, S. X.; Zhang, X. Z.; Zhuo, R. X. Biotinylated thermoresponsive micelle self-assembled from double-hydrophilic block copolymer for drug delivery and tumor target. *Biomaterials* **2008,** *29*, 497-505.

(131)   Lee, S.; Saito, K.; Lee, H. R.; Lee, M. J.; Shibasaki, Y.; Oishi, Y.; Kim, B. S. Hyperbranched double hydrophilic block copolymer micelles of poly (ethylene oxide) and polyglycerol for pH-responsive drug delivery. *Biomacromolecules* **2012,** *13*, 1190-1196.

(132)   He, C.; Kim, S. W.; Lee, D. S. In situ gelling stimuli-sensitive block copolymer hydrogels for drug delivery. *J. Control. Release* **2008,** *127*, 189-207.

(133)   Yao, C.; Wang, X.; Liu, G.; Hu, J.; Liu, S. Distinct morphological transitions of photoreactive and thermoresponsive vesicles for controlled release and nanoreactors. *Macromolecules* **2016,** *49*, 8282-8295.

(134) Ge, Z.; Xie, D.; Chen, D.; Jiang, X.; Zhang, Y.; Liu, H.; Liu, S. Stimuli-responsive double hydrophilic block copolymer micelles with switchable catalytic activity. *Macromolecules* **2007,** *40*, 3538-3546.

(135) Zhang, J.; Jiang, X.; Zhang, Y.; Li, Y.; Liu, S. Facile fabrication of reversible core cross-linked micelles possessing thermosensitive swellability. *Macromolecules* **2007,** *40*, 9125-9132.

(136) Ding, J.; Zhuang, X.; Xiao, C.; Cheng, Y.; Zhao, L.; He, C.; Tang, Z.; Chen, X. Preparation of photo-cross-linked pH-responsive polypeptide nanogels as potential carriers for controlled drug delivery. *J. Mater. Chem.* **2011,** *21*, 11383-11391.

(137) O'Reilly, R. K.; Hawker, C. J.; Wooley, K. L. Cross-linked block copolymer micelles: functional nanostructures of great potential and versatility. *Chem. Soc. Rev.* **2006,** *35*, 1068-1083.

(138) van Nostrum, C. F. Covalently cross-linked amphiphilic block copolymer micelles. *Soft Matter* **2011,** *7*, 3246-3259.

(139) Ding, J.; Chen, L.; Xiao, C.; Chen, L.; Zhuang, X.; Chen, X. Noncovalent interaction-assisted polymeric micelles for controlled drug delivery. *Chem. Commun.* **2014,** *50*, 11274-11290.

(140) Nishihara, M.; Imato, K.; Irie, A.; Kanehara, T.; Kano, A.; Maruyama, A.; Takahara, A.; Otsuka, H. Reversibly crosslinked polymeric micelles formed by autonomously exchangeable dynamic covalent bonds. *Chem. Lett.* **2013,** *42*, 377-379.

(141) Lee, A. L.; Venkataraman, S.; Sirat, S. B.; Gao, S.; Hedrick, J. L.; Yang, Y. Y. The use of cholesterol-containing biodegradable block copolymers to exploit hydrophobic interactions for the delivery of anticancer drugs. *Biomaterials* **2012,** *33*, 1921-1928.

(142) Hsieh, Y.-H.; Hsiao, Y.-T.; Jan, J.-S. Shell and core cross-linked poly (l-lysine)/poly (acrylic acid) complex micelles. *Soft matter* **2014,** *10*, 9568-9576.

(143) Bontha, S.; Kabanov, A. V.; Bronich, T. K. Polymer micelles with cross-linked ionic cores for delivery of anticancer drugs. *J. Control. Release* **2006,** *114*, 163-174.

(144) Zhang, J.; Ma, P. X. Host-guest interactions mediated nano-assemblies using cyclodextrin-containing hydrophilic polymers and their biomedical applications. *Nano Today* **2010,** *5*, 337-350.

(145) Ge, Z.; Liu, S. Facile fabrication of multistimuli-responsive metallo-supramolecular core cross-linked block copolymer micelles. *Macromol. Rapid Commun.* **2013,** *34*, 922-930.

(146) HaáHwang, G.; HyunáMin, K.; JaeáLee, H.; YoungáNam, H.; HyunáChoi, G.; JooáKim, B.; YoungáJeong, S.; CheonáLee, S. pH-Responsive robust polymer micelles with metal-ligand coordinated core cross-links. *Chem. Commun.* **2014,** *50*, 4351-4353.

(147) Kim, S. H.; Tan, J. P.; Nederberg, F.; Fukushima, K.; Colson, J.; Yang, C.; Nelson, A.; Yang, Y. Y.; Hedrick, J. L. Hydrogen bonding-enhanced micelle assemblies for drug delivery. *Biomaterials* **2010,** *31*, 8063-8071.

(148) Fan, J.; Zeng, F.; Wu, S.; Wang, X. Polymer micelle with pH-triggered hydrophobic-hydrophilic transition and de-cross-linking process in the core and its application for targeted anticancer drug delivery. *Biomacromolecules* **2012,** *13*, 4126-4137.

(149) Kuang, H.; Wu, S.; Meng, F.; Xie, Z.; Jing, X.; Huang, Y. Core-crosslinked amphiphilic biodegradable copolymer based on the complementary multiple hydrogen bonds of nucleobases: synthesis, self-assembly and in vitro drug delivery. *J. Mater. Chem.* **2012,** *22*, 24832-24840.

(150) Hauser, C. A.; Zhang, S. Designer self-assembling peptide nanofiber biological materials. *Chem. Soc. Rev.* **2010,** *39*, 2780-2790.

(151) Ishige, R.; Williams, G. A.; Higaki, Y.; Ohta, N.; Sato, M.; Takahara, A.; Guan, Z. In situ ultra-small-angle X-ray scattering study under uniaxial stretching of colloidal crystals prepared by silica nanoparticles bearing hydrogen-bonding polymer grafts. *IUCrJ* **2016,** *3*, 211-218.

(152) Montarnal, D.; Delbosc, N.; Chamignon, C.; Virolleaud, M. A.; Luo, Y.; Hawker, C. J.; Drockenmuller, E.; Bernard, J. Highly ordered nanoporous films from

supramolecular diblock copolymers with hydrogen-bonding junctions. *Angew. Chem. Int. Ed.* **2015,** *54*, 11117-11121.

(153)   Chollakup, R.; Smitthipong, W.; Chworos, A. Specific interaction of DNA-functionalized polymer colloids. *Polym. Chem.* **2010,** *1*, 658-662.

(154)   Chollakup, R.; Smitthipong, W.; Chworos, A. DNA-functionalized polystyrene particles and their controlled self-assembly. *RSC Adv.* **2014,** *4*, 30648-30653.

(155)   Klinger, D.; Robb, M. J.; Spruell, J. M.; Lynd, N. A.; Hawker, C. J.; Connal, L. A. Supramolecular guests in solvent driven block copolymer assembly: from internally structured nanoparticles to micelles. *Polym. Chem.* **2013,** *4*, 5038-5042.

(156)   Tian, S.; Liu, G.; Wang, X.; Wu, T.; Yang, J.; Ye, X.; Zhang, G.; Hu, J.; Liu, S. pH-Regulated reversible transition between polyion complexes (PIC) and hydrogen-bonding complexes (HBC) with tunable aggregation-induced emission. *ACS Appl. Mater. Interfaces* **2015,** *8*, 3693-3702.

(157)   Luo, S.; Liu, S.; Xu, J.; Liu, H.; Zhu, Z.; Jiang, M.; Wu, C. A stopped-flow kinetic study of the assembly of interpolymer complexes via hydrogen-bonding interactions. *Macromolecules* **2006,** *39*, 4517-4525.

(158)   Sawada, T.; Fujita, M. A single Watson-Crick G·C base pair in water: aqueous hydrogen bonds in hydrophobic cavities. *J. Am. Chem. Soc.* **2010,** *132*, 7194-7201.

(159)   Beijer, F. H.; Sijbesma, R. P.; Kooijman, H.; Spek, A. L.; Meijer, E. Strong dimerization of ureidopyrimidones via quadruple hydrogen bonding. *J. Am. Chem. Soc.* **1998,** *120*, 6761-6769.

(160)   Feldman, K. E.; Kade, M. J.; Meijer, E.; Hawker, C. J.; Kramer, E. J. Model transient networks from strongly hydrogen-bonded polymers. *Macromolecules* **2009,** *42*, 9072-9081.

(161)   Kieltyka, R. E.; Pape, A.; Albertazzi, L.; Nakano, Y.; Bastings, M. M.; Voets, I. K.; Dankers, P. Y.; Meijer, E. Mesoscale modulation of supramolecular ureidopyrimidinone-based poly (ethylene glycol) transient networks in water. *J. Am. Chem. Soc.* **2013,** *135*, 11159-11164.

(162)   Xu, J. F.; Niu, L. Y.; Chen, Y. Z.; Wu, L. Z.; Tung, C. H.; Yang, Q. Z. Hydrogen bonding directed self-assembly of small-molecule amphiphiles in water. *Org. Lett.* **2014,** *16*, 4016–4019.

(163)   Chen, Y.; Ballard, N.; Bon, S. A. Waterborne polymer nanogels non-covalently crosslinked by multiple hydrogen bond arrays. *Polym. Chem.* **2013,** *4*, 387-392.

(164)   Hofmann, C.; Schönhoff, M. Do additives shift the LCST of poly (N-isopropylacrylamide) by solvent quality changes or by direct interactions? *Colloid Polym. Sci.* **2009,** *287*, 1369-1376.

(165)   Liu, R.; Fraylich, M.; Saunders, B. R. Thermoresponsive copolymers: from fundamental studies to applications. *Colloid Polym. Sci.* **2009,** *287*, 627-643.

(166)   Folmer, B. J.; Sijbesma, R.; Versteegen, R.; Van der Rijt, J.; Meijer, E. Supramolecular polymer materials: chain extension of telechelic polymers using a reactive hydrogen-bonding synthon. *Adv. Mater.* **2000,** *12*, 874-878.

(167)   He, Y.; Lodge, T. P. Thermoreversible ion gels with tunable melting temperatures from triblock and pentablock copolymers. *Macromolecules* **2008,** *41*, 167-174.

(168)   Wilhelm, M.; Zhao, C. L.; Wang, Y.; Xu, R.; Winnik, M. A.; Mura, J. L.; Riess, G.; Croucher, M. D. Poly (styrene-ethylene oxide) block copolymer micelle formation in water: a fluorescence probe study. *Macromolecules* **1991,** *24*, 1033-1040.

(169)   Zhao, C.; Zhuang, X.; He, P.; Xiao, C.; He, C.; Sun, J.; Chen, X.; Jing, X. Synthesis of biodegradable thermo-and pH-responsive hydrogels for controlled drug release. *Polymer* **2009,** *50*, 4308-4316.

(170)   Hosono, N.; Gillissen, M. A.; Li, Y.; Sheiko, S. S.; Palmans, A. R.; Meijer, E. Orthogonal self-assembly in folding block copolymers. *J. Am. Chem. Soc.* **2012,** *135*, 501-510.

(171)   Zhang, L.; Eisenberg, A. Multiple morphologies of "crew-cut" aggregates of polystyrene-b-poly(acrylic acid) block copolymers. *Science* **1995,** *268*, 1728-1730.

(172)   Vangeyte, P.; Gautier, S.; Jérôme, R. About the methods of preparation of poly (ethylene oxide)-b-poly (ε-caprolactone) nanoparticles in water: Analysis by dynamic light scattering. *Colloids Surf., A* **2004,** *242*, 203-211.

(173)   Letchford, K.; Burt, H. A review of the formation and classification of amphiphilic block copolymer nanoparticulate structures: micelles, nanospheres, nanocapsules and polymersomes. *Eur. J. Pharm. Biopharm.* **2007,** *65*, 259-269.

(174)   Diehl, C.; Schlaad, H. Thermo-responsive polyoxazolines with widely tuneable LCST. *Macromol. Biosci.* **2009,** *9*, 157-161.

(175)   Ju, X. J.; Chu, L. Y.; Mi, P.; Song, H.; Lee, Y. M. Synthesis and characterization of a novel thermo-sensitive copolymer of N-isopropylacrylamide and dibenzo-18-crown-6-diacrylamide. *Macromol. Rapid Commun.* **2006,** *27*, 2072-2077.

(176)   Li, L.; Raghupathi, K.; Song, C.; Prasad, P.; Thayumanavan, S. Self-assembly of random copolymers. *Chem. Commun.* **2014,** *50*, 13417-13432.

(177)   Ta, T.; Convertine, A. J.; Reyes, C. R.; Stayton, P. S.; Porter, T. M. Thermosensitive liposomes modified with poly (N-isopropylacrylamide-co-propylacrylic acid) copolymers for triggered release of doxorubicin. *Biomacromolecules* **2010,** *11*, 1915-1920.

(178)   Yamada, T.; Hayamizu, Y.; Yamamoto, Y.; Yomogida, Y.; Izadi-Najafabadi, A.; Futaba, D. N.; Hata, K. A stretchable carbon nanotube strain sensor for human-motion detection. *Nat. Nanotechnol.* **2011,** *6*, 296-301.

(179)   Hammock, M. L.; Chortos, A.; Tee, B. C. K.; Tok, J. B. H.; Bao, Z. 25th anniversary article: the evolution of electronic skin (e-skin): a brief history, design considerations, and recent progress. *Adv. Mater.* **2013,** *25*, 5997-6038.

(180)   Guo, R.; Yu, Y.; Xie, Z.; Liu, X.; Zhou, X.; Gao, Y.; Liu, Z.; Zhou, F.; Yang, Y.; Zheng, Z. Matrix-assisted catalytic printing for the fabrication of multiscale, flexible, foldable, and stretchable metal conductors. *Adv. Mater.* **2013,** *25*, 3343-3350.

(181)   Benight, S. J.; Wang, C.; Tok, J. B.; Bao, Z. Stretchable and self-healing polymers and devices for electronic skin. *Prog. Polym. Sci.* **2013,** *38*, 1961-1977.

(182) Wang, X.; Dong, L.; Zhang, H.; Yu, R.; Pan, C.; Wang, Z. L. Recent progress in electronic skin. *Adv. Sci.* **2015,** *2*, No. 1500169.

(183) Lu, C.; Liu, Y.; Liu, X.; Wang, C.; Wang, J.; Chu, F. Sustainable Multiple and Multi-stimuli Shape Memory and Self-Healing Elastomers with Semi-interpenetrating network Derived from Biomass via Bulk Radical Polymerization. *ACS Sustainable Chemistry & Engineering* **2018**.

(184) Trung, T. Q.; Ramasundaram, S.; Hwang, B. U.; Lee, N. E. An all-elastomeric transparent and stretchable temperature sensor for body-attachable wearable electronics. *Adv. Mater.* **2016,** *28*, 502-509.

(185) Miao, J.; Liu, H.; Li, Y.; Zhang, X. Biodegradable transparent substrate based on edible starch-chitosan embedded with nature-inspired three-dimensionally interconnected conductive nanocomposites for wearable green electronics. *ACS Appl. Mater. Interfaces* **2018,** *10*, 23037-23047.

(186) Choi, S.; Lee, H.; Ghaffari, R.; Hyeon, T.; Kim, D. H. Recent advances in flexible and stretchable bio-electronic devices integrated with nanomaterials. *Adv. Mater.* **2016,** *28*, 4203-4218.

(187) Chen, D.; Pei, Q. Electronic muscles and skins: A review of soft sensors and actuators. *Chem. Rev.* **2017,** *117*, 11239-11268.

(188) Park, M.; Im, J.; Shin, M.; Min, Y.; Park, J.; Cho, H.; Park, S.; Shim, M. B.; Jeon, S.; Chung, D. Y. Highly stretchable electric circuits from a composite material of silver nanoparticles and elastomeric fibres. *Nat. Nanotechnol.* **2012,** *7*, 803-809.

(189) Park, M.; Park, J.; Jeong, U. Design of conductive composite elastomers for stretchable electronics. *Nano Today* **2014,** *9*, 244-260.

(190) Roh, E.; Hwang, B. U.; Kim, D.; Kim, B. Y.; Lee, N. E. Stretchable, transparent, ultrasensitive, and patchable strain sensor for human-machine interfaces comprising a nanohybrid of carbon nanotubes and conductive elastomers. *ACS Nano* **2015,** *9*, 6252-6261.

(191) Kim, D. H.; Rogers, J. A. Stretchable electronics: materials strategies and devices. *Adv. Mater.* **2008,** *20*, 4887-4892.

(192)   Guo, R.; Yu, Y.; Zeng, J.; Liu, X.; Zhou, X.; Niu, L.; Gao, T.; Li, K.; Yang, Y.; Zhou, F. Biomimicking topographic elastomeric petals (E-petals) for omnidirectional stretchable and printable electronics. *Adv. Sci.* **2015,** *2*, No. 1400021.

(193)   Fan, J. A.; Yeo, W. H.; Su, Y.; Hattori, Y.; Lee, W.; Jung, S. Y.; Zhang, Y.; Liu, Z.; Cheng, H.; Falgout, L. Fractal design concepts for stretchable electronics. *Nat. Commun.* **2014,** *5*, No. 3266.

(194)   Choi, S.; Han, S. I.; Kim, D.; Hyeon, T.; Kim, D. H. High-performance stretchable conductive nanocomposites: materials, processes, and device applications. *Chem. Soc. Rev.* **2019**, DOI: 10.1039/c8cs00706c.

(195)   D'Elia, E.; Barg, S.; Ni, N.; Rocha, V. G.; Saiz, E. Self-healing graphene-based composites with sensing capabilities. *Adv. Mater.* **2015,** *27*, 4788-4794.

(196)   Han, Y.; Wu, X.; Zhang, X.; Lu, C. Self-healing, highly sensitive electronic sensors enabled by metal-ligand coordination and hierarchical structure design. *ACS Appl. Mater. Interfaces* **2017,** *9*, 20106-20114.

(197)   Kim, Y.; Zhu, J.; Yeom, B.; Di Prima, M.; Su, X.; Kim, J. G.; Yoo, S. J.; Uher, C.; Kotov, N. A. Stretchable nanoparticle conductors with self-organized conductive pathways. *Nature* **2013,** *500*, 59-63.

(198)   Tee, B. C.; Wang, C.; Allen, R.; Bao, Z. An electrically and mechanically self-healing composite with pressure- and flexion-sensitive properties for electronic skin applications. *Nat. Nanotechnol.* **2012,** *7*, 825-832.

(199)   Mattmann, C.; Clemens, F.; Tröster, G. Sensor for measuring strain in textile. *Sensors* **2008,** *8*, 3719-3732.

(200)   Shang, S.; Zeng, W.; Tao, X. High stretchable MWNTs/polyurethane conductive nanocomposites. *J. Mater. Chem.* **2011,** *21*, 7274-7280.

(201)   Lin, L.; Liu, S.; Fu, S.; Zhang, S.; Deng, H.; Fu, Q. Fabrication of highly stretchable conductors via morphological control of carbon nanotube network. *Small* **2013,** *9*, 3620-3629.

(202)   Kim, H.; Miura, Y.; Macosko, C. W. Graphene/polyurethane nanocomposites for improved gas barrier and electrical conductivity. *Chem. Mater.* **2010,** *22*, 3441-3450.

(203)   Kim, H.; Abdala, A. A.; Macosko, C. W. Graphene/polymer nanocomposites. *Macromolecules* **2010,** *43*, 6515-6530.

(204)   Shi, Y.; Ma, C.; Peng, L.; Yu, G. Conductive "smart" hybrid hydrogels with PNIPAM and nanostructured conductive polymers. *Adv. Funct. Mater.* **2015,** *25*, 1219-1225.

(205)   Granero, A. J.; Wagner, P.; Wagner, K.; Razal, J. M.; Wallace, G. G.; in het Panhuis, M. Highly stretchable conducting SIBS-P3HT fibers. *Adv. Funct. Mater.* **2011,** *21*, 955-962.

(206)   Shi, Z.; Gao, H.; Feng, J.; Ding, B.; Cao, X.; Kuga, S.; Wang, Y.; Zhang, L.; Cai, J. In situ synthesis of robust conductive cellulose/polypyrrole composite aerogels and their potential application in nerve regeneration. *Angew. Chem. Int. Ed.* **2014,** *53*, 5380-5384.

(207)   He, Y.; Gui, Q.; Wang, Y.; Wang, Z.; Liao, S.; Wang, Y. A polypyrrole elastomer based on confined polymerization in a host polymer network for highly stretchable temperature and strain sensors. *Small* **2018,** *14*, No. 1800394.

(208)   Seyedin, M. Z.; Razal, J. M.; Innis, P. C.; Wallace, G. G. Strain-responsive polyurethane/PEDOT: PSS elastomeric composite fibers with high electrical conductivity. *Adv. Funct. Mater.* **2014,** *24*, 2957-2966.

(209)   Wu, Y.; Feng, S.; Zan, X.; Lin, Y.; Wang, Q. Aligned electroactive TMV nanofibers as enabling scaffold for neural tissue engineering. *Biomacromolecules* **2015,** *16*, 3466-3472.

(210)   Zhang, Q.; Liu, L.; Pan, C.; Li, D. Review of recent achievements in self-healing conductive materials and their applications. *J. Mater. Sci.* **2018,** *53*, 27-46.

(211)   Maeda, T.; Otsuka, H.; Takahara, A. Dynamic covalent polymers: reorganizable polymers with dynamic covalent bonds. *Prog. Polym. Sci.* **2009,** *34*, 581-604.

(212)   Wang, T.; Zhang, Y.; Liu, Q.; Cheng, W.; Wang, X.; Pan, L.; Xu, B.; Xu, H. A self-healable, highly stretchable, and solution processable conductive polymer composite for ultrasensitive strain and pressure sensing. *Adv. Funct. Mater.* **2018,** *28*, No. 1705551.

(213)   Shi, Y.; Wang, M.; Ma, C.; Wang, Y.; Li, X.; Yu, G. A conductive self-healing hybrid gel enabled by metal-ligand supramolecule and nanostructured conductive polymer. *Nano Lett.* **2015,** *15*, 6276-6281.

(214)   Jing, X.; Mi, H. Y.; Lin, Y. J.; Enriquez, E.; Peng, X. F.; Turng, L. S. Highly stretchable and biocompatible strain sensors based on mussel-inspired super-adhesive self-healing hydrogels for human motion monitorinm. *ACS Appl. Mater. Interfaces* **2018,** *10*, 20897–20909.

(215)   Zhu, B.; Jasinski, N.; Benitez, A.; Noack, M.; Park, D.; Goldmann, A. S.; Barner-Kowollik, C.; Walther, A. Hierarchical nacre mimetics with synergistic mechanical properties by control of molecular interactions in self-healing polymers. *Angew. Chem. Int. Ed.* **2015,** *54*, 8653-8657.

(216)   Zhou, B.; He, D.; Hu, J.; Ye, Y.; Peng, H.; Zhou, X.; Xie, X.; Xue, Z. A flexible, self-healing and highly stretchable polymer electrolyte via quadruple hydrogen bonding for lithium-ion batteries. *J. Mater. Chem. A* **2018,** *6*, 11725-11733.

(217)   Hu, J.; Liu, S. Supramolecular assembly-assisted synthesis of responsive polymeric materials with controlled chain topologies. *Macromol. Chem. Phys.* **2015,** *216*, 591-604.

(218)   Liu, S.; Jiang, M.; Liang, H.; Wu, C. Intermacromolecular complexes due to specific interactions. 13. Formation of micelle-like structure from hydrogen-bonding graft-like complexes in selective solvents. *Polymer* **2000,** *41*, 8697-8702.

(219)   Lu, Q.; Danner, E.; Waite, J. H.; Israelachvili, J. N.; Zeng, H.; Hwang, D. S. Adhesion of mussel foot proteins to different substrate surfaces. *J. Royal Soc. Interface* **2013,** *10*, No. 20120759.

(220)   Chen, J.; Yan, B.; Wang, X.; Huang, Q.; Thundat, T.; Zeng, H. Core cross-linked double hydrophilic block copolymer micelles based on multiple hydrogen-bonding interactions. *Polym. Chem.* **2017,** *8*, 3066-3073.

(221)   Söntjens, S. H.; Sijbesma, R. P.; van Genderen, M. H.; Meijer, E. Stability and lifetime of quadruply hydrogen bonded 2-ureido-4[1H]-pyrimidinone dimers. *J. Am. Chem. Soc.* **2000,** *122*, 7487-7493.

(222)   Wang, Y.; Shi, Y.; Pan, L.; Ding, Y.; Zhao, Y.; Li, Y.; Shi, Y.; Yu, G. Dopant-enabled supramolecular approach for controlled synthesis of nanostructured conductive polymer hydrogels. *Nano Lett.* **2015,** *15*, 7736-7741.

(223)   Liang, S.; Zhang, Y.; Wang, H.; Xu, Z.; Chen, J.; Bao, R.; Tan, B.; Cui, Y.; Fan, G.; Wang, W. Paintable and rapidly bondable conductive hydrogels as therapeutic cardiac patches. *Adv. Mater.* **2018,** *30*, No. 1704235.

(224)   Wang, H. L.; Fernandez, J. E. Blends of polypyrrole and poly(vinyl alcohol). *Macromolecules* **1993,** *26*, 3336-3339.

(225)   Smitthipong, W.; Suethao, S.; Shah, D.; Vollrath, F. Interesting green elastomeric composites: Silk textile reinforced natural rubber. *Polym. Test.* **2016,** *55*, 17-24.

(226)   Müller, D.; Rambo, C.; Recouvreux, D.; Porto, L.; Barra, G. Chemical in situ polymerization of polypyrrole on bacterial cellulose nanofibers. *Synth. Met.* **2011,** *161*, 106-111.

(227)   Ballav, N.; Maity, A.; Mishra, S. B. High efficient removal of chromium (VI) using glycine doped polypyrrole adsorbent from aqueous solution. *Chem. Eng. J.* **2012,** *198*, 536-546.

(228)   Wei, D.; Lin, X.; Li, L.; Shang, S.; Yuen, M. C.; Yan, G.; Yu, X. Controlled growth of polypyrrole hydrogels. *Soft Matter* **2013,** *9*, 2832-2836.

(229)   Hur, J.; Im, K.; Kim, S. W.; Kim, J.; Chung, D. Y.; Kim, T. H.; Jo, K. H.; Hahn, J. H.; Bao, Z.; Hwang, S. Polypyrrole/agarose-based electronically conductive and reversibly restorable hydrogel. *ACS Nano* **2014,** *8*, 10066-10076.

(230)   Li, B.; Kan, L.; Zhang, S.; Liu, Z.; Li, C.; Li, W.; Zhang, X.; Wei, H.; Ma, N. Planting carbon nanotubes onto supramolecular polymer matrixes for waterproof non-contact self-healing. *Nanoscale* **2018,** *11*, 467-473.

(231) Heinzmann, C.; Weder, C.; de Espinosa, L. M. Supramolecular polymer adhesives: advanced materials inspired by nature. *Chem. Soc. Rev.* **2016,** *45*, 342-358.

(232) Liu, X.; Zhang, Q.; Gao, Z.; Hou, R.; Gao, G. Bioinspired adhesive hydrogel driven by adenine and thymine. *ACS Appl. Mater. Interfaces* **2017,** *9*, 17645-17652.

(233) Shao, C.; Wang, M.; Meng, L.; Chang, H.; Wang, B.; Xu, F.; Yang, J.; Wan, P. Mussel-inspired cellulose nanocomposite tough hydrogels with synergistic self-healing, adhesive, and strain-sensitive properties. *Chem. Mater.* **2018,** *30*, 3110-3121.

(234) Ding, Q.; Xu, X.; Yue, Y.; Mei, C.; Huang, C.; Jiang, S.; Wu, Q.; Han, J. Nanocellulose-mediated electroconductive self-healing hydrogels with high strength, plasticity, viscoelasticity, stretchability, and biocompatibility toward multifunctional applications. *ACS Appl. Mater. Interfaces* **2018,** *10*, 27987–28002.

(235) Das, N. C.; Chaki, T. K.; Khastgir, D. Effect of axial stretching on electrical resistivity of short carbon fibre and carbon black filled conductive rubber composites. *Polym. Int.* **2002,** *51*, 156-163.

(236) Hoffman, A. S. Hydrogels for biomedical applications. *Adv. Drug Deliv. Rev.* **2012,** *64*, 18-23.

(237) Chakraborty, P.; Guterman, T.; Adadi, N.; Yadid, M.; Brosh, T.; Adler-Abramovich, L.; Dvir, T.; Gazit, E. A self-healing, all-organic, conducting, composite peptide hydrogel as pressure sensor and electrogenic cell soft substrate. *ACS Nano* **2018,** *13*, 163-175.

(238) Lu, B.; Yuk, H.; Lin, S.; Jian, N.; Qu, K.; Xu, J.; Zhao, X. Pure PEDOT: PSS hydrogels. *Nat. Commun.* **2019,** *10*, No. 1043.

(239) Guiseppi-Elie, A. Electroconductive hydrogels: synthesis, characterization and biomedical applications. *Biomaterials* **2010,** *31*, 2701-2716.

(240) Kim, H.; Kim, K.; Lee, S. J. Nature-inspired thermo-responsive multifunctional membrane adaptively hybridized with PNIPAm and PPy. *NPG Asia Mater.* **2017,** *9*, No. e445.

(241) Duan, J.; Liang, X.; Guo, J.; Zhu, K.; Zhang, L. Ultra-stretchable and force-sensitive hydrogels reinforced with chitosan microspheres embedded in polymer networks. *Adv. Mater.* **2016,** *28*, 8037-8044.

(242) Yuk, H.; Lu, B.; Zhao, X. Hydrogel bioelectronics. *Chem. Soc. Rev.* **2018**, 10.1039/C8CS00595H.

(243) Zhang, B.; Korolj, A.; Lai, B. F. L.; Radisic, M. Advances in organ-on-a-chip engineering. *Nat. Rev. Mater.* **2018,** *3*, 257–278.

(244) Sarkar, D.; Liu, W.; Xie, X.; Anselmo, A. C.; Mitragotri, S.; Banerjee, K. MoS2 field-effect transistor for next-generation label-free biosensors. *ACS Nano* **2014,** *8*, 3992-4003.

(245) You, J. O.; Auguste, D. T. Conductive, physiologically responsive hydrogels. *Langmuir* **2010,** *26*, 4607-4612.

(246) Jin, Y.; Hwang, S.; Ha, H.; Park, H.; Kang, S. W.; Hyun, S.; Jeon, S.; Jeong, S. H. Buckled Au@ PVP nanofiber networks for highly transparent and stretchable conductors. *Adv. Electron. Mater.* **2016,** *2*, 1500302.

(247) Cai, G.; Wang, J.; Qian, K.; Chen, J.; Li, S.; Lee, P. S. Extremely stretchable strain sensors based on conductive self-healing dynamic cross-links hydrogels for human-motion detection. *Adv. Sci.* **2017,** *4*, No. 1600190.

(248) Ahadian, S.; Huyer, L. D.; Estili, M.; Yee, B.; Smith, N.; Xu, Z.; Sun, Y.; Radisic, M. Moldable elastomeric polyester-carbon nanotube scaffolds for cardiac tissue engineering. *Acta Biomater.* **2017,** *52*, 81-91.

(249) Jing, X.; Mi, H. Y.; Peng, X. F.; Turng, L. S. Biocompatible, self-healing, highly stretchable polyacrylic acid/reduced graphene oxide nanocomposite hydrogel sensors via mussel-inspired chemistry. *Carbon* **2018,** *136*, 63-72.

(250) Xia, Y.; Zhu, H. Polyaniline nanofiber-reinforced conducting hydrogel with unique pH-sensitivity. *Soft Matter* **2011,** *7*, 9388-9393.

(251)   Huang, H.; Yao, J.; Li, L.; Zhu, F.; Liu, Z.; Zeng, X.; Yu, X.; Huang, Z. Reinforced polyaniline/polyvinyl alcohol conducting hydrogel from a freezing-thawing method as self-supported electrode for supercapacitors. *J. Mater. Sci.* **2016,** *51*, 8728-8736.

(252)   Balint, R.; Cassidy, N. J.; Cartmell, S. H. Conductive polymers: towards a smart biomaterial for tissue engineering. *Acta Biomater.* **2014,** *10*, 2341-2353.

(253)   Ding, H.; Zhong, M.; Kim, Y. J.; Pholpabu, P.; Balasubramanian, A.; Hui, C. M.; He, H.; Yang, H.; Matyjaszewski, K.; Bettinger, C. J. Biologically derived soft conducting hydrogels using heparin-doped polymer networks. *ACS Nano* **2014,** *8*, 4348-4357.

(254)   Huang, H.; Zeng, X.; Li, W.; Wang, H.; Wang, Q.; Yang, Y. Reinforced conducting hydrogels prepared from the in situ polymerization of aniline in an aqueous solution of sodium alginate. *J. Mater. Chem. A* **2014,** *2*, 16516-16522.

(255)   Pan, L.; Chortos, A.; Yu, G.; Wang, Y.; Isaacson, S.; Allen, R.; Shi, Y.; Dauskardt, R.; Bao, Z. An ultra-sensitive resistive pressure sensor based on hollow-sphere microstructure induced elasticity in conducting polymer film. *Nat. Commun.* **2014,** *5*, No. 3002.

(256)   Dai, T.; Jia, Y. Supramolecular hydrogels of polyaniline-poly (styrene sulfonate) prepared in concentrated solutions. *Polymer* **2011,** *52*, 2550-2558.

(257)   Li, W.; Zeng, X.; Wang, H.; Wang, Q.; Yang, Y. Polyaniline-poly (styrene sulfonate) conducting hydrogels reinforced by supramolecular nanofibers and used as drug carriers with electric-driven release. *Eur. Polym. J.* **2015,** *66*, 513-519.

(258)   Darabi, M. A.; Khosrozadeh, A.; Mbeleck, R.; Liu, Y.; Chang, Q.; Jiang, J.; Cai, J.; Wang, Q.; Luo, G.; Xing, M. Skin-inspired multifunctional autonomic-intrinsic conductive self-healing hydrogels with pressure sensitivity, stretchability, and 3D printability. *Adv. Mater.* **2017,** *29*, No. 1700533.

(259)   Han, B.; Yang, Y.; Shi, X.; Zhang, G.; Gong, L.; Xu, D.; Zeng, H.; Wang, C.; Gu, M.; Deng, Y. Spontaneous repairing liquid metal/Si nanocomposite as a smart conductive-additive-free anode for lithium-ion battery. *Nano energy* **2018,** *50*, 359-366.

(260)   Cao, Y.; Morrissey, T. G.; Acome, E.; Allec, S. I.; Wong, B. M.; Keplinger, C.; Wang, C. A transparent, self-healing, highly stretchable ionic conductor. *Adv. Mater.* **2017,** *29*, No. 1605099.

(261)   Narkar, A. R.; Lee, B. P. Incorporation of anionic monomer to tune the reversible catechol-boronate complex for pH responsive, reversible adhesion. *Langmuir* **2018,** *34*, 9410–9417.

(262)   Tuncaboylu, D. C.; Sari, M.; Oppermann, W.; Okay, O. Tough and self-healing hydrogels formed via hydrophobic interactions. *Macromolecules* **2011,** *44*, 4997-5005.

(263)   Chen, J.; Wu, M.; Gong, L.; Zhang, J.; Yan, B.; Liu, J.; Zhang, H.; Thundat, T.; Zeng, H. Mechanistic understanding and nanomechanics of multiple hydrogen-bonding interaction in aqueous environment. *J. Phys. Chem. C* **2019,** *123*, 4540–4548.

(264)   Zhang, G.; Yang, Y.; Chen, Y.; Huang, J.; Zhang, T.; Zeng, H.; Wang, C.; Liu, G.; Deng, Y. A quadruple hydrogen-bonded supramolecular binder for high-performance silicon anodes in lithium-ion batteries. *Small* **2018,** *14*, 1801189.

(265)   Hou, S.; Wang, X.; Park, S.; Jin, X.; Ma, P. X. Rapid self-integrating, injectable hydrogel for tissue complex regeneration. *Adv. Healthc. Mater.* **2015,** *4*, 1491-1495.

(266)   Liao, H.; Liao, S.; Tao, X.; Liu, C.; Wang, Y. Intrinsically recyclable and self-healable conductive supramolecular polymer for customizable electronic sensors. *J. Mater. Chem. C* **2018,** *6*, 12992-12999.

(267)   Almdal, K.; Dyre, J.; Hvidt, S.; Kramer, O. Towards a phenomenological definition of the term 'gel'. *Polym. Gels Networks* **1993,** *1*, 5-17.

(268)   Zhang, G.; Ngai, T.; Deng, Y.; Wang, C. An injectable hydrogel with excellent self-healing property based on quadruple hydrogenbonding. *Macromol. Chem. Phys.* **2016,** *217*, 2172-2181.

(269)   Jang, J.; Ha, J.; Cho, J. Fabrication of water-dispersible polyaniline-poly (4-styrenesulfonate) nanoparticles for inkjet-printed chemical-sensor applications. *Adv. Mater.* **2007,** *19*, 1772-1775.

(270)   Dai, T.; Jiang, X.; Hua, S.; Wang, X.; Lu, Y. Facile fabrication of conducting polymer hydrogels via supramolecular self-assembly. *Chem. Commun.* **2008**, 4279-4281.

(271)   Wang, Z.; Chen, J.; Cong, Y.; Zhang, H.; Xu, T.; Nie, L.; Fu, J. Ultra stretchable strain sensors and arrays with high sensitivity and linearity based on super tough conductive hydrogels. *Chem. Mater.* **2018,** *30*, 8062–8069.

(272)   Dai, C.; Zhou, Z.; Guan, Z.; Wu, Y.; Liu, Y.; He, J.; Yu, P.; Tu, L.; Zhang, F.; Chen, D. A multifunctional metallohydrogel with injectability, self-ealing, and multistimulus-responsiveness for bioadhesives. *Macromol. Mater. Eng.* **2018,** *303*, No. 1800305.

(273)   Liu, Y. J.; Cao, W. T.; Ma, M. G.; Wan, P. B. Ultrasensitive wearable soft strain sensors of conductive, self-healing, and elastic hydrogels with synergistic "soft and hard" hybrid networks. *ACS Appl. Mater. Interfaces* **2017,** *9*, 25559-25570.

(274)   Balkenende, D. W.; Monnier, C. A.; Fiore, G. L.; Weder, C. Optically responsive supramolecular polymer glasses. *Nat. Commun.* **2016,** *7*, 10995.

(275)   Liu, S.; Zhu, H.; Zhao, H.; Jiang, M.; Wu, C. Interpolymer hydrogen-bonding complexation induced micellization from polystyrene-b-poly(methyl methacrylate) and PS(OH) in toluene. *Langmuir* **2000,** *16*, 3712-3717.

(276)   Zhang, H.; Xia, H.; Zhao, Y. Poly(vinyl alcohol) hydrogel can autonomously self-heal. *ACS Macro Lett.* **2012,** *1*, 1233-1236.

(277)   Rehm, T.; Schmuck, C. How to achieve self-assembly in polar solvents based on specific interactions? Some general guidelines. *Chem. Commun.* **2008,** *0*, 801-813.

(278)   Cui, Y.; Tan, M.; Zhu, A.; Guo, M. Non-covalent interaction cooperatively induced stretchy, tough and stimuli-responsive polyurethane–urea supramolecular (PUUS) hydrogels. *J. Mater. Chem. B* **2015,** *3*, 2834-2841.

(279)   Ghatee, M. H.; Zolghadr, A. R. Local depolarization in hydrophobic and hydrophilic ionic liquids/water mixtures: car–parrinello and classical molecular dynamics simulation. *J. Phys. Chem. C* **2013,** *117*, 2066-2077.

(280)   Reinecke, A.; Bertinetti, L.; Fratzl, P.; Harrington, M. J. Cooperative behavior of a sacrificial bond network and elastic framework in providing self-healing capacity in mussel byssal threads. *J. Struct. Biol.* **2016,** *196*, 329-339.

(281)   Zheng, R.; Arora, J.; Boonkaew, B.; Raghavan, S.; Kaplan, D.; He, J.; Pesika, N.; John, V. Liposomes tethered to a biopolymer film through the hydrophobic effect create a highly effective lubricating surface. *Soft matter* **2014,** *10*, 9226-9229.

(282)   Kristiansen, K.; Stock, P.; Baimpos, T.; Raman, S.; Harada, J. K.; Israelachvili, J. N.; Valtiner, M. Influence of molecular dipole orientations on long-range exponential interaction forces at hydrophobic contacts in aqueous solutions. *ACS Nano* **2014,** *8*, 10870-10877.

(283)   Hirschberg, J. K.; Brunsveld, L.; Ramzi, A.; Vekemans, J. A.; Sijbesma, R. P.; Meijer, E. Helical self-assembled polymers from cooperative stacking of hydrogen-bonded pairs. *Nature* **2000,** *407*, 167-170.

(284)   Obert, E.; Bellot, M.; Bouteiller, L.; Andrioletti, F.; Lehen-Ferrenbach, C.; Boué, F. Both water-and organo-soluble supramolecular polymer stabilized by hydrogen-bonding and hydrophobic interactions. *J. Am. Chem. Soc.* **2007,** *129*, 15601-15605.

(285)   Némethy, G.; Steinberg, I. Z.; Scheraga, H. A. Influence of water structure and of hydrophobic interactions on the strength of side‐chain hydrogen bonds in proteins. *Biopolymers* **1963,** *1*, 43-69.

(286)   Yu, M. L.; Wang, S. M.; Feng, K.; Khoury, T.; Crossley, M. J.; Yang, F.; Zhang, J. P.; Tung, C. H.; Wu, L. Z. Photoinduced electron transfer and charge-recombination in 2-ureido-4[1H]-pyrimidinone quadruple hydrogen-bonded porphyrin–fullerene assemblies. *J. Phys. Chem. C* **2011,** *115*, 23634-23641.

(287)   Hou, S.; Wang, X.; Park, S.; Jin, X.; Ma, P. X. Rapid self‐integrating, injectable hydrogel for tissue complex regeneration. *Adv. Healthc. Mater.* **2015,** *4*, 1491-1495.

(288)   Iliafar, S.; Wagner, K.; Manohar, S.; Jagota, A.; Vezenov, D. Quantifying interactions between DNA oligomers and graphite surface using single molecule force spectroscopy. *J. Phys. Chem. C* **2012,** *116*, 13896-13903.

(289)   Stroh, C.; Wang, H.; Bash, R.; Ashcroft, B.; Nelson, J.; Gruber, H.; Lohr, D.; Lindsay, S.; Hinterdorfer, P. Single-molecule recognition imaging microscopy. *Proc. Natl. Acad. Sci. U.S.A.* **2004,** *101*, 12503-12507.

(290)   Yuan, C.; Chen, A.; Kolb, P.; Moy, V. T. Energy landscape of streptavidin−biotin complexes measured by atomic force microscopy. *Biochemistry* **2000,** *39*, 10219-10223.

(291)   Zhang, J.; Lu, X.; Shi, C.; Yan, B.; Gong, L.; Chen, J.; Xiang, L.; Xu, H.; Liu, Q.; Zeng, H. Unraveling the molecular interaction mechanism between graphene oxide and aromatic organic compounds with implications on wastewater treatment. *Chem. Eng. J.* **2019,** *358*, 842-849.

(292)   Zou, S.; Schönherr, H.; Vancso, G. J. Stretching and rupturing individual supramolecular polymer chains by AFM. *Angew. Chem. Int. Ed.* **2005,** *44*, 956-959.

(293)   Zou, S.; Schönherr, H.; Vancso, G. J. Force spectroscopy of quadruple H-bonded dimers by AFM: dynamic bond rupture and molecular time−temperature superposition. *J. Am. Chem. Soc.* **2005,** *127*, 11230-11231.

(294)   Embrechts, A.; Schönherr, H.; Vancso, G. J. Rupture force of single supramolecular bonds in associative polymers by AFM at fixed loading rates. *J. Phys. Chem. B* **2008,** *112*, 7359-7362.

(295)   Hosono, N.; Kushner, A. M.; Chung, J.; Palmans, A. R.; Guan, Z.; Meijer, E. Forced unfolding of single-chain polymeric nanoparticles. *J. Am. Chem. Soc.* **2015,** *137*, 6880-6888.

(296)   Chung, J.; Kushner, A. M.; Weisman, A. C.; Guan, Z. Direct correlation of single-molecule properties with bulk mechanical performance for the biomimetic design of polymers. *Nat. Mater.* **2014,** *13*, 1055-1062.

(297)   Hörner, G.; Lewandowska, A.; Hug, G. L.; Marciniak, B. Solvent effects on the intramolecular hydrogen-atom transfer between tyrosine and benzophenone. Diverting reaction mechanisms in protic and nonprotic media. *J. Phys. Chem. C* **2009,** *113*, 11695-11703.

(298)   Cui, S.; Albrecht, C.; Kühner, F.; Gaub, H. E. Weakly bound water molecules shorten single-stranded DNA. *J. Am. Chem. Soc.* **2006,** *128*, 6636-6639.

(299)   Cui, S.; Yu, J.; Kühner, F.; Schulten, K.; Gaub, H. E. Double-stranded DNA dissociates into single strands when dragged into a poor solvent. *J. Am. Chem. Soc.* **2007,** *129*, 14710-14716.

(300)   Fersht, A. R.; Shi, J.-P.; Knill-Jones, J.; Lowe, D. M.; Wilkinson, A. J.; Blow, D. M.; Brick, P.; Carter, P.; Waye, M. M.; Winter, G. Hydrogen bonding and biological specificity analysed by protein engineering. *Nature* **1985,** *314*, 235-238.

(301)   Zhang, Y.; Yu, Y.; Jiang, Z.; Xu, H.; Wang, Z.; Zhang, X.; Oda, M.; Ishizuka, T.; Jiang, D.; Chi, L. Single-molecule study on intermolecular interaction between C60 and porphyrin derivatives: toward understanding the strength of the multivalency. *Langmuir* **2009,** *25*, 6627-6632.

(302)   Schmid, N.; Eichenberger, A. P.; Choutko, A.; Riniker, S.; Winger, M.; Mark, A. E.; van Gunsteren, W. F. Definition and testing of the GROMOS force-field versions 54A7 and 54B7. *Eur. Biophys. J.* **2011,** *40*, 843-856.

(303)   York, D. M.; Darden, T. A.; Pedersen, L. G. The effect of long‐range electrostatic interactions in simulations of macromolecular crystals: A comparison of the Ewald and truncated list methods. *J. Chem. Phys.* **1993,** *99*, 8345-8348.

(304)   Kumar, S.; Rosenberg, J. M.; Bouzida, D.; Swendsen, R. H.; Kollman, P. A. The weighted histogram analysis method for free‐energy calculations on biomolecules. I. The method. *J. Comput. Chem.* **1992,** *13*, 1011-1021.

(305)   Wang, C.; Hu, R.; Morrissey, J. J.; Kharasch, E. D.; Singamaneni, S. Single molecule force spectroscopy to compare natural versus artificial antibody-antigen interaction. *Small* **2017,** *13*, 1604255.

(306)   Ray, C.; Brown, J. R.; Kirkpatrick, A.; Akhremitchev, B. B. Pairwise interactions between linear alkanes in water measured by AFM force spectroscopy. *J. Am. Chem. Soc.* **2008,** *130*, 10008-10018.

(307)   Stock, P.; Utzig, T.; Valtiner, M. Soft matter interactions at the molecular scale: interaction forces and energies between single hydrophobic model peptides. *Phys. Chem. Chem. Phys.* **2017,** *19*, 4216-4221.

(308)   Schlierf, M.; Berkemeier, F.; Rief, M. Direct observation of active protein folding using lock-in force spectroscopy. *Biophys. J.* **2007,** *93*, 3989-3998.

(309)   Li, Y.; Qin, M.; Li, Y.; Cao, Y.; Wang, W. Single molecule evidence for the adaptive binding of DOPA to different wet surfaces. *Langmuir* **2014,** *30*, 4358-4366.

(310)   Friddle, R. W.; Noy, A.; De Yoreo, J. J. Interpreting the widespread nonlinear force spectra of intermolecular bonds. *Proc. Natl. Acad. Sci. U.S.A.* **2012,** *109,* 13573-13578.

(311)   Sluysmans, D.; Devaux, F.; Bruns, C. J.; Stoddart, J. F.; Duwez, A. S. Dynamic force spectroscopy of synthetic oligorotaxane foldamers. *Proc. Natl. Acad. Sci. U. S. A.* **2017,** *115*, 9362-9366.

(312)   Israelachvili, J. N. *Intermolecular and surface forces;* Academic press, 2011.

(313)   Mitchell, J. B.; Laskowski, R. A.; Alex, A.; Thornton, J. M. BLEEP—potential of mean force describing protein–ligand interactions: I. Generating potential. *J. Comput. Chem.* **1999,** *20,* 1165-1176.

(314)   Ray, C.; Brown, J. R.; Akhremitchev, B. B. Rupture force analysis and the associated systematic errors in force spectroscopy by AFM. *Langmuir* **2007,** *23,* 6076-6083.

(315)   Ray, C.; Brown, J. R.; Akhremitchev, B. B. Correction of systematic errors in single-molecule force spectroscopy with polymeric tethers by atomic force microscopy. *J. Phys. Chem. B* **2007,** *111*, 1963-1974.

(316)   de Jong, D. H.; Periole, X.; Marrink, S. J. Dimerization of amino acid side chains: lessons from the comparison of different force fields. *J. Chem. Theory Comput.* **2012,** *8*, 1003-1014.

Appendices

Appendix A   Supporting Information for Chapter 2
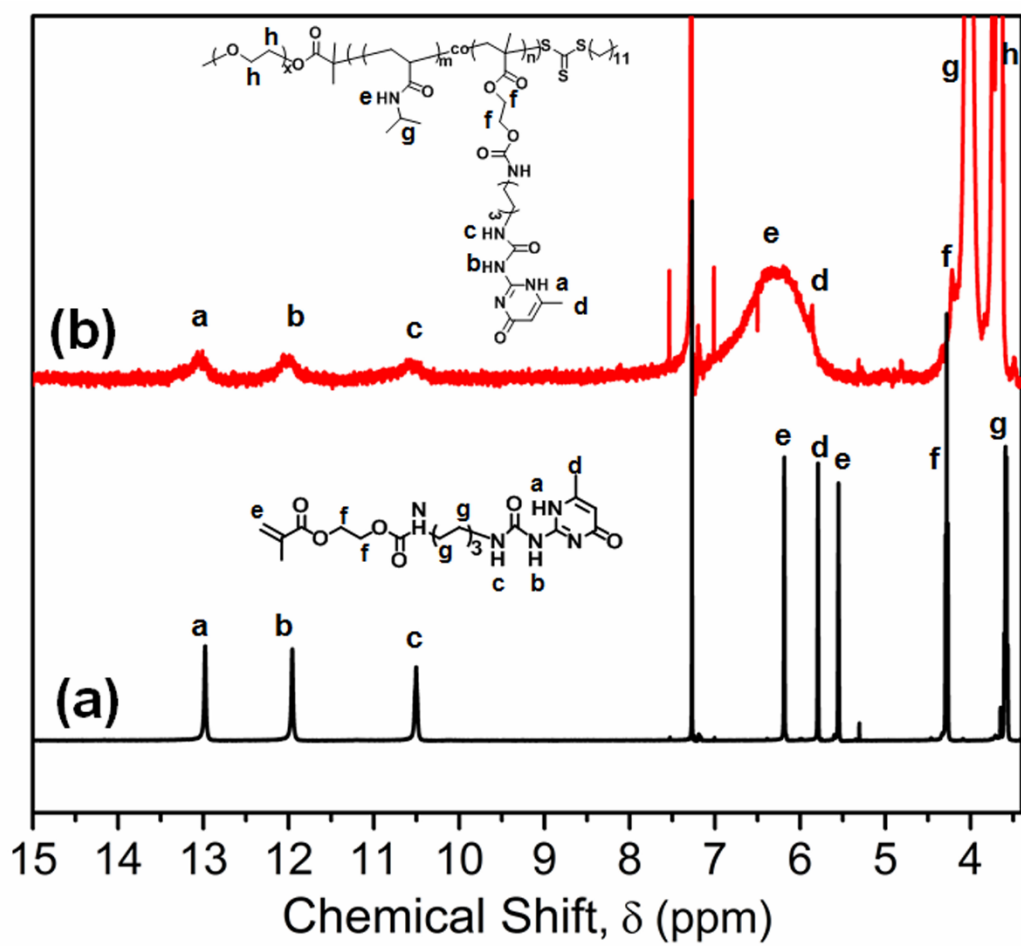
Figure S2.1. ^{1}H NMR spectra of (a) HEMA-UPy monomer and (b) BC-U6 diblock copolymer in CDCl$_3$.
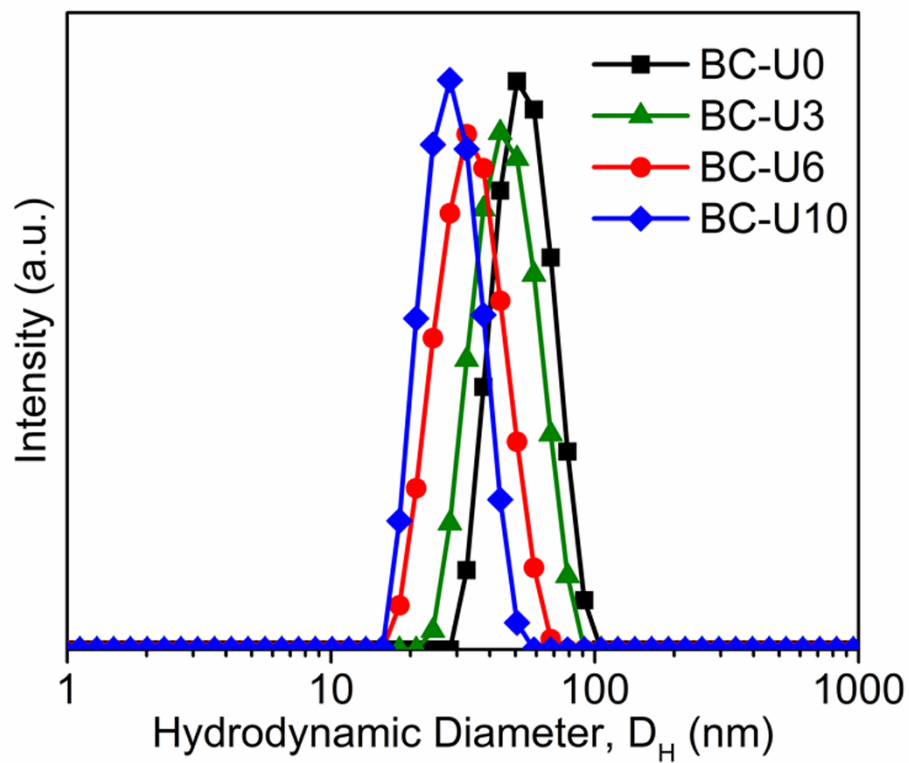
Figure S2.2. Hydrodynamic diameter distributions obtained from aqueous solutions of synthesized polymers BC-U0, BC-U3, BC-U6 and BC-U10 at 40 °C.

Appendix B   Supporting Information for Chapter 3
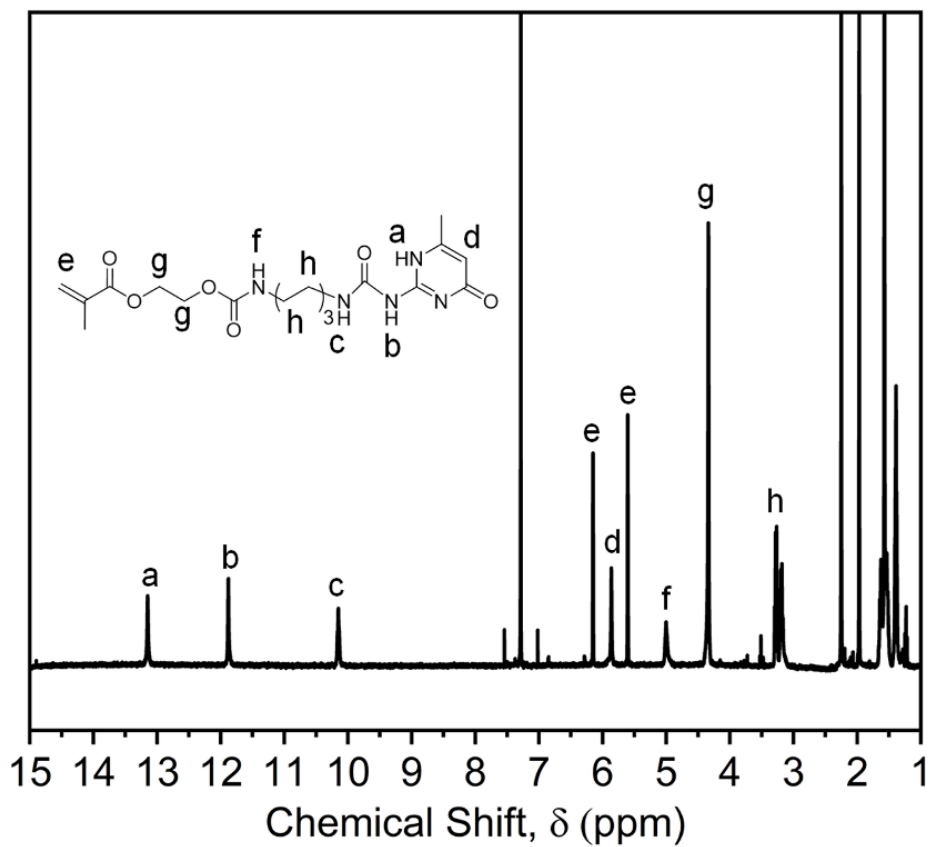
Figure S3.1. [superscript]1H NMR spectrum of the synthesized HEMA-UPy monomer in CDCl$_3$.
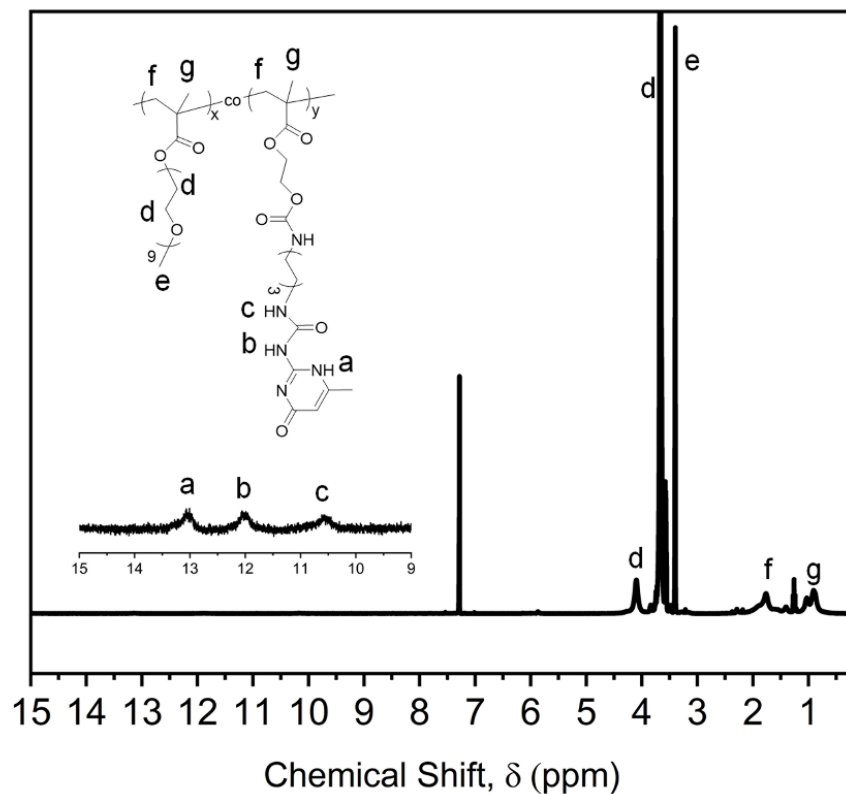
Figure S3.2. ^{1}H NMR spectrum of copolymer PEG-5UPy in CDCl$_3$.
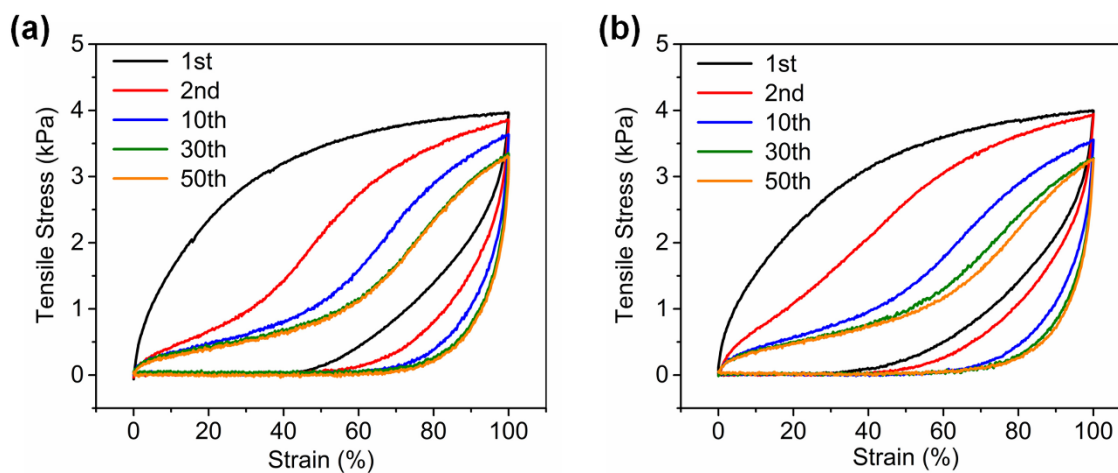
Figure S3.3. Successive loading-unloading cycles of the (a) original PEG-5UPy elastomer and (b) self-healed PEG-5UPy elastomer with a healing time of 10 min.
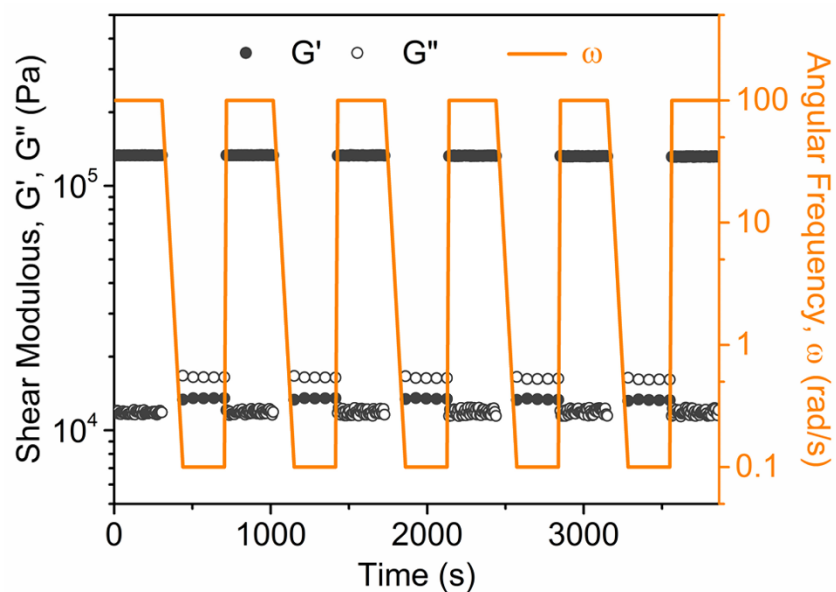
Figure S3.4. Variation of the shear moduli during cyclic steps with angular frequency

shifting between 100 rad/s and 0.1 rad/s.
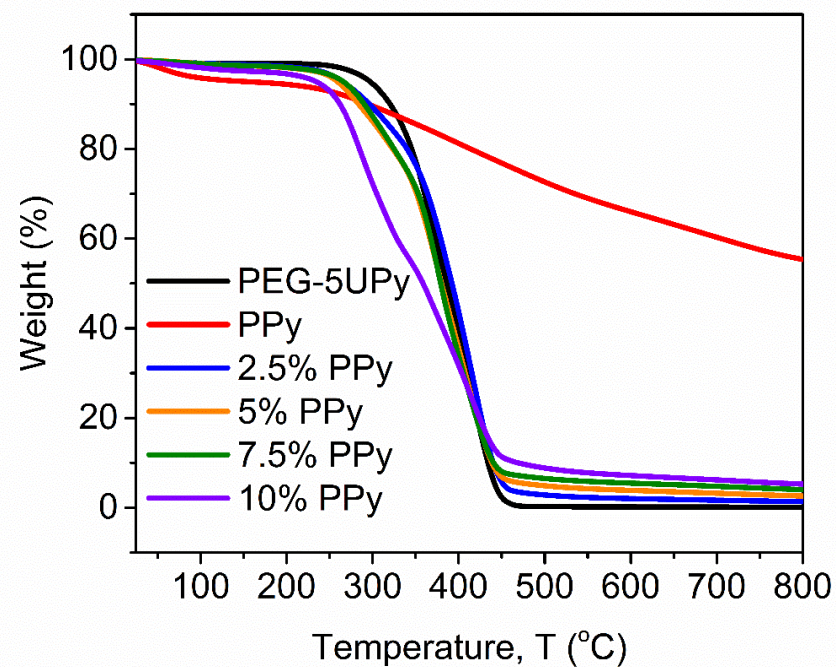
Figure S3.5. TGA curves of PEG-5UPy, PPy and elastic composites with different PPy
contents.
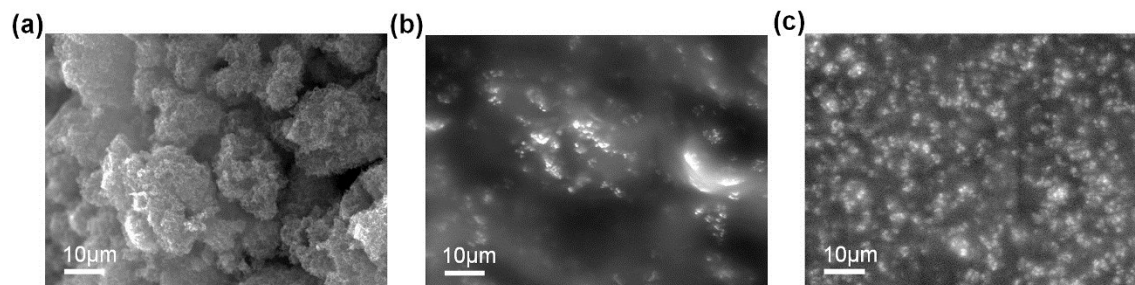
Figure S3.6. SEM images of (a) PPy particle, (b) elastomer composite formed by direct mixing of PEG-5UPy and 7.5 wt% PPy, (c) PPy/PEG-5UPy composite formed by in situ polymerization of 7.5 wt% PPy within PEG-5UPy matrix.
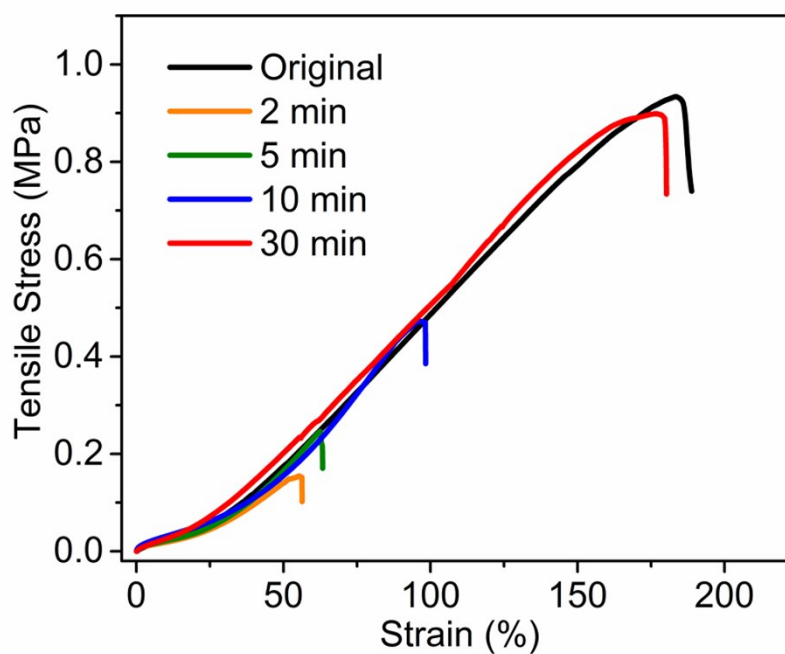
Figure S3.7. Typical stress-strain curves of the original and self-healed composites with 10% wt% PPy at different healing time.
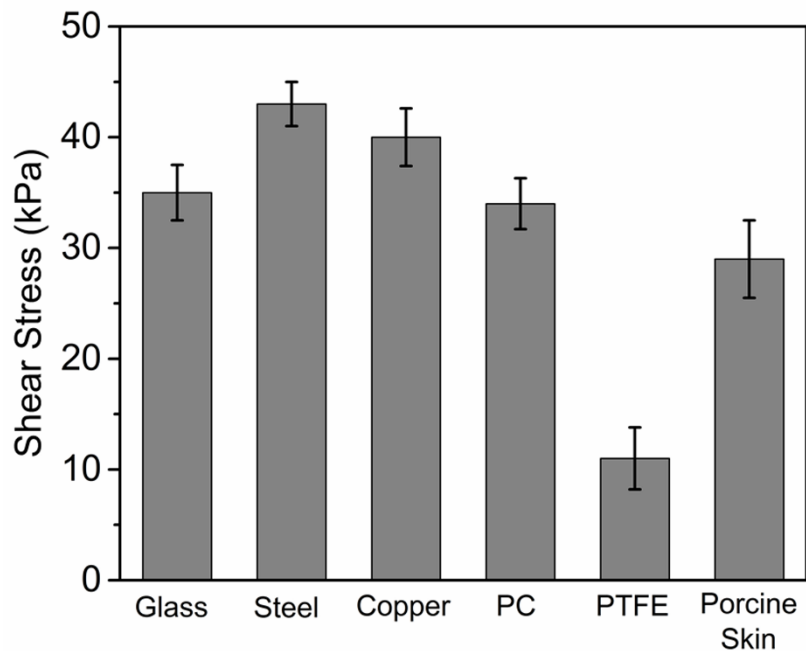
Figure S3.8. Adhesive strengths of the composite with 10 wt% PPy to different substrates.
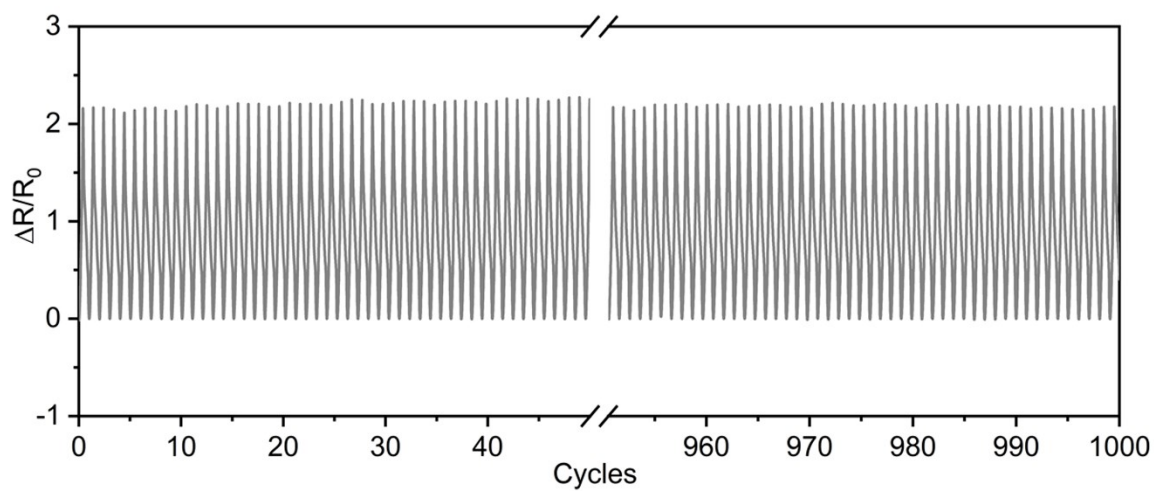
Figure S3.9. Relative resistance change of the composite with 7.5 wt% PPy during 1000 stretching-releasing cycles of 50% strain.
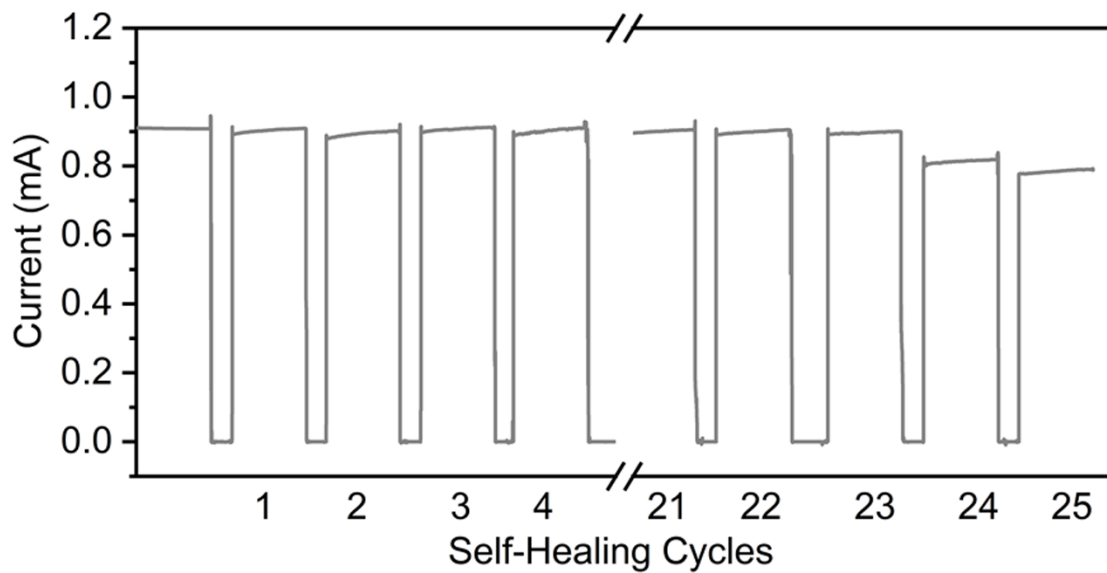
Figure S3.10. Current change of the composite with 25 cut (15 s) and healing (60 s) cycles.

.

Appendix C   Supporting Information for Chapter 4
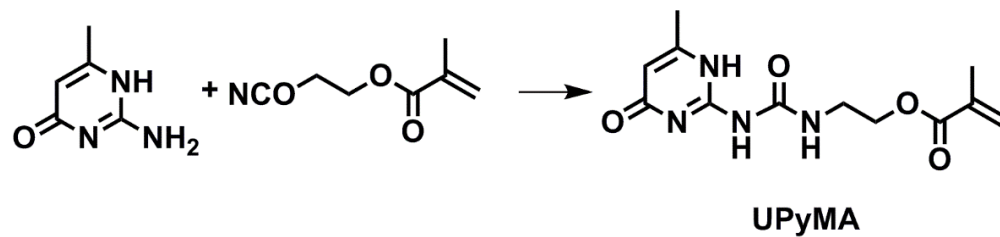
Figure S4.1. Synthesis route of hydrogen-bonding monomer UPyMA.
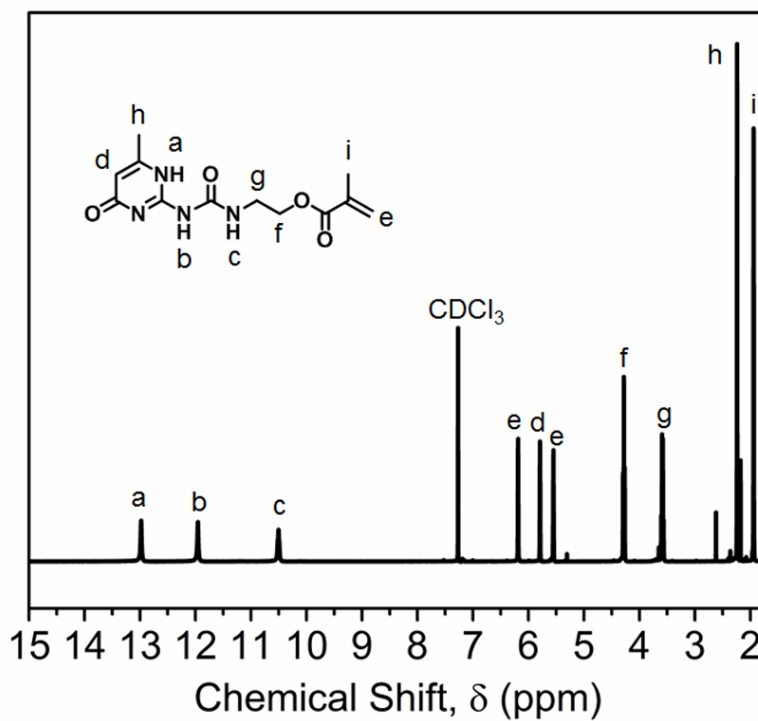
Figure S4.2. ^{1}H NMR spectrum of the synthesized UPyMA monomer in CDCl$_3$.
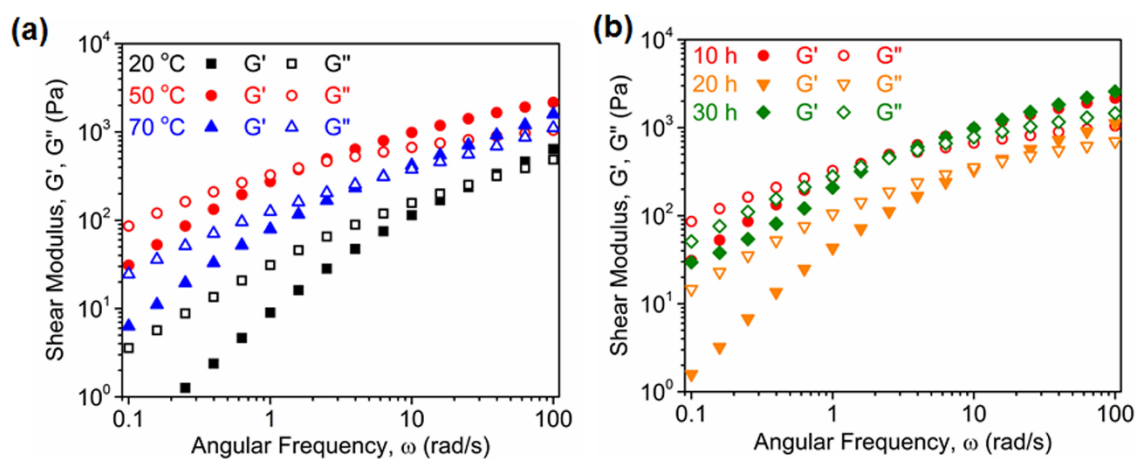
Figure S4.3. Frequency sweep measurements of PSS-20UPy hydrogel prepared at (a) 20 °C, 50 °C, and 70 °C for 20 h and (b) 50 °C for 10 h, 20 h, and 30 h.
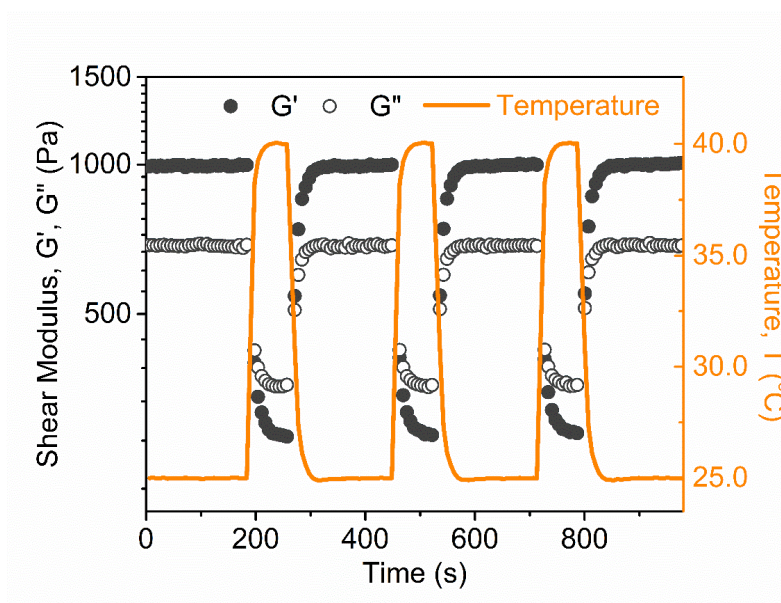
Figure S4.4. Variation of the shear moduli of PSS-20UPy hydrogel during multiple heating-cooling cycles between 25 °C and 40 °C.

160

Table S4.1. Water content and PANI fraction of the prepared hydrogels.

Sample	Water content (wt%)	PANI fraction in polymer network (wt%)	
		Feed	Product
PSS-20UPy (before soaking)	72.8	None	None
PSS-20UPy without ANI (after soaking)	80.9	None	None
PSS-20UPy with 0.1 M ANI (after soaking)	80.3	3.5	3.4
PSS-20UPy with 0.2 M ANI (after soaking))	79.4	6.7	6.5
PSS-20UPy with 0.3 M ANI (after soaking)	78.0	9.7	9.4
PSS-20UPy with 0.4 M ANI (after soaking)	76.8	12.5	12.0
PSS-10 UPy with 0.3 M ANI (after soaking)	hydrogel dissolves	9.7	N/A
PSS-15UPy with 0.3 M ANI (after soaking)	hydrogel dissolves	9.7	N/A
PSS-25 UPy with 0.3 M ANI (after soaking)	75.7	9.7	9.3
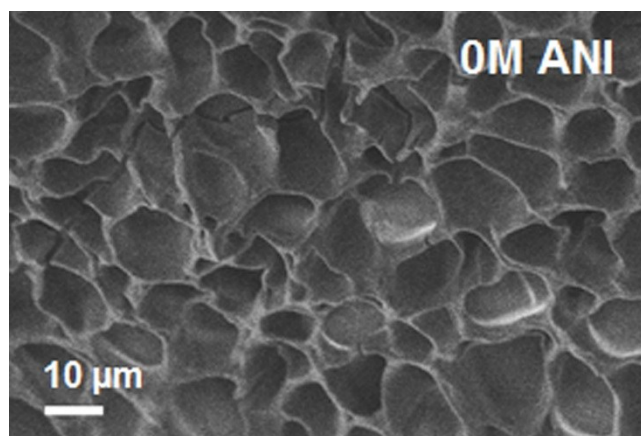
Figure S4.5. Representative SEM image of PSS-20UPy hydrogel after immersing in FeCl$_3$ solution without addition of ANI.
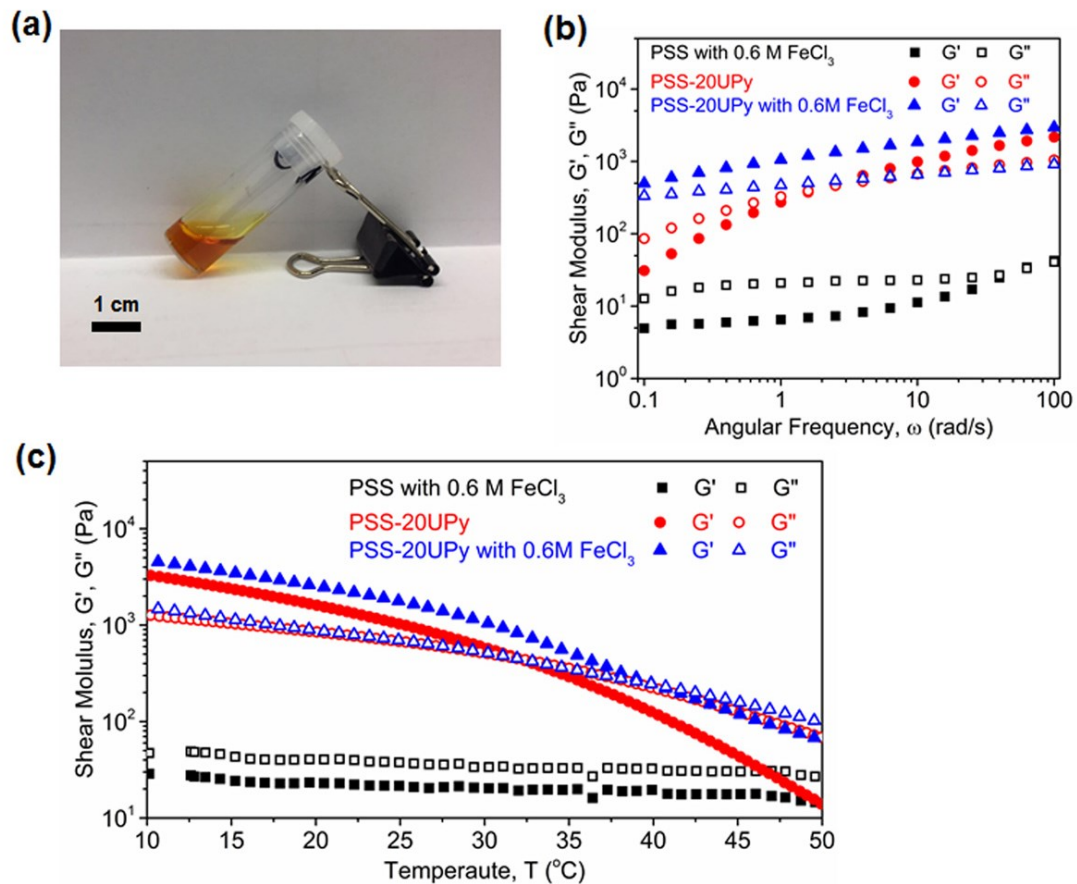
Figure S4.6. (a) Optical image of PSS solution (1 M NaSS) added with 0.6 M FeCl$_3$. (b) Frequency sweep measurements at 25 °C and (c) temperature sweep measurements at 10 rad/s of PSS solution with 0.6 M FeCl$_3$, PSS-20UPy hydrogel, and PSS-20UPy hydrogel soaked in 0.6 M FeCl$_3$, respectively.
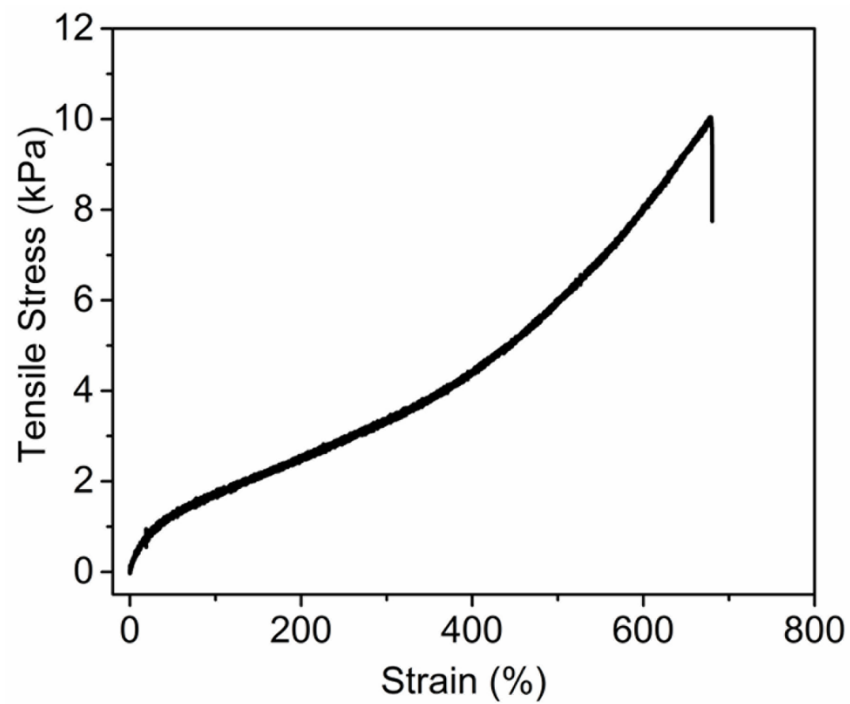
Figure S4.7. Typical stress-strain curve of the PANI/PSS-20UPy hybrid hydrogel with
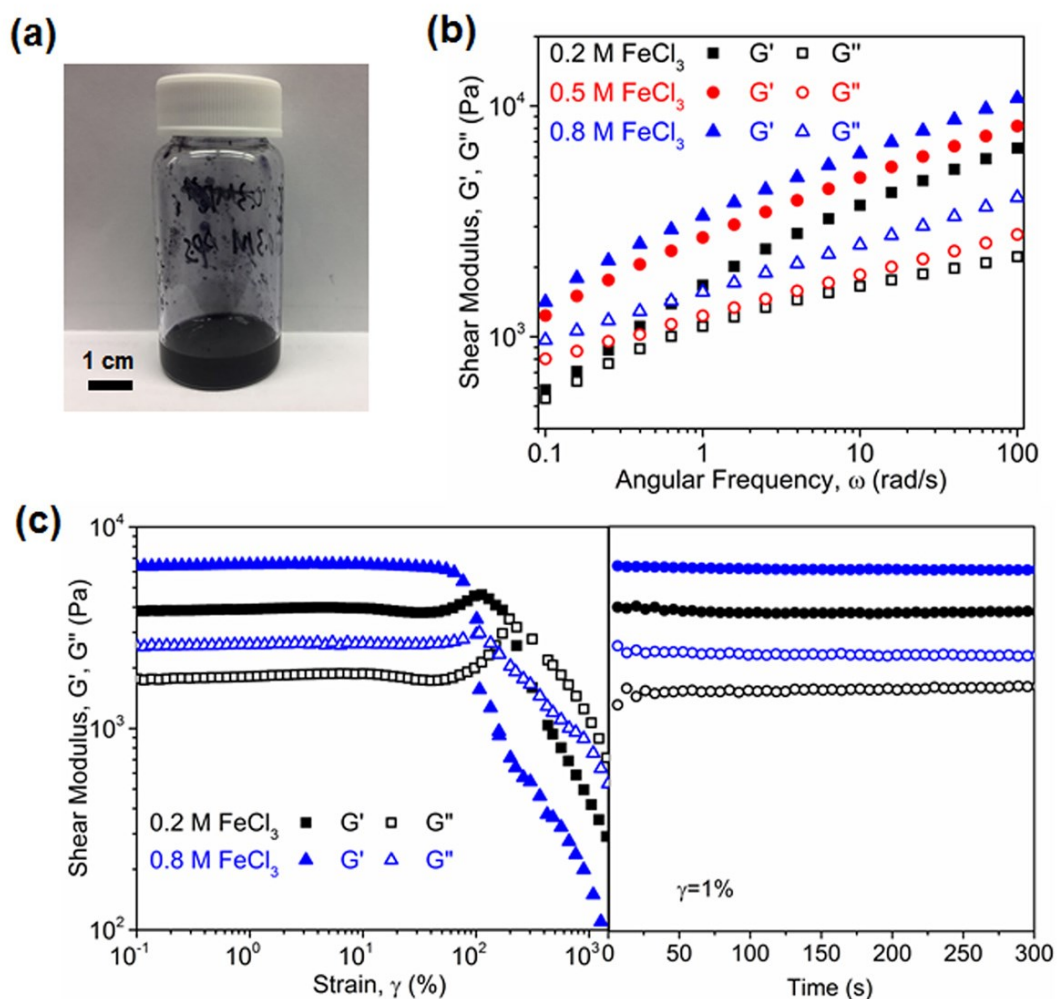
0.3 M ANI.

Figure S4.8. PANI/PSS-20UPy hydrogel with 0.3 M ANI polymerized in different solutions. (a) Optical image of the hydrogel polymerized in 0.3 M APS solution. (b) Frequency sweep measurements of the hydrogels polymerized in $FeCl_3$ solution with a concentration of 0.2 M, 0.5 M, 0.8 M, respectively. (c)Strain sweep measurements (left) followed by time sweep measurement of recovery (right) of the hydrogels polymerized in $FeCl_3$ solution with a concentration of 0.2 M and 0.8 M.
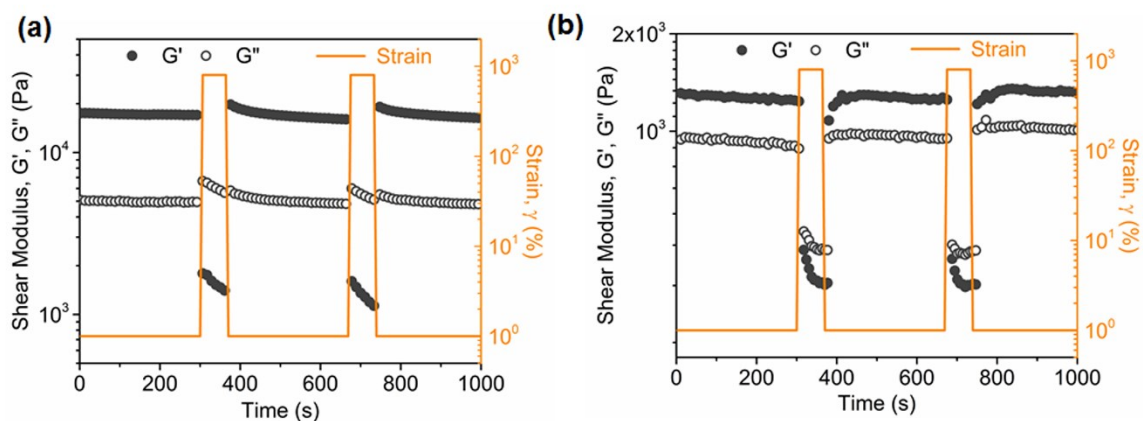
Figure S4.9. Variation of the shear moduli of PANI/PSS-20UPy hydrogel with 0.3 M ANI during cyclic steps with strain shifting between 1% and 800% at (a) 5 °C and (b) 40°C.

Table S4.2. Summary of recently reported conductive hydrogels prepared with conducting polymers for flexible electronics.

Hydrogel	Conductivity	Stretchability	Self-healing ability
PANI and PPy with phytic acid[1-2]	11 S/m and 50 S/m	Slight compression	Not reported
PNIPAM/PANI and PNIPAM/PPy[3]	0.2 S/m and 0.8 S/m	Compression by 50%	Not reported
PANI microsphere-structured hydrogel[4]	5 S/m	900%	Not reported
PPy in Zn-tpy gel[5]	12 S/m	67% on PDMS	Yes
PNIPAM with CNT and PPy[6]	34.93 S/m	515%	Yes
CNF-PPy in PVA[7]	3.65 S/m	600%	Yes
PDA-PPy in PVA[8]	12 S/m	2000%	Not reported
PANI and PAA with phytic acid[9]	12 S/m	500%	24 h (slow)
PANI in P(AAm-co-HEMA)[10]	8.14 S/m	>300%	Not reported
PEDOT: PSS[11]	4000 S/m	>35%	Not reported

References

(1)   Pan, L.; Yu, G.; Zhai, D.; Lee, H. R.; Zhao, W.; Liu, N.; Wang, H.; Tee, B. C.-K.; Shi, Y.; Cui, Y. Hierarchical nanostructured conducting polymer hydrogel with high electrochemical activity. *Proc. Natl. Acad. Sci. U.S.A.* **2012,** *109*, 9287-9292.

(2)   Pan, L.; Chortos, A.; Yu, G.; Wang, Y.; Isaacson, S.; Allen, R.; Shi, Y.; Dauskardt, R.; Bao, Z. An ultra-sensitive resistive pressure sensor based on hollow-sphere microstructure induced elasticity in conducting polymer film. *Nat. Commun.* **2014,** *5*, No.3002.

(3)   Shi, Y.; Ma, C.; Peng, L.; Yu, G. Conductive "smart" hybrid hydrogels with PNIPAM and nanostructured conductive polymers. *Adv. Funct. Mater.* **2015,** *25*, 1219-1225.

(4)   Duan, J.; Liang, X.; Guo, J.; Zhu, K.; Zhang, L. Ultra-stretchable and force-sensitive hydrogels reinforced with chitosan microspheres embedded in polymer networks. *Adv. Mater.* **2016,** *28*, 8037-8044.

(5)   Shi, Y.; Wang, M.; Ma, C.; Wang, Y.; Li, X.; Yu, G. A conductive self-healing hybrid gel enabled by metal-ligand supramolecule and nanostructured conductive polymer. *Nano Lett.* **2015,** *15*, 6276-6281.

(6)   Deng, Z.; Guo, Y.; Zhao, X.; Ma, P. X.; Guo, B. Multifunctional stimuli-responsive hydrogels with self-healing, high conductivity, and rapid recovery through host-guest interactions. *Chem. Mater.* **2018,** *30*, 1729–1742.

(7)   Ding, Q.; Xu, X.; Yue, Y.; Mei, C.; Huang, C.; Jiang, S.; Wu, Q.; Han, J. Nanocellulose-mediated electroconductive self-Healing hydrogels with high strength, plasticity, viscoelasticity, stretchability, and biocompatibility toward multifunctional applications. *ACS Appl. Mater. Interfaces* **2018,** *10*, 27987–28002.

(8)   Han, L.; Yan, L.; Wang, M.; Wang, K.; Fang, L.; Zhou, J.; Fang, J.; Ren, F.; Lu, X. Transparent, adhesive, and conductive hydrogel for soft bioelectronics based on light-transmitting polydopamine-doped polypyrrole nanofibrils. *Chem. Mater.* **2018,** *30*, 5561-5572.

(9)   Wang, T.; Zhang, Y.; Liu, Q.; Cheng, W.; Wang, X.; Pan, L.; Xu, B.; Xu, H. A self-healable, highly stretchable, and solution processable conductive polymer composite for ultrasensitive strain and pressure sensing. *Adv. Funct. Mater.* **2018,** *28*, No. 1705551.

(10)   Wang, Z.; Chen, J.; Cong, Y.; Zhang, H.; Xu, T.; Nie, L.; Fu, J. Ultra stretchable strain sensors and arrays with high sensitivity and linearity based on super tough conductive hydrogels. *Chem. Mater.* **2018,** *30*, 8062–8069.

(11)   Lu, B.; Yuk, H.; Lin, S.; Jian, N.; Qu, K.; Xu, J.; Zhao, X. Pure PEDOT: PSS hydrogels. *Nat. Commun.* **2019,** *10*, No. 1043.

Appendix D   Supporting Information for Chapter 5

S5.1 Experimental Section: Synthesis

2-(6-isocyanatohexylaminocarbonylamino)-6-methyl-4[1H]-pyrimidinone (OCN-C6-UPy). 2-amino-4-hydroxy-6-methylpyrimidine (5.00 g, 0.04 mol) was suspended in hexamethylene diisocyanate (40.32 g, 0.24 mol) and the mixture was stirred at 100 ºC under argon atmosphere for 20 h. After cooling to room temperature, 50 mL pentane was added in the flask and the resulting precipitate was filtered and washed with excess pentane for 3 times. The white powder was then dried under vacuum overnight. ^{1}H NMR (CDCl$_3$, 400 MHz): δ_H (ppm) = 13.1 (s, 1H, CH$_3$CN$\underline{H}$), 11.9 (s, 1H, CH$_2$NH(C=O)N$\underline{H}$), 10.2 (s, 1H, CH$_2$N$\underline{H}$(C=O)NH), 5.8 (s, 1H, C$\underline{H}$=CCH$_3$), 3.3 (m, 4H, NH(C=O)NHC$\underline{H}_2$ + C$\underline{H}_2$NCO), 2.2 (s, 3H, C$\underline{H}_3$C=CH), 1.6 (m, 4H, NCH$_2$C$\underline{H}_2$), 1.4 (m, 4H, CH$_2$CH$_2$C$\underline{H}_2$CH$_2$CH$_2$).

2-(12-isocyanatododecylaminocarbonylamino)-6-methyl-4[1H]-pyrimidinone (OCN-C12-UPy). A mixture of 2-amino-4-hydroxy-6-methylpyrimidine (0.375 g, 3 mmol) in 1,12-diisocyanatododecane (4.542 g, 18 mmol) was stirred at 90 ºC under argon atmosphere for 20 h. 5 mL hexane was added in the flask after reaction with stirring and then the suspension was poured into 50 mL hexane. The precipitate was filtered, washed with hexane for 3 times and dried under vacuum overnight. ^{1}H NMR (CDCl$_3$, 400 MHz): δ_H (ppm) = 13.1 (s, 1H, CH$_3$CN$\underline{H}$), 11.9 (s, 1H, CH$_2$NH(C=O)N$\underline{H}$), 10.2 (s, 1H, CH$_2$N$\underline{H}$(C=O)NH), 5.8 (s, 1H, C$\underline{H}$=CCH$_3$), 3.3 (m, 4H, NH(C=O)NHC$\underline{H}_2$ + C$\underline{H}_2$NCO), 2.2 (s, 3H, C$\underline{H}_3$C=CH), 1.6-1.4 (m, 20H, CH$_2$C$\underline{H}_2$CH$_2$).

2-(1-imidazolylcarbonylamino)-6-methyl-4[1H]-pyrimidinone (Im-Py). 2-amino-4-hydroxy-6-methylpyrimidine (1.25 g, 10 mmol) and 1,1′-Carbonyldiimidazole (2.43 g, 15 mmol) were suspended in 20 mL DMSO and stirred at 60 ºC under argon atmosphere for 8 h. After the addition of 50 mL acetone in the flask, the resulting solid was filtered and washed with excess acetone. The obtained white powder was dried in vacuum overnight.

TA-PEG-OH. PEG1500 (4.5 g, 3 mmol), DCC (0.619g, 3 mmol) and DMAP (0.037 g, 0.3 mmol) were dissolved in 40 mL DCM. The mixture was cooled to 0 ºC in an ice bath and purged with argon for 20 min. TA (0.619 g, 3 mmol) was dissolved in another 10 mL DCM and added dropwise into the stirring contents. After 1 h, the solution was allowed to gradually warm to room temperature and then stirred for 20 h. The solids were filtered off and the filtrate was concentrated to about 10 mL by rotation evaporation. Then TA-PEG-OH was isolated by precipitation in diethyl ether and dried under vacuum. ^{1}H NMR (CDCl$_3$, 400 MHz): δ_H (ppm) = 4.2 (t, 2H, C$\underline{H}_2$O(C=O)), 3.7-3.5 (m, ~130H, CH$_2$CH$_2$O + C$\underline{H}$SS), 3.1 (m, 2H, CH$_2$C$\underline{H}_2$S), 2.8 (Br. s. 1H, CH$_2$CH$_2$O$\underline{H}$), 2.4+1.9 (m, 2H, C$\underline{H}_2$CHS), 2.3 (m, 2H, CH$_2$C$\underline{H}_2$(C=O)), 1.7-1.4 (m, 6H, CH$_2$C$\underline{H}_2$CH$_2$).

TA-PEG-NH$_2$. The synthesis was performed as described for TA-PEG-OH, using NH$_2$-PEG-NH$_2$ instead of PEG1500. ^{1}H NMR (CDCl$_3$, 400 MHz): δ_H (ppm) =6.3 (s, 1H, CH$_2$N$\underline{H}$(C=O)), 3.7-3.5 (m, ~130 H, CH$_2$C$\underline{H}_2$O + C$\underline{H}$SS), 3.4 (t, 2H, C$\underline{H}_2$NH(C=O)), 3.1 (m, 2H, CH$_2$C$\underline{H}_2$S), 2.8 (m, 2H, CH$_2$ C$\underline{H}_2$NH$_2$), 2.4+1.9 (m, 2H, C$\underline{H}_2$CHS), 2.3 (m, 2H, CH$_2$C$\underline{H}_2$(C=O)), 1.7-1.4 (m, 10H, CH$_2$C$\underline{H}_2$CH$_2$).

PEG-C6-UPy. Prepared TA-PEG-OH (0.844 g, 0.5 mmol) was dissolved in 20 mL anhydrous chloroform, and OCN-C6-UPy (0.293g, 1 mmol) was added to the

solution. After addition of two drops of dibutyltin dilaurate as catalyst, the mixture was refluxed and stirred at 60 ºC for 20 h. After the reaction, another 20 mL chloroform was added, and the suspension was filtered to remove the solids. After concentrating the filtrate back to 20 mL by rotation evaporation, 1 g silica and 1 drop of dibutyltin dilaurate were added, and the mixture was heated at 60 ºC for 1h. The silica was removed by filtration and the prepared PEG-C6-UPy was obtained by precipitation in diethyl ether and dried under vacuum. ^{1}H NMR (CDCl$_3$, 400 MHz): δ_H (ppm) = 13.1 (s, 1H, CH$_3$CN<u>H</u>), 11.9 (s, 1H, CH$_2$NH(C=O)N<u>H</u>), 10.2 (s, 1H, CH$_2$N<u>H</u>(C=O)NH), 5.8 (s, 1H, C<u>H</u>=CCH$_3$), 4.2 (t, 2H, C<u>H</u>$_2$O(C=O)), 3.7-3.5 (m, ~130H, CH$_2$C<u>H</u>$_2$O + C<u>H</u>SS), 3.3 (m, 4H, NH(C=O)NHC<u>H</u>$_2$ + C<u>H</u>$_2$NCO), 3.1 (m, 2H, CH$_2$C<u>H</u>$_2$S), 2.4+1.9 (m, 2H, C<u>H</u>$_2$CHS), 2.3-2.2 (m, 5H, C<u>H</u>$_3$C=CH + CH$_2$C<u>H</u>$_2$(C=O)), 1.7-1.4 (m, 14H, CH$_2$C<u>H</u>$_2$CH$_2$).

PEG-C12-UPy. The synthesis was performed as described for PEG-C6-UPy, using OCN-C12-UPy instead of OCN-C6-UPy. ^{1}H NMR (CDCl$_3$, 400 MHz): δ_H (ppm) = 13.1 (s, 1H, CH$_3$CN<u>H</u>), 11.9 (s, 1H, CH$_2$NH(C=O)N<u>H</u>), 10.2 (s, 1H, CH$_2$N<u>H</u>(C=O)NH), 5.8 (s, 1H, C<u>H</u>=CCH$_3$), 4.2 (t, 2H, C<u>H</u>$_2$O(C=O)), 3.7-3.5 (m, ~130H, CH$_2$C<u>H</u>$_2$O + C<u>H</u>SS), 3.3 (m, 4H, NH(C=O)NHC<u>H</u>$_2$ + C<u>H</u>$_2$NCO), 3.1 (m, 2H, CH$_2$C<u>H</u>$_2$S), 2.4+1.9 (m, 2H, C<u>H</u>$_2$CHS), 2.3-2.2 (m, 5H, C<u>H</u>$_3$C=CH + CH$_2$C<u>H</u>$_2$(C=O)), 1.7-1.4 (m, 26H, CH$_2$C<u>H</u>$_2$CH$_2$).

PEG-C3-UPy. Prepared Im-Py (0.221g, 1 mmol) and TA-PEG-NH$_2$ (0.844g, 0.5 mmol) were added to 20 mL anhydrous chloroform and refluxed at 60 ºC for 2 days. With completion of the reaction, another 20 mL chloroform was added and the solids were removed by filtration. After the solution concentrated by rotation evaporation, PEG-C3-UPy was isolated by precipitation in diethyl ether and dried under vacuum. ^{1}H NMR (CDCl$_3$, 400 MHz): δ_H (ppm) = 13.1 (s, 1H, CH$_3$CN<u>H</u>), 11.9 (s, 1H, CH$_2$NH(C=O)N<u>H</u>),

10.2 (s, 1H, CH₂NH(C=O)NH), 6.3 (s, 1H, CH₂NH(C=O)), 5.8 (s, 1H, CH=CCH₃), 3.7-3.5 (m, ~130H, CH₂CH₂O + CHSS), 3.4 (m, 4H, CH₂NH(C=O)), 3.1 (m, 2H, CH₂CH₂S), 2.4+1.9 (m, 2H, CH₂CHS), 2.3-2.2 (m, 5H, CH₃C=CH + CH₂CH₂(C=O)), 1.7-1.4 (m, 10H, CH₂CH₂CH₂).

PEG-C6. TA-PEG-OH (844 mg, 0.5 mmol), DCC (1.3 mg, 0.5 mmol) and DMAP (6 mg, 0.05 mmol) were dissolved in 25 mL DCM. The mixture was cooled in an ice bath and purged with argon for 20 min. Heptanoic acid (130 mg, 1 mmol) was dissolved in another 5 mL DCM and added dropwise into the stirring mixture. After 1 h, the solution was moved from ice bath to room temperature and stirred for 20 h. The solids were removed by filtration and the solution was concentrated by rotation evaporation. Then TA-PEG-OH was collected by precipitation in diethyl ether and dried under vacuum. ¹H NMR (CDCl₃, 400 MHz): δ_H (ppm) = 4.2 (m, 4H, CH₂O(C=O)), 3.7-3.5 (m, ~130H, CH₂CH₂O + CHSS), 3.1 (m, 2H, CH₂CH₂S), 2.4+1.9 (m, 2H, CH₂CHS), 2.3 (m, 4H, CH₂CH₂(C=O)), 1.7-1.3 (m, 14H, CH₂CH₂CH₂ + CH₂CH₂CH₃), 0.9 (m, 3H, CH₂CH₂CH₃).

PEG-C12. The synthesis was performed as described for PEG-C6, using tridecanoic acid as reagent. ¹H NMR (CDCl₃, 400 MHz): δ_H (ppm) = 4.2 (m, 4H, CH₂O(C=O)), 3.7-3.5 (m, ~130H, CH₂CH₂O + CHSS), 3.1 (m, 2H, CH₂CH₂S), 2.4+1.9 (m, 2H, CH₂CHS), 2.3 (m, 4H, CH₂CH₂(C=O)), 1.7-1.3 (m, 26H, CH₂CH₂CH₂ + CH₂CH₂CH₃), 0.9 (m, 3H, CH₂CH₂CH₃).

S5.2 Supplementary Figures

S5.2.1 Force-Extension Curves
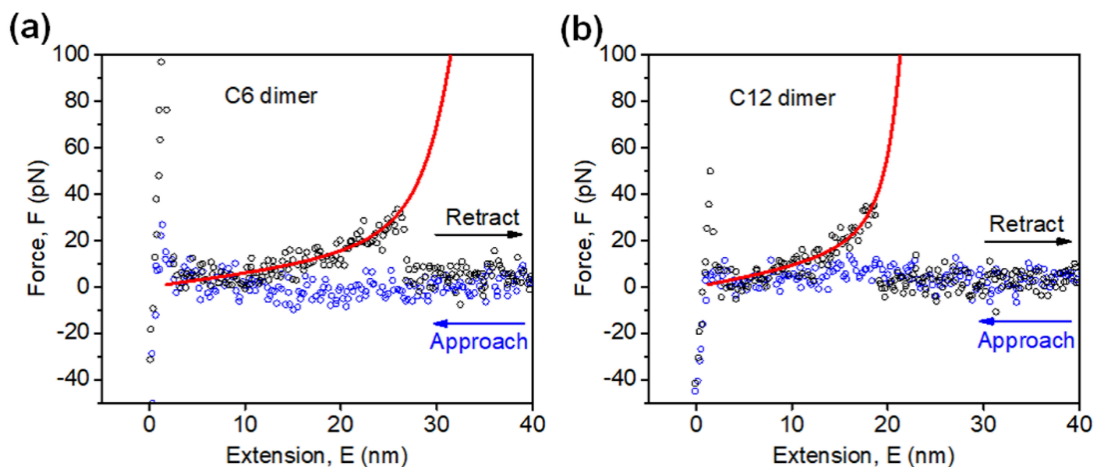
Figure S5.1. Representative force-extension curves measured between (a) C6 dimers at $R_f = 1.9 \times 10^5 \, \text{pN/s}$ and (b) C12 dimers at $R_f = 2.0 \times 10^5 \, \text{pN/s}$. The red curves correspond to modified freely-jointed chain (M-FJC) fitting to the rupture events.

S5.2.2 Force Histograms at Different Force Loading Rates
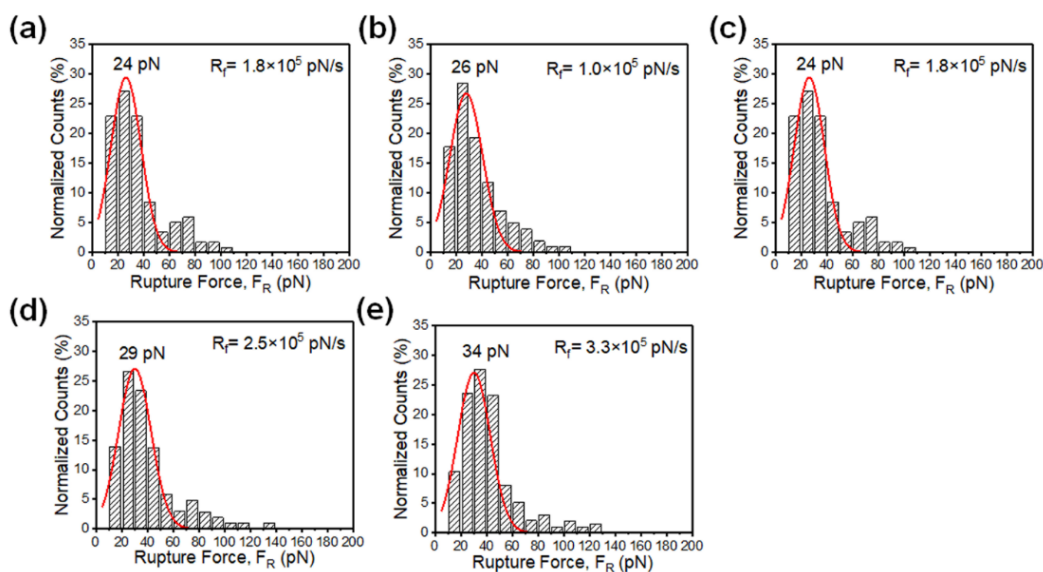
Figure S5.2. Histograms of rupture forces for C3-UPy dimers at loading rate of (a) $4.4 \times 10^4 \, \text{pN/s}$, (b) $1.0 \times 10^5 \, \text{pN/s}$, (c) $1.8 \times 10^5 \, \text{pN/s}$, (d) $2.5 \times 10^5 \, \text{pN/s}$, and (e) $3.3 \times 10^5 \, \text{pN/s}$. The red curves are Gaussian fits to the corresponding histograms.
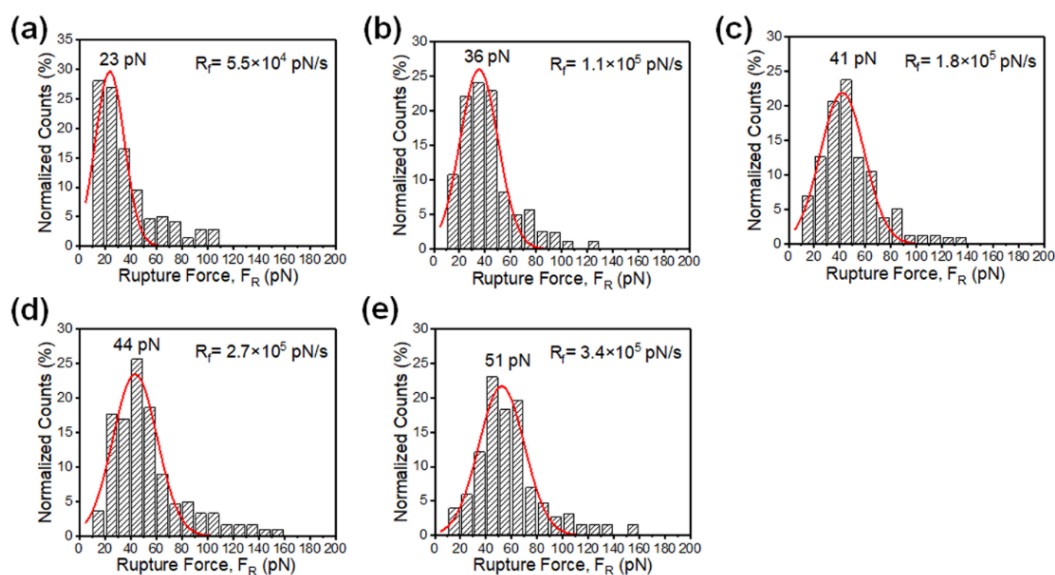
Figure S5.3. Histograms of rupture forces for C6-UPy dimers at loading rate of (a) 5.5×10^4 pN/s , (b) 1.0×10^5 pN/s , (c) 1.8×10^5 pN/s , (d) 2.7×10^5 pN/s , and (e) 3.4×10^5 pN/s . The red curves are Gaussian fits to the corresponding histograms.
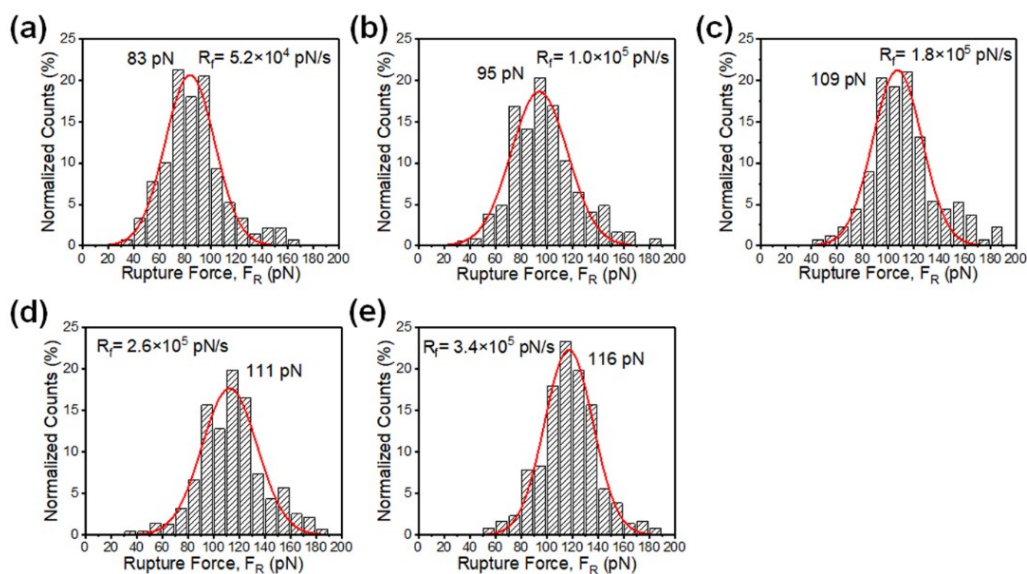
Figure S5.4. Histograms of rupture forces for C12-UPy dimers at loading rate of (a) 5.2×10^4 pN/s , (b) 1.0×10^5 pN/s , (c) 1.8×10^5 pN/s , (d) 2.6×10^5 pN/s , and (e) 3.4×10^5 pN/s . The red curves are Gaussian fits to the corresponding histograms.
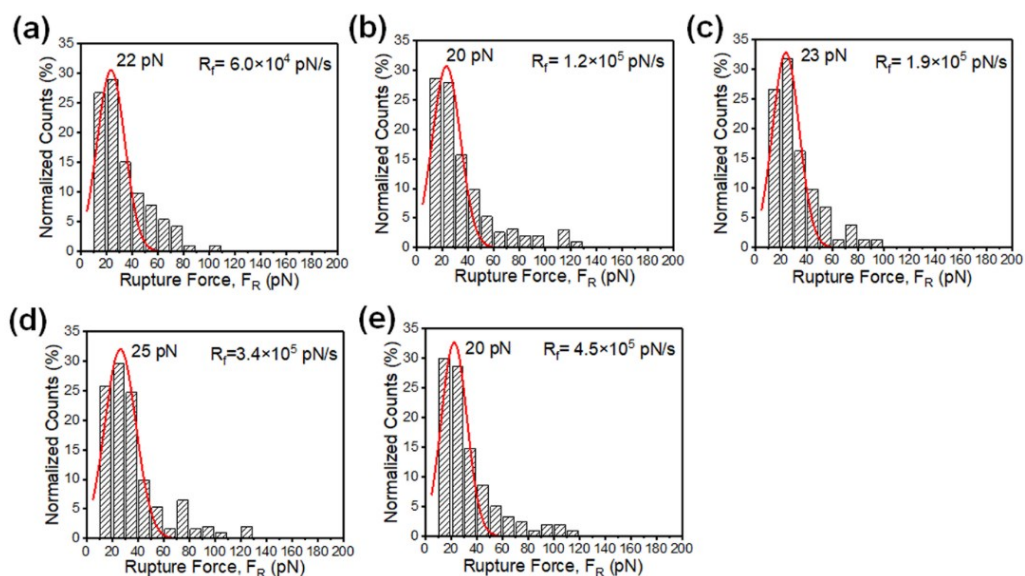
Figure S5.5. Histograms of rupture forces for C6 dimers at loading rate of (a) $6.0{\times}10^{4}\,\mathrm{pN/s}$, (b) $1.2{\times}10^{5}\,\mathrm{pN/s}$, (c) $1.9{\times}10^{5}\,\mathrm{pN/s}$, (d) $3.4{\times}10^{5}\,\mathrm{pN/s}$, and (e) $4.5{\times}10^{5}\,\mathrm{pN/s}$. The red curves are Gaussian fits to the corresponding histograms.
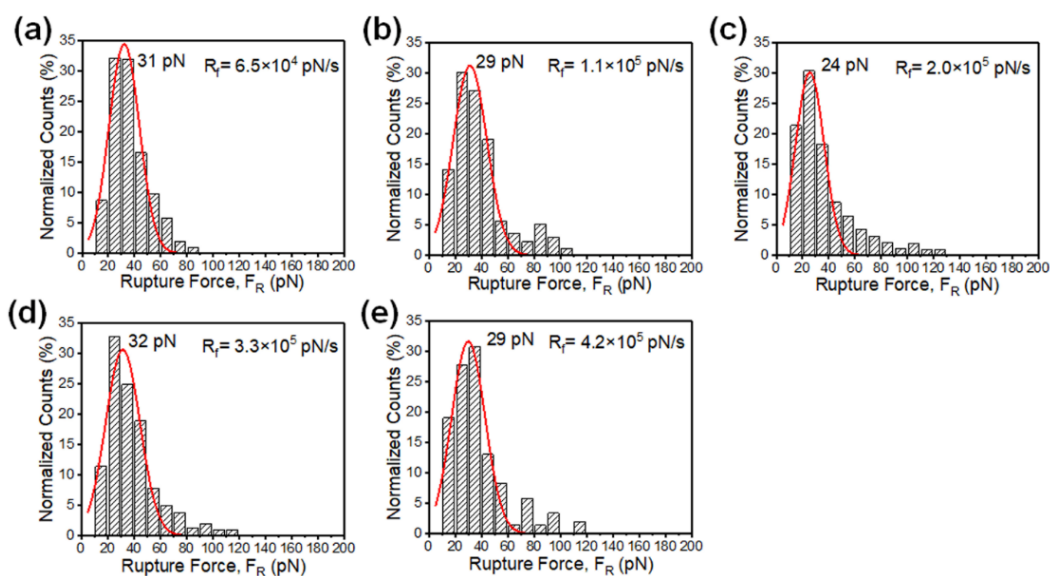
Figure S5.6. Histograms of rupture forces for C12 dimers at loading rate of (a) $6.5{\times}10^{4}\,\mathrm{pN/s}$, (b) $1.1{\times}10^{5}\,\mathrm{pN/s}$, (c) $2.0{\times}10^{5}\,\mathrm{pN/s}$, (d) $3.3{\times}10^{5}\,\mathrm{pN/s}$, and (e) $4.2{\times}10^{5}\,\mathrm{pN/s}$. The red curves are Gaussian fits to the corresponding histograms.

S5.2.3 Molecular Dynamics Simulation
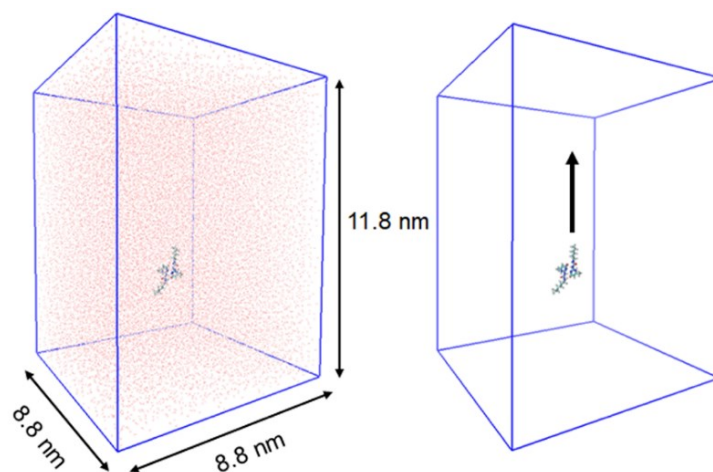
Figure S5.7. Initial configuration of C6-UPy dimer in a bulk explicit water box with dimension of $8.8 \times 8.8 \times 11.8$ nm^3. Umbrella sampling was conducted by pulling one molecule along a reaction coordinate with 0.1 nm step.
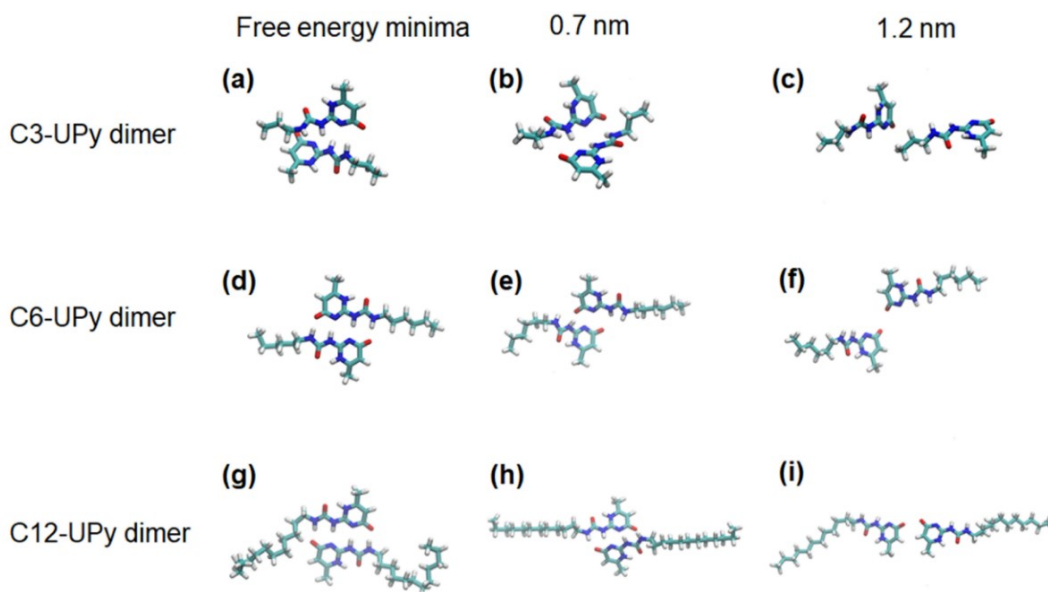
Figure S5.8. Snapshots showing representative structures of Cn-UPy (n=3, 6, 12) dimers at different center-of-mass distances.